

**UNIVERSIDADE FEDERAL DO RIO GRANDE DO SUL
INSTITUTO DE GEOCIÊNCIAS
PROGRAMA DE PÓS-GRADUAÇÃO EM GEOCIÊNCIAS**

**CONEXÕES CLIMÁTICAS ENTRE OS ANDES
TROPICAIS E A AMAZÔNIA NO REGISTRO DE
AEROSSÓIS EM TESTEMUNHO DE GELO DO
NEVADO ILLIMANI**

FILIPE GAUDIE LEY LINDAU

ORIENTADOR Prof. Dr. Jefferson Cardia Simões
COORIENTADORA Profa. Dra. Barbara Delmonte

Volume I

Porto Alegre – 2020

**UNIVERSIDADE FEDERAL DO RIO GRANDE DO SUL
INSTITUTO DE GEOCIÊNCIAS
PROGRAMA DE PÓS-GRADUAÇÃO EM GEOCIÊNCIAS**

**CONEXÕES CLIMÁTICAS ENTRE OS ANDES
TROPICAIS E A AMAZÔNIA NO REGISTRO DE
AEROSSÓIS EM TESTEMUNHO DE GELO DO
NEVADO ILLIMANI**

FILIPE GAUDIE LEY LINDAU

ORIENTADOR – Prof. Dr. Jefferson Cardia Simões – Instituto de Geociências,
Universidade Federal do Rio Grande do Sul

COORIENTADORA – Profa. Dra. Barbara Delmonte – Department of Earth and
Environmental Sciences, Università degli Studi di Milano-Bicocca

BANCA EXAMINADORA

Prof. Dr. Alexandre Lima Correia – Instituto de Física, Universidade de
São Paulo

Profa. Dra. Franciéle Schwanck Carlos – Instituto de Pesquisas
Hidráulicas, Universidade Federal do Rio Grande do Sul

Prof. Dr. Heitor Evangelista da Silva – Instituto de Biologia Roberto
Alcântara Gomes, Universidade do Estado do Rio de Janeiro

Tese de Doutorado apresentada como
requisito parcial para a obtenção do Título
de Doutor em Ciências

Porto Alegre – 2020

CIP - Catalogação na Publicação

Lindau, Filipe Gaudie Ley
Conexões climáticas entre os Andes tropicais e a Amazônia no registro de aerossóis em testemunho de gelo do Nevado Illimani / Filipe Gaudie Ley Lindau. -- 2020.

145 f.
Orientador: Jefferson Cardia Simões.

Coorientadora: Barbara Delmonte.

Tese (Doutorado) -- Universidade Federal do Rio Grande do Sul, Instituto de Geociências, Programa de Pós-Graduação em Geociências, Porto Alegre, BR-RS, 2020.

1. Testemunhos de gelo. 2. Andes tropicais. 3. Bacia Amazônica. 4. Poeira atmosférica. I. Simões, Jefferson Cardia, orient. II. Delmonte, Barbara, coorient. III. Título.

À Heloísa, João Carlos e Jade

Agradecimentos

Agradeço ao Prof. Jefferson C. Simões pela orientação, pela confiança, pelo amplo acesso aos laboratórios de glacioquímica do CPC e pela sua dedicação na pesquisa dos testemunhos de gelo. Também, às oportunidades de participação em expedições na Antártica (2014/15) e nos Andes (2017), em campanhas de amostragem no CCI (2013, 2015 e 2019) e ao incentivo na participação nos principais eventos e congressos voltados a temática dos testemunhos de gelo.

Agradeço à Profa. Barbara Delmonte pela coorientação e pela sua imensa motivação em revelar os segredos congelados no Nevado Illimani. E também, por me fornecer total autonomia de trabalho no EuroCold durante o meu período de doutorado sanduíche e pela sua detalhada revisão dos resultados.

Ao Patrick Ginot por me acolher na expedição Ice Memory ao Nevado Illimani e pelo seu esforço para que o terceiro testemunho (o utilizado nesse trabalho) fosse perfurado, mesmo que a expedição tenha sofrido atrasos pelas condições meteorológicas pouco favoráveis. E também, por me receber no IGE para dividirmos o testemunho e por revisar os artigos com entusiasmo.

Ao Prof. Rafael Ribeiro por sempre me lembrar de focar o meu olhar na Amazônia, pela disposição em revisar os artigos, pelos dados glaciológicos e pelas ideias compartilhadas.

Aos mais de 90 integrantes da expedição Ice Memory. Em especial a Stanislav Kutuzov e Luc Piard pela insistência em consertar o gerador da perfuradora, operada por eles, para que o terceiro testemunho fosse extraído. Ao Bruno Jordain pela organização das amostras. Ao Nicolas Caillon por negociar minha subida ao acampamento no topo do Illimani. Ao Juvenal Condori e Félix Vargas por me guiarem com aparente tranquilidade em meio a tempestades, fendas e precipícios que separavam os acampamentos no Illimani.

Agradeço à equipe do DISAT. Ao Giovanni Baccolo por estar sempre disposto a ajudar nas análises, por me apresentar a técnica de absorção

neutrônica e por revisar os artigos. À Chiara Paleari por me apresentar a técnica de microespectrometria Raman. À Elena Di Stefano por completar as análises por INAA. À Cristina Canella pela ajuda na descontaminação das amostras. À Agnese Petteni por vir ao Brasil ajudar na interpretação dos resultados. A Marco Filippazzi pelas dicas de trabalho na câmara fria. Aos professores Valter Maggi, Sergio Andó e Eduardo Garzanti por me conferirem amplo acesso aos seus laboratórios e por revisarem os resultados.

À equipe do CCI. Ao prof. Paul Mayewski e ao Mariusz Potocki por assegurarem o transporte do testemunho da Itália para os EUA. À Elena Korotkikh pelas análises de IC. Ao Michael Handley pelas análises de ICP-SMFS. Ao Douglas Introne pelas análises isotópicas.

À equipe do CPC. Ao Ronaldo Bernardo, Franciéle Schwanck, Flávia Tavares e Cláudia Uchôa pelo empenho na campanha de subamostragem do testemunho em fevereiro de 2019 no CCI. Ao Isaías Thoen, Luciano Marquetto, Jeffrey Auger, José Mauro Dalla Rosa, José Celso, Pedro Reis, Ildo Parnov, Ana Sanches, Rafael dos Reis e prof. Francisco Aquino por compartilharem experiências, conhecimentos e referências.

Agradeço ao Programa Antártico Brasileiro pelo empréstimo de material de campo. Ao PPGGEO e ao CNPq pelas oportunidades.

À minha família. À Jade pela companhia, pelo incentivo e por enfrentar comigo a nevasca que quase impediu o transporte do testemunho da França para a Itália. À Heloísa, João Carlos e Marcos pelo apoio nos meus projetos.

Resumo

As geleiras tropicais Andinas arquivam informações ambientais importantes para a validação de modelos climáticos utilizados na previsão de tendências na precipitação sobre a América do Sul tropical, que possibilitam o desenvolvimento de estratégias de mitigação e adaptação frente aos cenários de mudança climática nessa região. Nesse contexto, esta tese investiga um testemunho de *firn* com 23,8 m de profundidade perfurado no Nevado Illimani (16°37'S; 67°46'O, 6.350 m acima do nível do mar, Bolívia), com o objetivo de obter *proxies* ambientais, principalmente relacionadas ao transporte de umidade da bacia Amazônica para os Andes. O testemunho passou por etapas de processamento e análise em três laboratórios, no EuroCold (Universidade Milano-Bicocca, Itália), no *Climate Change Institute* (Universidade do Maine, EUA) e no *Institut des Géosciences de l'Environnement* (Universidade Grenoble-Alpes, França). As partículas de poeira presentes no testemunho foram analisadas quanto a sua concentração, distribuição de tamanhos, mineralogia e composição. Na integralidade da matriz de *firn* foram determinados os íons majoritários, os elementos traço e as razões de isótopos estáveis (δD e $\delta^{18}O$). O testemunho cobre um período de 18 anos (1999–2017), conforme datação baseada na variabilidade sazonal das concentrações de poeira e Ca^{2+} , e de δD . A comparação das análises com informações atmosféricas atuais (observações meteorológicas, modelos de reanálise e imagens de satélite) permitiu a identificação de *proxies* ambientais. Foi observado que a proporção de partículas gigantes (diâmetro > 20 μm), quando considerada junto com o δD , responde à convecção profunda sobre o Altiplano Boliviano durante o verão, que por sua vez está relacionada ao fenômeno El Niño-Oscilação Sul. Os fatores de enriquecimento do Mn estão correlacionados (no nível de significância de 95%) com a intensidade dos jatos de baixos níveis sobre a bacia Amazônica durante o inverno. A expansão temporal do registro de poeira pelo uso dos dados de um testemunho extraído do Illimani em 1999, permitiu investigar a relação entre a poeira e o rápido degelo dos Andes tropicais nas últimas décadas. A proporção de partículas de poeira grossa (diâmetro entre 10 e 20 μm) durante o período 1919–2017 responde a uma troposfera mais quente e à redução no transporte de umidade da bacia Amazônica para os Andes, causada pelo aquecimento do oceano Atlântico tropical norte. Em contrapartida, a contaminação por Cr durante o século XXI mostrou uma redução quando comparada ao final do século XX, provavelmente devido ao maior controle na emissão de poluentes em atividades ligadas à mineração.

Palavras-chave: Testemunhos de gelo; Andes tropicais; Bacia Amazônica; Poeira atmosférica.

Abstract

Andean tropical glaciers store valuable environmental information to validate climate models used to forecast precipitation trends over tropical South America, which enable the development of mitigation and adaptation strategies for climate change scenarios in that region. In this context, this thesis investigates a 23.8 m deep firn core from Nevado Illimani (16°37'S; 67°46'W, 6.350 m above the sea level, Bolivia) in order to obtain environmental proxies, in particular the moisture transport from the Amazon basin towards the Andes. The core was processed and analyzed in three laboratories: the EuroCold (University Milano-Bicocca, Italy), the Climate Change Institute (University of Maine, USA) and the *Institut des Géosciences de l'Environnement* (University Grenoble-Alps, France). Dust particles were analyzed for their concentration, size distribution, mineralogy and composition. The bulk firn matrix was analyzed for major ions, trace elements and stable isotopes (δD and $\delta^{18}O$). The core spans 18 years (1999–2017) based on seasonal oscillations of dust and Ca^{2+} concentrations, and δD . Environmental proxies were obtained by comparing the measurements with recent atmospheric information (meteorological observations, reanalysis models and satellite images). The proportion of giant dust particles (diameter > 20 μm), when considered together with δD , responds to summer deep convection over the Bolivian Altiplano, which in turn is related to the El Niño Southern Oscillation. The Mn enrichment factors are correlated (at the 95% significance level) with the winter low level jets intensity over the Amazon basin. The temporal expansion of the dust record, by using data from an ice core drilled in 1999 at the Illimani, allowed a relationship between the dust and the fast retreat of the tropical Andean glaciers over the last decades. The proportion of coarse dust particles (diameters between 10 and 20 μm) during the 1919–2017 period responds to a warmer troposphere and to the reduction in moisture transport from the Amazon basin to the Andes, caused by the warming of the tropical North Atlantic Ocean. On the other hand, Cr contamination reduced during the 21st century, when compared to the late 20th century, most probably because a higher pollutant emission control by mining related activities.

Keywords: Ice cores; Tropical Andes; Amazon basin; Atmospheric dust

Sumário

Agradecimentos.....	5
Resumo.....	7
Abstract.....	8
1 Introdução.....	11
1.1 Considerações iniciais.....	11
1.2 O registro dos aerossóis em geleiras.....	12
1.3 Objetivos.....	13
1.4 Estrutura da tese.....	14
2 O registro ambiental dos testemunhos de gelo nos Andes Centrais.....	16
2.1 A transição do Último Máximo Glacial para o Holoceno.....	17
2.2 O Holoceno.....	19
2.3 O último século.....	20
3 Área de estudo.....	23
3.1 Aspectos climáticos.....	23
3.2 Aspectos glaciológicos.....	25
3.3 Expedições ao Nevado Illimani.....	26
4 Metodologia.....	28
4.1 Coleta do testemunho de <i>firn</i>	28
4.2 Processamento do testemunho.....	29
4.3 Análise da Poeira.....	32
4.3.1 Concentração e distribuição de tamanhos.....	34
4.3.2 Composição elementar.....	35
4.3.3 Composição mineralógica.....	37
4.4 Análise dos isótopos estáveis.....	39
4.5 Análise das impurezas na matriz de neve e <i>firn</i>	39
4.5.1 Elementos traço.....	40
4.5.2 Íons majoritários.....	41
4.6 O testemunho de gelo extraído em 1999.....	42
4.7 Dados atmosféricos.....	42
5 Resultados.....	44
5.1 Giant dust particles at Nevado Illimani: a proxy of summertime deep convection over the Bolivian Altiplano.....	44

5.2 Proxies for atmospheric circulation over the Amazon basin from the aerosol composition in a Nevado Illimani firn core, Bolivia.....	74
5.3 Dust record in an ice core from tropical Andes (Nevado Illimani – Bolivia), potential for climate variability analyses in the Amazon basin.....	105
6 Conclusões.....	130
7 Referências.....	132
Anexo I.....	139
Anexo II.....	141
Anexo III.....	143
Anexo IV.....	145

1 Introdução

1.1 Considerações iniciais

Entender o comportamento da circulação atmosférica durante o passado é um tópico de alta prioridade do estudo paleoclimatógico. Isso possibilita a validação de modelos climáticos que poderão ser usados no desenvolvimento de estratégias de mitigação e/ou adaptação com base em cenários de mudanças climáticas futuras. Arquivos paleoclimáticos dos últimos ~20.000 anos (com resolução anual nos últimos ~1.000 anos) estão armazenados em geleiras da cordilheira dos Andes (Vimeux *et al.*, 2009). Tais arquivos são obtidos por testemunhos verticalmente coletados nas camadas de neve, *firn*¹ e gelo, localizadas nos divisores das bacias de drenagem, onde as taxas de escoamento dessas camadas são mínimas. Os testemunhos de gelo extraídos de geleiras da Bolívia e do Peru são de particular interesse por arquivarem informações de um ambiente tropical, algo raro no estudo de testemunhos de gelo, já que 99% das geleiras tropicais estão nos Andes (Kaser e Osmaston, 2002).

Os Andes tropicais estão fortemente expostos a potenciais impactos das mudanças climáticas que poderão afetar a segurança alimentar e hídrica de aproximadamente 90 milhões de pessoas (Espinoza *et al.*, 2020). Na Bolívia, o degelo da Cordilheira Andina ameaça o suprimento de água da região metropolitana de La Paz (Soruco *et al.*, 2015), além de outras centenas de cidades ao longo dos Andes. De fato, o degelo nessa região intensificou-se nas últimas décadas devido a uma atmosfera mais quente, atingindo as maiores taxas de derretimento já registradas desde a metade do século XVII (Rabatel *et al.*, 2013). Na Bolívia, entre a década de 1970 e o ano de 2017, o Grupo de Trabalho em Neve e Gelo do Programa Hidrológico Internacional (GTHN-PHI-UNESCO) estimou que a superfície glacial na Bolívia sofreu uma redução de 50%. O degelo dos Andes afeta, ainda, a

¹ *Firn*: estágio intermediário entre a neve e o gelo, com densidade entre 0,4 e 0,8 g cm⁻³. Caracterizado por cristais soldados uns aos outros, porém ainda com espaços intergranulares e permeável (Simões, 2004).

preservação dos testemunhos de gelo. A perda do sinal climático sazonal já foi sentida a uma altitude de 5.670 m acima do nível do mar (anm) nas camadas de *firn* da calota de gelo Quelccaya ($13^{\circ}54'S$; $70^{\circ}48'W$, Peru), devido ao derretimento da superfície e percolação através do *firn* (Thompson *et al.*, 2017). Porém camadas mais elevadas (6.350 m anm) no Nevado Illimani ($16^{\circ}37'S$, $67^{\circ}46'W$, Bolívia) estão, por enquanto, preservadas.

Um potencial agravante desse acelerado degelo é o corrente desmatamento da floresta Amazônica, já que uma redução na quantidade de vapor d'água gerada pela evapotranspiração pode afetar a precipitação de neve sobre as geleiras (Zemp *et al.*, 2014; Staal *et al.*, 2018). Um maior entendimento da conectividade entre os Andes tropicais e a Amazônia depende de uma detalhada identificação dos mecanismos atmosféricos interligando esses ambientes (Espinoza *et al.*, 2020). A presente tese parte da hipótese de que aerossóis depositados ao longo do tempo nas camadas de *firn* e gelo do Nevado Illimani respondem à variabilidade de condições atmosféricas conectando a bacia Amazônica e os Andes tropicais.

1.2 O registro dos aerossóis em geleiras

Existem numerosas interações entre a atmosfera, outros reservatórios geoquímicos (biosfera, hidrosfera, criossfera e litosfera) e atividades antrópicas (e.g., queima de biomassa, uso de combustíveis fósseis, fundição de metais), que levam à formação de uma variedade de aerossóis (suspensões atmosféricas sólidas ou líquidas). Grandes quantidades do aerossol classificado como poeira são emitidas do Altiplano Boliviano (Prospero *et al.*, 2001; Gaiero *et al.*, 2013), principalmente durante o inverno (estação seca), e depositados em geleiras próximas.

A concentração absoluta de poeira em testemunhos de *firn* e gelo depende de fatores que incluem a acumulação de neve, a intensidade da fonte (que considera a aridez do solo, a cobertura vegetal e qualquer outro fator influenciando a quantidade de partículas disponível para deflação), assim como processos de transporte, que afetam o tempo de residência das partículas na atmosfera (Delmonte, 2003). Em contrapartida, a distribuição de tamanhos e a relativa proporção de partículas com determinado tamanho de grão dependem geralmente das condições de transporte

(Delmonte *et al.*, 2004, 2017). Ou seja, partículas com um maior tamanho de grão estão relacionadas a um menor transporte atmosférico e, portanto, são geralmente provenientes de fontes mais próximas. A variabilidade na presença de partículas relativamente maiores em um testemunho de gelo da Groenlândia foi recentemente utilizada como *proxy* da extensão daquele manto de gelo, pois o recuo da área glacial aumenta a exposição de áreas ricas em sedimentos que, por sua vez, tornam-se uma fonte de partículas relativamente mais grossas ao local de perfuração do testemunho (Simonsen *et al.*, 2019).

A variabilidade na concentração de poeira depositada em geleiras também pode ser inferida pela presença de elementos que majoritariamente constituem os minerais de regiões áridas. A partir do aumento nas concentrações de cálcio ao longo dos últimos 200 anos, em testemunho de gelo extraído do Cáucaso (Rússia), observou-se um aumento da intensidade da fonte em regiões do Oriente Médio e, portanto, concluiu-se que elas apresentam, nas últimas décadas, as condições mais áridas ao longo do período estudado (Kutuzov *et al.*, 2019). Um detalhado estudo da composição dos aerossóis permite ainda a identificação de aerossóis provenientes de diversas fontes. Por exemplo, foi observado que a variabilidade nas concentrações de urânio e arsênio em partículas depositadas em diferentes regiões do manto de gelo da Antártica estão diretamente relacionadas às emissões provenientes de fundições na Austrália e nos Andes, respectivamente (Potocki *et al.*, 2016; Schwanck *et al.*, 2016).

Nas geleiras Andinas são encontradas, além de aerossóis provenientes das regiões áridas do Altiplano e das atividades antrópicas ligadas à mineração, suspensões biogênicas e fuligem provenientes da bacia Amazônica. Uma observação interessante é que a combinação de elevadas concentrações de fuligem e de poeira na superfície de geleiras Bolivianas pode aumentar a sua taxa anual de derretimento em aproximadamente 5% (Magalhães *et al.*, 2019).

1.3 Objetivos

O objetivo desta tese é investigar a variabilidade climática e ambiental a partir das camadas de neve, *firn* e gelo armazenadas em um testemunho de gelo do

Nevado Illimani (Bolívia), identificando possíveis conexões entre os Andes tropicais e a bacia Amazônica.

Metas:

- a) Extrair um testemunho de *firn* do Nevado Illimani que forneça uma quantidade de amostras necessárias para identificação dos ciclos sazonais anuais e que possa ser integrado ao testemunho extraído no mesmo local, no ano de 1999. Para ao novo testemunho,
- b) Determinar a concentração de poeira, sua distribuição de tamanhos e sua composição mineralógica e elementar;
- c) Determinar a composição das impurezas presentes na matriz de *firn*, assim como a razão de isótopos estáveis da água;
- d) Datar o testemunho observando a variabilidade sazonal dos parâmetros analisados;
- e) Estabelecer relações entre as variáveis analisadas no testemunho e parâmetros atmosféricos, buscando a identificação de *proxies* ambientais e climáticas;
- f) Integrar resultados obtidos com dados ainda não estudados do testemunho de gelo extraído em 1999 no mesmo local.
- g) Reconstruir condições climáticas e ambientais desde o início do século XX a partir da caracterização da poeira depositada no Nevado Illimani.

1.4 Estrutura da tese

No primeiro capítulo (Introdução) são apresentadas as considerações iniciais sobre a relevância do estudo de testemunhos de gelo nos Andes tropicais. No capítulo 2 (O registro ambiental dos testemunhos de gelo dos Andes Centrais) é apresentada uma revisão sobre as principais informações ambientais e climáticas obtidas a partir do estudo de testemunhos de gelo dessa região. No capítulo 3 (Área de estudo) é caracterizada a área geográfica deste estudo, focando nos aspectos climáticos e glaciológicos. O capítulo 4 (Metodologia) apresenta os métodos utilizados para a perfuração do testemunho de *firn* estudado, além da preparação e da análise das amostras. O capítulo 5 (Resultados) é composto por três artigos

submetidos em periódicos internacionais. O primeiro artigo (*Giant dust particles at Nevado Illimani: a proxy of summertime deep convection over the Bolivian Altiplano*) apresenta uma caracterização detalhada da poeira depositada no Illimani e relações com a convecção profunda sobre o Altiplano. O segundo artigo (*Proxies for atmospheric circulation over the Amazon basin from the aerosol composition in a Nevado Illimani firn core, Bolivia*) explora detalhadamente a composição das impurezas depositadas no Illimani, buscando relações com a circulação atmosférica sobre a bacia Amazônica. Por fim, o terceiro artigo (*Dust record in an ice core from tropical Andes (Nevado Illimani – Bolivia), potential for climate variability analyses in the Amazon basin*) amplia a escala temporal do registro de poeira, analisando os efeitos da variabilidade climática recente nesse registro. O fechamento da tese com a integração dos três artigos é realizado no capítulo 6 (Conclusões).

2 O registro ambiental dos testemunhos de gelo nos Andes Centrais

A região dos Andes Centrais (ou Andes tropicais do sul) é definida como a porção da Cordilheira Andina entre 15° e 23°S, abrangendo o norte do Chile e da Argentina, a Bolívia, e o sul do Peru. Nessa região a cordilheira se divide em duas cadeias de montanhas com elevações que ultrapassam os 6500 m anm (Cordilheira Oriental e Ocidental) separadas por um platô de altitude média de aproximadamente 4000 m anm, conhecido como o Altiplano. A Figura 2.1 indica os locais dos Andes Centrais onde foram obtidos testemunhos de gelo, além do Nevado Huascarán que apresenta um registro climático similar ao observado nos Andes Centrais (Hoffman *et al.*, 2003).

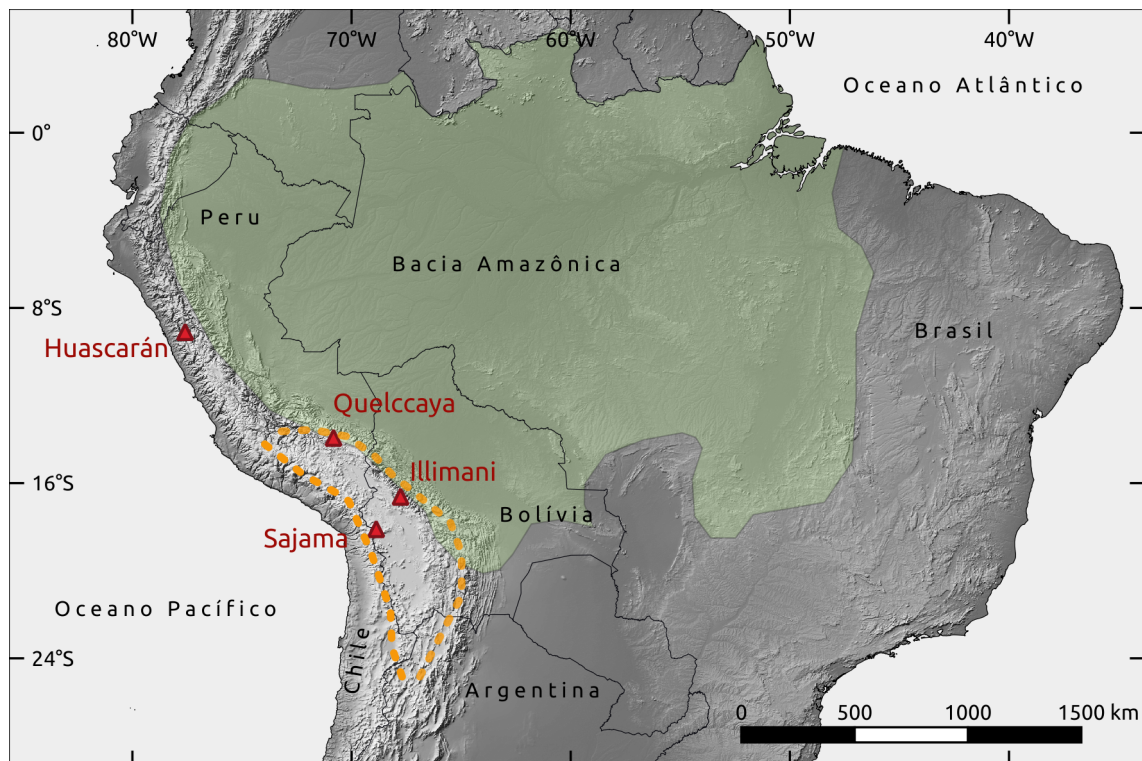


Figura 2.1: Localização dos sítios onde foram extraídos os testemunhos de gelo (triângulos vermelhos) discutidos no Capítulo 2. A bacia Amazônica está demarcada pela área em verde e as linhas tracejadas laranja indicam a divisão dos Andes em cordilheira Ocidental e Oriental.

2.1 A transição do Último Máximo Glacial para o Holoceno

A determinação cronológica das camadas de gelo nesse período é complexa devido à sua extrema compactação. Embora os registros dos testemunhos de gelo dos Andes Centrais cubram os últimos ~20 ka, a maior parte das suas camadas de gelo referem-se aos últimos 1000 anos (Vimeux *et al.*, 2009). Isso é um reflexo das altas acumulações anuais de neve nessa região, em comparação com os polos, o que resulta em elevada compactação das camadas mais profundas. No Illimani, por exemplo, os últimos 1000 anos estão contidos em ~90% do testemunho (Knüsel *et al.*, 2003), enquanto que os 10 m mais profundos englobam mais do que 15 ka de registros paleoambientais.

Os testemunhos de gelo do Illimani, Sajama e Huascarán mostraram um coerente aumento dos valores isotópicos na transição do Último Máximo Glacial (UGM) para o Holoceno (Figura 2.2a). O UGM, por sua vez, foi atribuído a um intervalo de 1000 anos centrado nos menores valores isotópicos de cada testemunho (Vimeux, 2009). Observações modernas da composição isotópica da precipitação nos Andes Centrais mostram que ela é afetada por um grande número de fatores (Hoffman *et al.*, 2003), mas principalmente controlada pela precipitação local e por ciclos de precipitação na bacia Amazônica e no Oceano Atlântico tropical (Vimeux *et al.*, 2005). Com base no entendimento do registro isotópico das camadas de neve recentes, estima-se que a precipitação nos Andes Centrais durante o UGM foi de 5 a 7% maior do que a dos dias atuais (Vimeux, 2009). Porém, segundo essa autora, isso representa um balanço líquido de precipitação, resultante da integração de todos os sinais isotópicos que constituem as massas de ar que chegam aos Andes Centrais, portanto respondendo a um possível mosaico de condições mais úmidas e mais secas na América do Sul tropical.

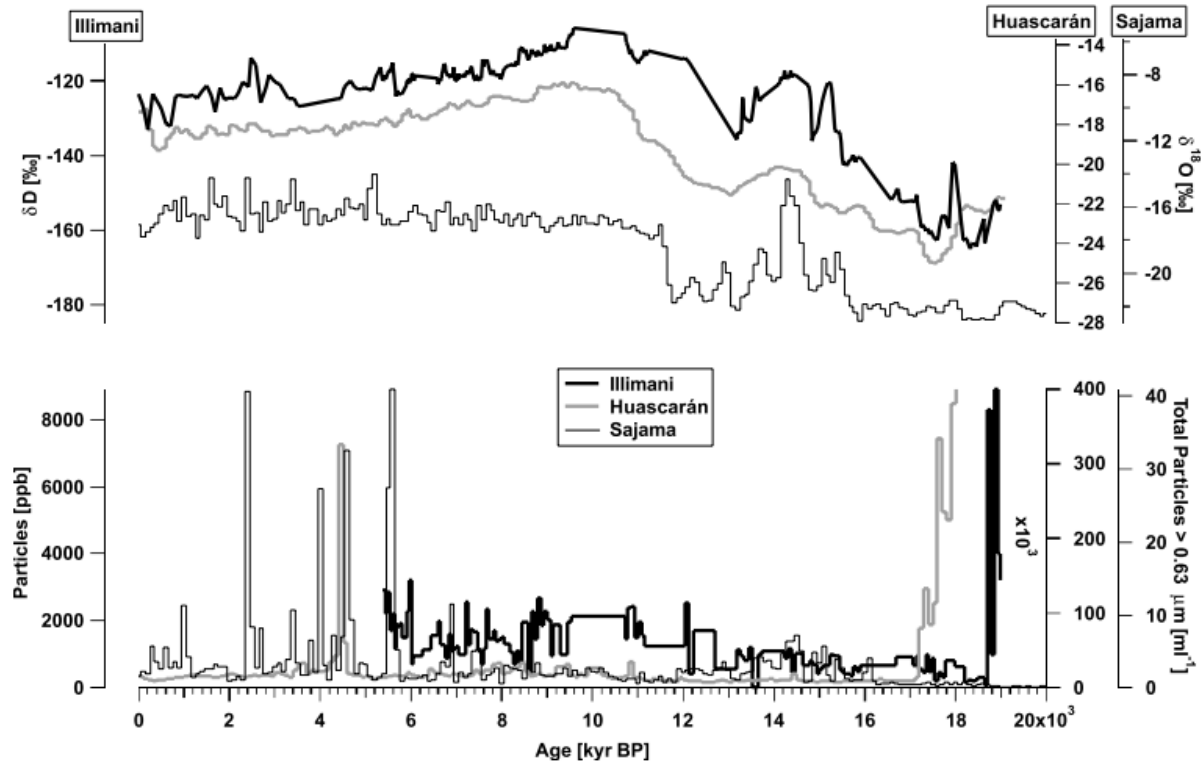


Figura 2.2: Comparação entre os registros dos testemunhos de gelo Illimani, Huascarán e Sajama ao longo dos últimos ~20 ka. (a) Os registros isotópicos (δD e $\delta^{18}\text{O}$); (b) As concentrações de poeira. Extraído de Ramirez *et al.* (2003).

Outro parâmetro observado nos testemunhos de gelo dos Andes Centrais durante a transição do UGM para o Holoceno foi a concentração de poeira (Figura 2.2b), que registrou um aumento em 8x no Sajama (Thompson *et al.*, 1998) e de 2,5x no Illimani (Ramirez *et al.*, 2003). Esse aumento durante períodos mais quentes é contrário à tendência esperada sob uma perspectiva global, expressa por testemunhos de gelo extraídos nas regiões polares, na qual o ciclo da poeira é reduzido durante períodos quentes (Maher *et al.*, 2010). Tal comportamento nos Andes Centrais foi atribuído às condições locais, onde as temperaturas mais elevadas do Holoceno geraram um aumento na altitude da linha de equilíbrio das geleiras da região (Thompson *et al.*, 1998; Ramirez *et al.*, 2003), ou seja, houve aumento da área de ablação das geleiras. Com isso, foi exposta uma maior superfície de solo com alto potencial de ter micropartículas suspensas pelo vento, aumentando a concentração de poeira na atmosfera.

2.2 O Holoceno

O Holoceno na América do Sul tropical, de acordo com os registros dos testemunhos de gelo dos Andes Centrais, apresentou uma elevada variabilidade climática. Episódios como o Younger Dryas (há 8 ka), o Ótimo Climático do Holoceno (de 7 a 3 ka atrás), a Anomalia Climática Medieval (entre os séculos X e XIV) e a Pequena Idade do Gelo ou *Little Ice Age* (LIA, entre os séculos XV e XVIII) foram detectados no Illimani a partir de aerossóis de amônio (subproduto da atividade biológica no solo e na vegetação) e também, a partir do carbono negro ou *Black Carbon* (BC, resultante de processos de combustão). Essas espécies são transportados em maior quantidade para o Nevado Illimani nos períodos de temperatura mais elevada na bacia Amazônica (principal fonte dessas espécies) (Kellerhals *et al.*, 2010; Osmont *et al.*, 2019). Além do Nevado Illimani, a LIA é bem marcada nos testemunhos Quelccaya e Huascarán. Menores razões de $\delta^{18}\text{O}$ e poeira no Huascarán durante a LIA sugerem condições mais úmidas nos Andes Centrais, resultantes de uma possível intensificação da Monção Sul Americana (Capítulo 3.1), gerando uma maior atividade convectiva ao longo da trajetória das massas de ar que atingem os Andes Centrais e portanto, um sinal de $\delta^{18}\text{O}$ mais depletado (Vimeux *et al.*, 2009). O registro do Quelccaya durante a LIA indica uma migração para o sul da Zona de Convergência Intertropical, resultando em condições mais úmidas no sudoeste da bacia Amazônica (Thompson *et al.*, 2013). Tal conclusão teve como base uma correlação positiva entre concentrações de amônio e o parâmetro climático água precipitável na porção sudoeste da Amazônia durante o século XX.

Além de fatores climáticos, os testemunhos de gelo dos Andes Centrais registram 2700 anos de atividade antrópica na América do Sul, observados a partir das concentrações de cobre e chumbo no Illimani (Eichler *et al.*, 2015; Eichler *et al.*, 2017). A partir de 1540 (início do período colonial), aproximadamente, a concentração de metais no Quelccaya indica evidente e contínuo sinal antrópico, marcando a introdução do processo de amalgamação para a extração da prata (Uglietti *et al.*, 2015). Mudanças no uso da terra impostas durante o período colonial também estão registradas nas camadas de gelo dos Andes Centrais a partir de

significativas alterações nos tipos de pólen depositados no Illimani, principalmente a partir do século XVIII (Brugger *et al.*, 2019).

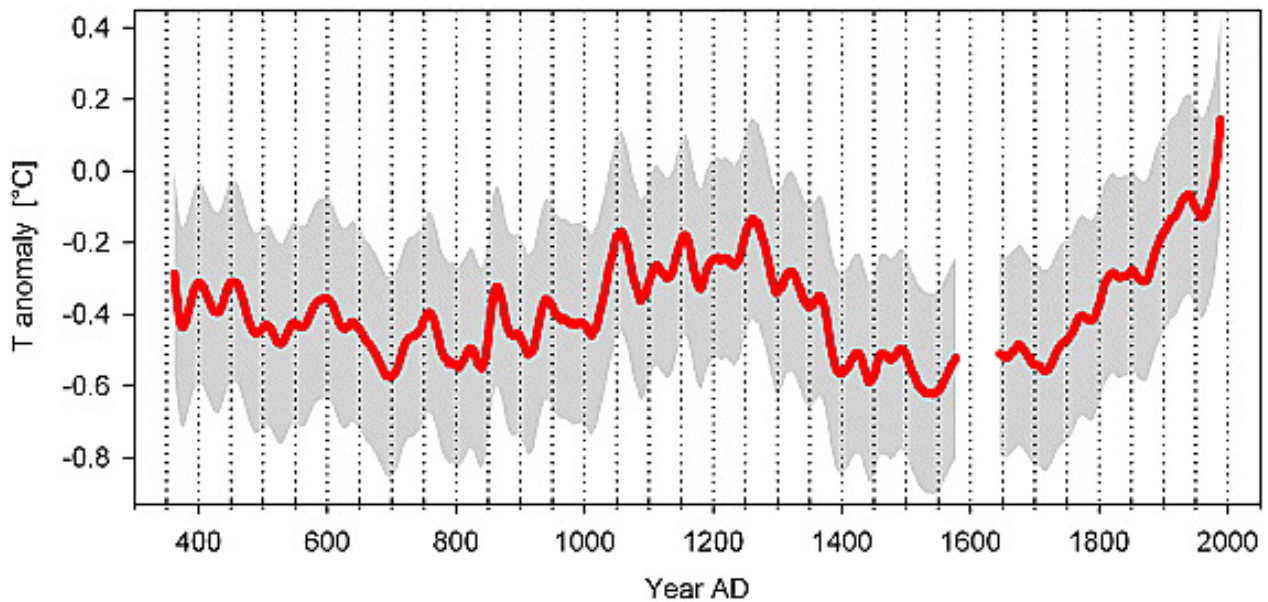


Figura 2.3: Reconstrução da variabilidade da temperatura durante o Holoceno a partir do registro de amônio no testemunho de gelo do Illimani. Fonte: Kellerhals *et al.* (2010).

2.3 O último século

Os testemunhos de gelo Illimani, Quelccaya e Sajama mostram concentrações sem precedentes nos elementos associados à mineração ao longo do último século (Hong *et al.*, 2004; Eichler *et al.*, 2015; Ugliesti *et al.*, 2015; Eichler *et al.*, 2017). O chumbo, por sua vez, tem máxima concentração devido ao uso da gasolina contendo chumbo, com pico no consumo durante os anos 1970. Porém, elementos associados à queima de combustível fóssil (nitrato e partículas carbonáceas esféricas) continuam mostrando tendência crescente (Eichler *et al.*, 2015; Brugger *et al.*, 2019). As concentrações atuais de *black carbon* assemelham-se às registradas durante a Anomalia Climática Medieval, entretanto uma tendência de aumento está em curso desde 1730, em decorrência do aumento das temperaturas e do desmatamento na bacia Amazônica (Osmont *et al.*, 2019).

Os registros atuais possibilitam, ainda, uma validação dos parâmetros obtidos nos testemunhos de gelo frente a observações meteorológicas, a reanálises climáticas e a imagens de satélite. Essa validação é fundamental para a interpretação dos testemunhos de gelo durante períodos pretéritos com escassa informação climática. Conforme discutido na Seção 2.1, a comparação do registro isotópico nos 4 testemunhos de gelo dos Andes Centrais durante o século XX (Índice Isotópico Andino, IIA), com modelos de circulação atmosférica e com dados meteorológicos indica que tais registros são basicamente controlados pela variabilidade da precipitação na bacia Amazônica (Hoffman *et al.*, 2003). O IIA reflete ainda a reorganização oceânica atmosférica de larga escala ocorrida no Oceano Pacífico durante a década de 1970 (Figura 2.4), com consequências à variabilidade na temperatura e na precipitação nos Andes Centrais, acelerando o degelo nessa região (Francou *et al.*, 2003). A influência do Pacífico expressa em eventos El Niño persistentes foi observada pelo aumento na concentração das espécies iônicas associadas à poeira no Illimani (Knüsel *et al.*, 2005). Segundo esses autores, durante tais eventos há a intensificação de ventos oeste sobre os Andes Centrais, impedindo a entrada de umidade da bacia Amazônica e portanto, favorecendo o maior transporte e deposição de poeira no Illimani. Registros em alta resolução temporal da composição das impurezas depositadas no Illimani mostram o predomínio da poeira oriunda dos Andes Centrais (principalmente no inverno) durante o século XX (Correia *et al.*, 2003; Knüsel *et al.*, 2005). Assim, há uma ofuscamento dos sinais vindos da bacia Amazônica (geralmente associados à queima de biomassa) durante os meses de inverno (Correia *et al.*, 2003).

Testemunhos de *firn* (testemunhos rasos que não atingem as densas camadas de gelo) referentes às últimas décadas permitiram comparar o sinal isotópico do Quelccaya e do Huascarán com dados atmosféricos de alta resolução espacial. Correlações significativas entre o $\delta^{18}\text{O}$ e a temperatura no topo de nuvens convectivas sugerem uma relação entre a razão isotópica na precipitação nas geleiras dos Andes Centrais e a temperatura durante a condensação sobre o norte da bacia Amazônica e ao longo da face leste dos Andes Centrais (Thompson *et al.*, 2017). Tal relação espacial foi reforçada pela observação de que o $\delta^{18}\text{O}$ é mais depletado quando os jatos de baixos níveis na bacia Amazônica logo à leste dos Andes Centrais são mais intensos e há mais umidade sobre o Quelccaya (Guy *et al.*, 2019). Ainda, a comparação da variabilidade do $\delta^{18}\text{O}$ e da acumulação de neve em

um testemunho raso Quelccaya com medidas atmosféricas locais mostra as relações entre o sinal isotópico e a incursão de massas de ar frio sobre os Andes Centrais (Hurley *et al.*, 2015; Hurley *et al.*, 2016).

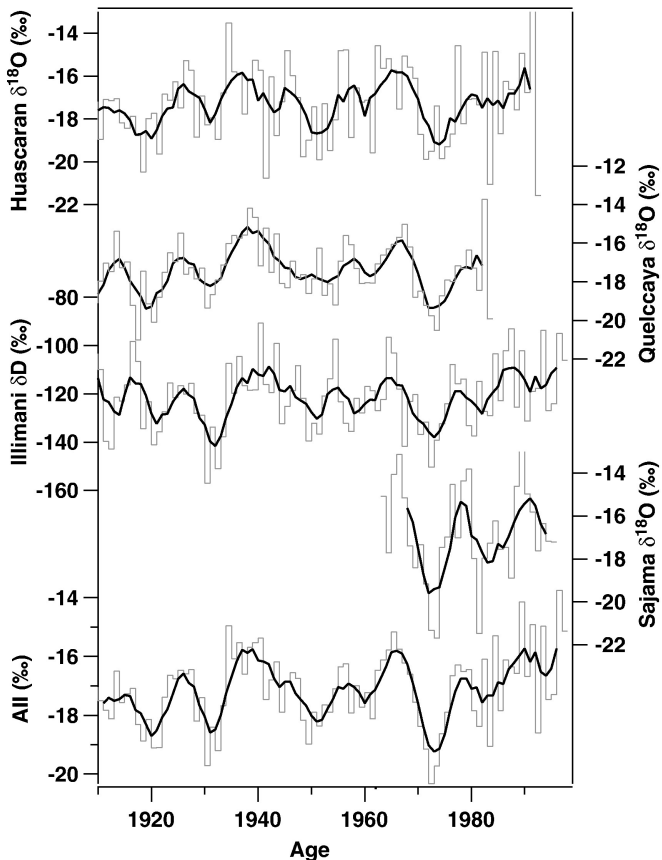


Figura 2.4: Comparação do registro isotópico nos testemunhos de gelo Huascarán, Quelccaya, Illimani e Sajama durante o século XX. AII representa a variabilidade comum entre os perfis dos quatro testemunhos (Índice Isotópico Andino). Extraído de Vimeux *et al.* (2009).

Testemunhos rasos permitem, portanto, a calibração de parâmetros analisados no *firn* frente a uma complexa rede de interações atmosféricas, o que possibilita o aperfeiçoamento de modelos paleoclimáticos. Entretanto, o intenso aquecimento atmosférico em curso nas geleiras dos Andes Centrais gera derretimento e percolação no *firn*, ameaçando o seu registro ambiental. Em consequência, o sinal isotópico recente no Quelccaya já sofreu atenuação, embora camadas de poeira ainda preservem uma sazonalidade (Thompson *et al.*, 2017).

3 Área de estudo

O Nevado Illimani ($16^{\circ}38'S$; $67^{\circ}44'W$, Bolívia) está localizado na Cordilheira Real, distante 50 km da cidade de La Paz. Ele apresenta dimensões aproximadas de 10 por 4 km e alguns picos ultrapassam os 6000 m anm. O Nevado Illimani é formado por um pluton granodiorítico do Oligoceno tardio, com um pequeno cinturão composto por um fluxo dacítico, contemporâneo à formação do pluton e localizado próximo a sua borda sudoeste (McBride *et al.*, 1983; Jiménez e López-Velásques, 2008).

3.1 Aspectos climáticos

Os Andes Centrais formam uma barreira climática entre as condições contrastantes da bacia Amazônica e do Oceano Pacífico. O transporte de massas de ar úmido dessa bacia até os Andes Centrais ocorre majoritariamente nos meses de verão do hemisfério sul, favorecido pela fase madura da Monção Sul Americana (Zhou & Lau, 1998; Vera *et al.*, 2006). Uma das principais características da Monção Sul Americana é a formação da Alta da Bolívia (Figura 3.1), um sistema anticiclônico na alta troposfera posicionado sobre a Bolívia (Lenters & Cook, 1997). Quando esse sistema está bem desenvolvido, ventos leste na baixa troposfera da bacia Amazônica são intensificados e massas de ar úmido atravessam de forma turbulenta a Cordilheira Oriental, ocasionando precipitação na forma de convecção profunda nos Andes Centrais (Garreaud, 1999). Essa circulação sobre a bacia Amazônica é definida como Jatos de Baixos Níveis da América do Sul (JBN). Esses jatos são responsáveis por distribuir uma vasta quantidade de umidade gerada no oceano Atlântico e/ou Amazônia para a Bolívia, Paraguai, sul do Brasil e norte da Argentina, também ocorrendo em outras estações do ano (Marengo *et al.*, 2004). Durante o inverno, porém, a precipitação nos Andes Centrais é muito escassa, devido à advecção de ar seco do Pacífico que é favorecida por uma circulação predominantemente de oeste, resultante da expansão da zona dos jatos subtropicais para o norte (Vuille, 1999).

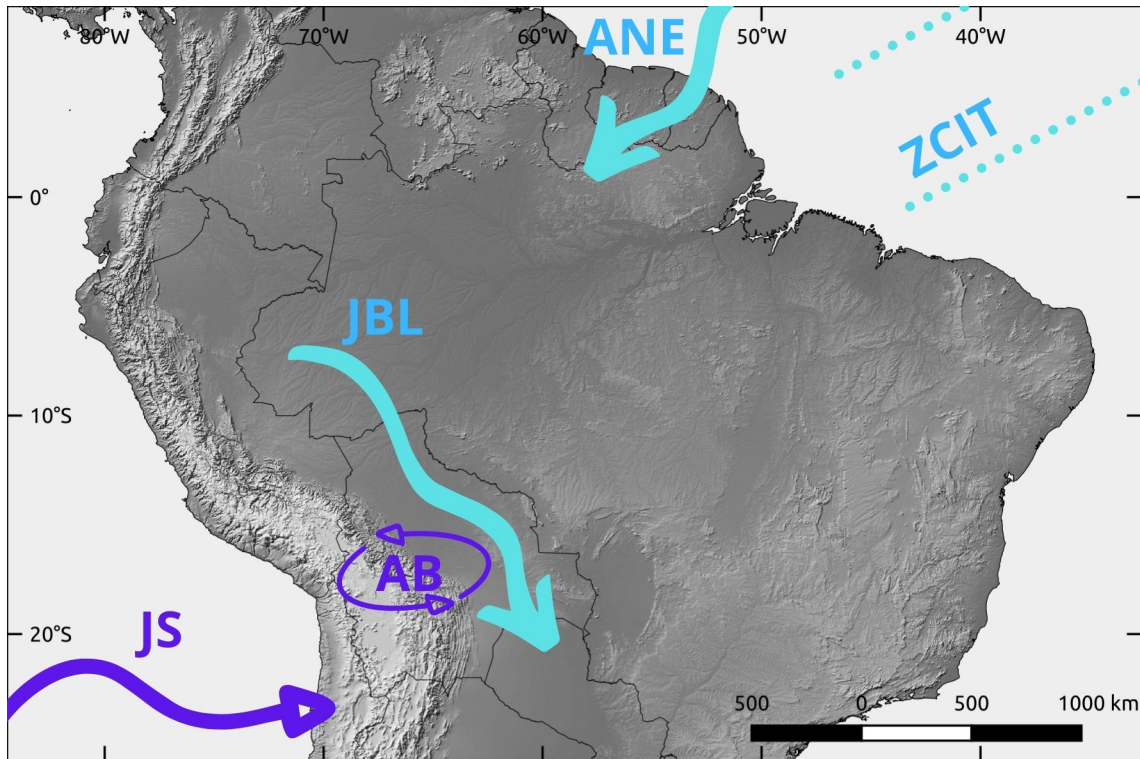


Figura 3.1: Representação esquemática dos sistemas atmosféricos, comentados no texto, na baixa troposfera (azul claro) e na alta troposfera (roxo) atuantes na América do Sul. Em relação à baixa troposfera tem-se os Ventos Alísios de Nordeste (ANE), os Jatos de Baixos Níveis (JBN) e a Zona de Convergência Intertropical (ZCIT). Em relação à alta troposfera tem-se a Alta da Bolívia (AB) e o Jato Subtropical (JS).

A variabilidade interanual da precipitação nos Andes Centrais é portanto influenciada pelas condições no oceano Pacífico tropical, controladas principalmente pelo fenômeno El Niño–Oscilação Sul (ENOS). Fases positivas do ENOS promovem o aquecimento da troposfera tropical, aumentando o fluxo de ar no sentido oeste sobre os Andes Centrais, o que inibe a advecção de ar úmido vindo da bacia Amazônica (Garreaud & Aceituno, 2001). O inverso se aplica às fases negativas do ENOS. Porém, desde o início do século XXI, o oceano Atlântico passou a ter um papel mais relevante na variabilidade interanual da precipitação sobre os Andes Centrais (Segura *et al.*, 2020). O aumento das temperaturas na superfície do Atlântico tropical norte durante as últimas décadas mudou o posicionamento da Zona de Convergência Intertropical (ZCIT) (Yoon & Zeng, 2010). A ZCIT deslocou-se para o norte, diminuindo a intensidade dos ventos alísios que levam umidade do Atlântico para o sudoeste da bacia Amazônica (Espinoza *et al.*, 2019). A redução na precipitação por convecção nessa parte da região Amazônica diminui o transporte de umidade para os Andes Centrais (Segura *et al.*, 2020). Houve ainda o deslocamento

dos JBN, que ao longo dos últimos anos vêm se encontrando com a Cordilheira mais ao norte, além de mostrarem um aumento na sua frequência e intensidade, favorecendo a precipitação na Cordilheira Oriental Boliviana (Jones, 2019), portanto sobre o Nevado Illimani.

A precipitação sobre o Nevado Illimani ao longo do ano é distribuída durante 9 meses (Vimeux *et al.*, 2009). Há uma distinção bem marcada entre a estação seca (abril a agosto, inverno austral) e a estação úmida (novembro a março, verão austral). Esses dois períodos são separados por uma transição abrupta entre março e abril e condições intermediárias em setembro e outubro (Vimeux *et al.*, 2005).

O acentuado aquecimento troposférico nas últimas décadas é um tema especialmente relevante em regiões de geleiras como os Andes Centrais. A evolução da temperatura do ar no Nevado Illimani a 6350 m anm foi estimada a partir das camadas de neve e gelo (Gilbert *et al.*, 2010). Esses autores quantificaram um aumento de $1,1 \pm 0,2^{\circ}\text{C}$ durante o século XX. Campanhas realizadas nesse sítio entre 1999 e 2001 mediram temperaturas abaixo dos -10°C entre maio e junho (Wagnon *et al.*, 2003). Seguindo estimativas do aquecimento global, essa região do Nevado Illimani poderia tornar-se temperada entre 2050 e 2060 (Gilbert *et al.*, 2010).

3.2 Aspectos glaciológicos

Entre os anos de 1956 e 2009, o Nevado Illimani perdeu 35% (aproximadamente $9,5 \text{ km}^2$) de sua área total de gelo, permanecendo com uma superfície de $17,9 \text{ km}^2$ (Figura 3.3; Ribeiro *et al.*, 2013). De fato, um generalizado e rápido recuo das geleiras bolivianas ocorreu a partir dos anos 1980, de maneira sem precedentes desde a Pequena Idade do Gelo (entre a metade do século XVII e o início do século XVIII) (Rabatel *et al.*, 2013). Na geleira Chacaltaya ($16^{\circ}20'\text{S}$, $68^{\circ}07'\text{O}$, 5.400 m anm) o período 1983–1998 foi marcado por um recuo tão drástico que acarretou no seu completo derretimento (Ramirez *et al.*, 2001). Esse acelerado recuo em Chacaltaya foi atribuído, além do aquecimento troposférico, a uma alteração na evolução de eventos El Niño, incluindo sua maior frequência e intensidade (Francou *et al.*, 2003). Em 2005, um forte balanço de massa negativo (ablação muito maior do que a acumulação) foi observado na geleira Zongo

($16^{\circ}15'S$, $68^{\circ}10'W$, 6.000 m anm) devido a condições áridas resultantes do acentuado aquecimento do Atlântico tropical norte naquele ano (Ribeiro *et al.*, 2018). Durante o século XXI o recuo das geleiras dos Andes Centrais continua acentuado, estima-se um balanço de massa negativo de $-0,42 \pm 0,24$ m de equivalentes em água por ano (Dussaillant *et al.*, 2019).

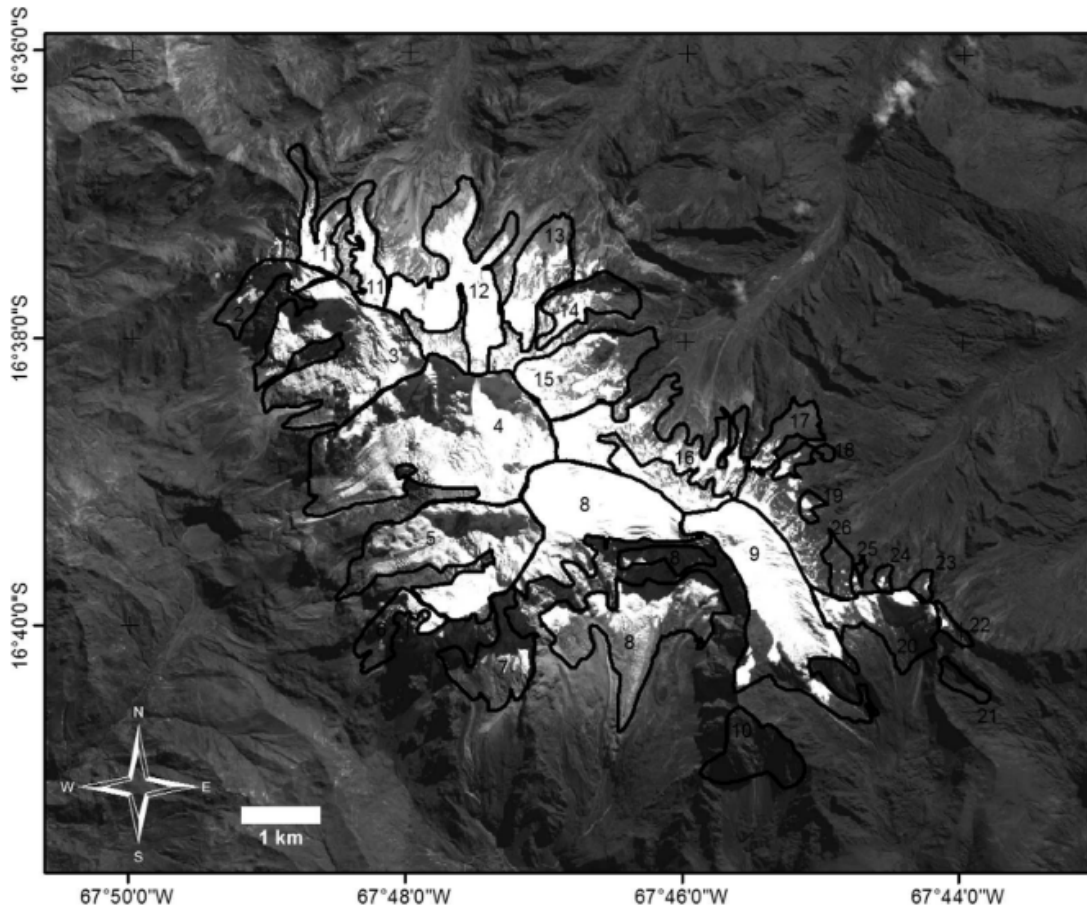


Figura 3.2: Imagem de satélite de 2009 do Nevado Illimani, incluindo a subdivisão em bacias de drenagem glacial (indicada pelos números). O traçado delimita a extensão das geleiras em 1963. Fonte: Ribeiro *et al.* (2013).

3.3 Expedições ao Nevado Illimani

Duas expedições ao Nevado Illimani extraíram testemunhos de gelo na altitude de 6350 m anm atingindo o embasamento rochoso. A primeira ocorreu em junho de 1999 envolvendo pesquisadores do *Institut de Recherche pour le Developpement* (IRD, França) e do Instituto Paul Scherrer (PSI, Suíça). Foram extraídos 2

testemunhos que atingiram a profundidades de 137 e 139 m. Em junho de 2017 realizou-se a expedição do projeto Ice Memory (<https://www.ice-memory.org>), coordenada por um grupo de pesquisadores da França e com participação de pesquisadores da Rússia, Bolívia e Brasil. Foram extraídos dois testemunhos de gelo (136 e 134 m de profundidade) e um testemunho de *firn* com 24 m de profundidade (alvo deste estudo). Nessa expedição, 4,5 toneladas de equipamento, distribuídas em três acampamentos, foram transportadas por 61 carregadores do vilarejo de Pinaya (Bolívia) e por 16 carregadores de alta altitude, coordenados por 3 guias de montanha.

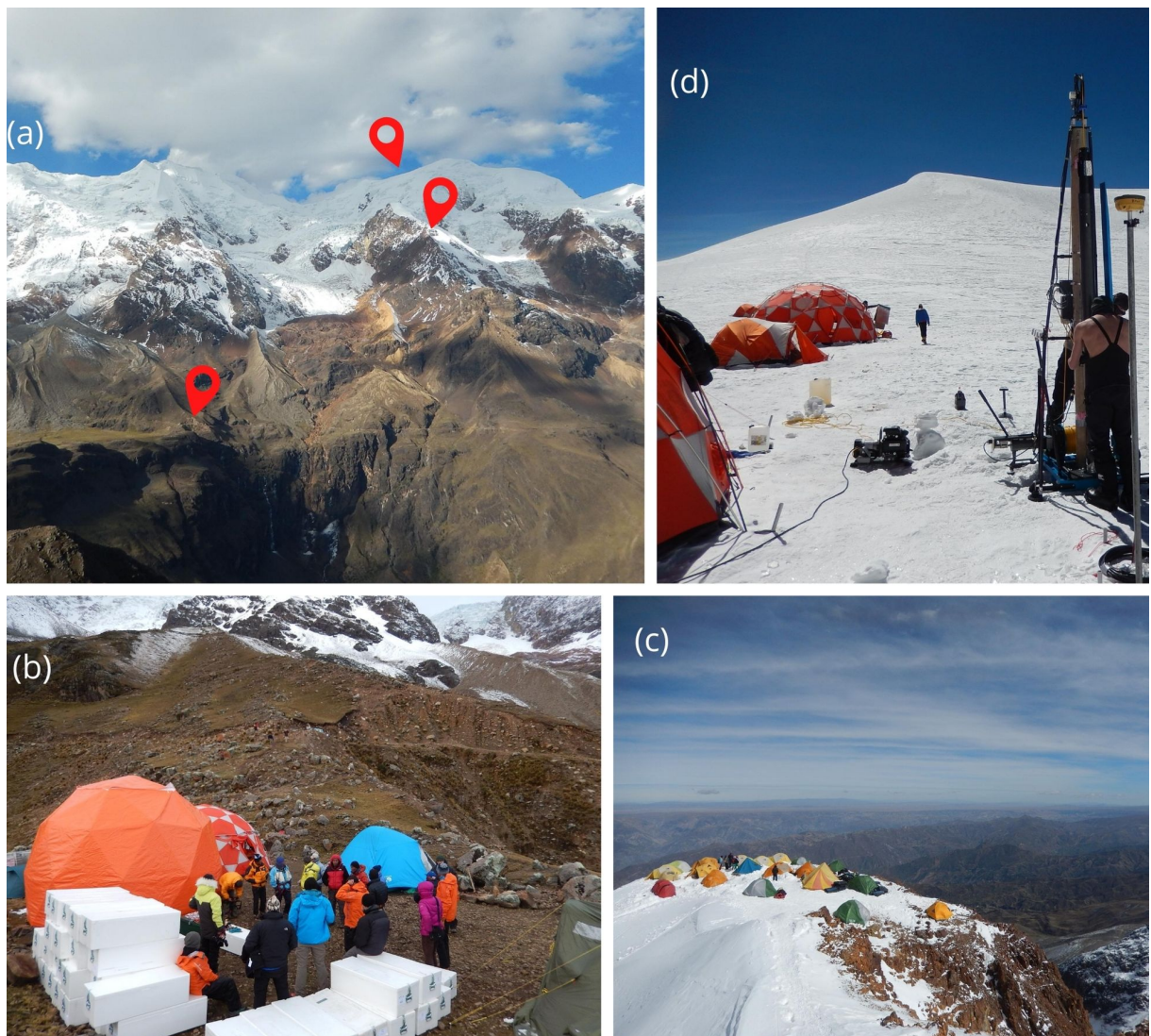


Figura 3.3: A expedição Ice Memory de 2017: (a) foto do Nevado Illimani indicando a posição dos três acampamentos montados; (b) acampamento base (4500 m anm); (c) acampamento intermediário (5500 m anm); (d) acampamento da perfuração (6350 m anm).

4 Metodologia

4.1 Coleta do testemunho de *firn*

Um testemunho de neve e *firn* com 23,8 m de comprimento e diâmetro de 10 cm foi extraído durante a expedição Ice Memory ao Nevado Illimani ocorrida em 2017 na altitude de 6.350 m anm. A perfuração ocorreu no mesmo local onde foram extraídos os testemunhos profundos da expedição de 1999, ou seja, na região de sela entre os dois cumes mais elevados (Fig. 4.1a).

Utilizou-se a perfuradora eletromecânica modelo EM-100-1000 produzida pela *Cryosphere Research Solutions* (Columbus, OH, EUA) composta por um motor submersível com sistema anti-torque ajustável, conectado a um barril (para coleta do testemunho) de 110 cm de comprimento (Fig. 4.1b). Os cortadores eram adaptados à perfuração de gelo temperado (*i.e.*, gelo perto do ponto de fusão sob pressão) em sua base. As partes mais pesadas do sistema de perfuração eram o tambor do cabo com 22 kg e a caixa de engrenagens do motor com 23 kg, o que ainda era adequado para ser transportado pelos carregadores até o local da perfuração.

O testemunho extraído (identificado como IL2017) era composto por 24 seções, com no máximo 3 quebras por seção e comprimento aproximado de 1 m. Após a medida da profundidade de cada quebra, as seções eram acondicionadas em tubos plásticos onde eram identificados o número da seção e a extremidade referente ao topo. Em seguida, esse material era colocado dentro dos cilindros de transporte e estocados em um abrigo escavado na neve (Fig. 4.1c). No final de cada dia de perfuração cada um dos 16 carregadores de alta altitude transportavam 3 cilindros até o acampamento intermediário (Fig. 4.1d). No período da noite, a outra equipe de carregadores transportava os cilindros do acampamento intermediário até o acampamento base, onde os testemunhos eram colocados dentro de caixas de isopor que eram transportadas por um veículo 4 x 4 que partia diariamente às 6h da manhã até um contêiner frigorífico na cidade de La Paz.



Figura 4.1: (a) local da perfuração apontado por P. Ginot (foto de X. Fain); (b) a perfuradora operada por L. Piard e S. Kutuzov; (c) estoque dos cilindros preenchidos com amostras; (d) transporte dos cilindros do local de perfuração até o acampamento intermediário (foto de X. Fain).

4.2 Processamento do testemunho

A Figura 4.2 apresenta um fluxograma com as etapas do processamento do testemunho de *firn* IL2017.

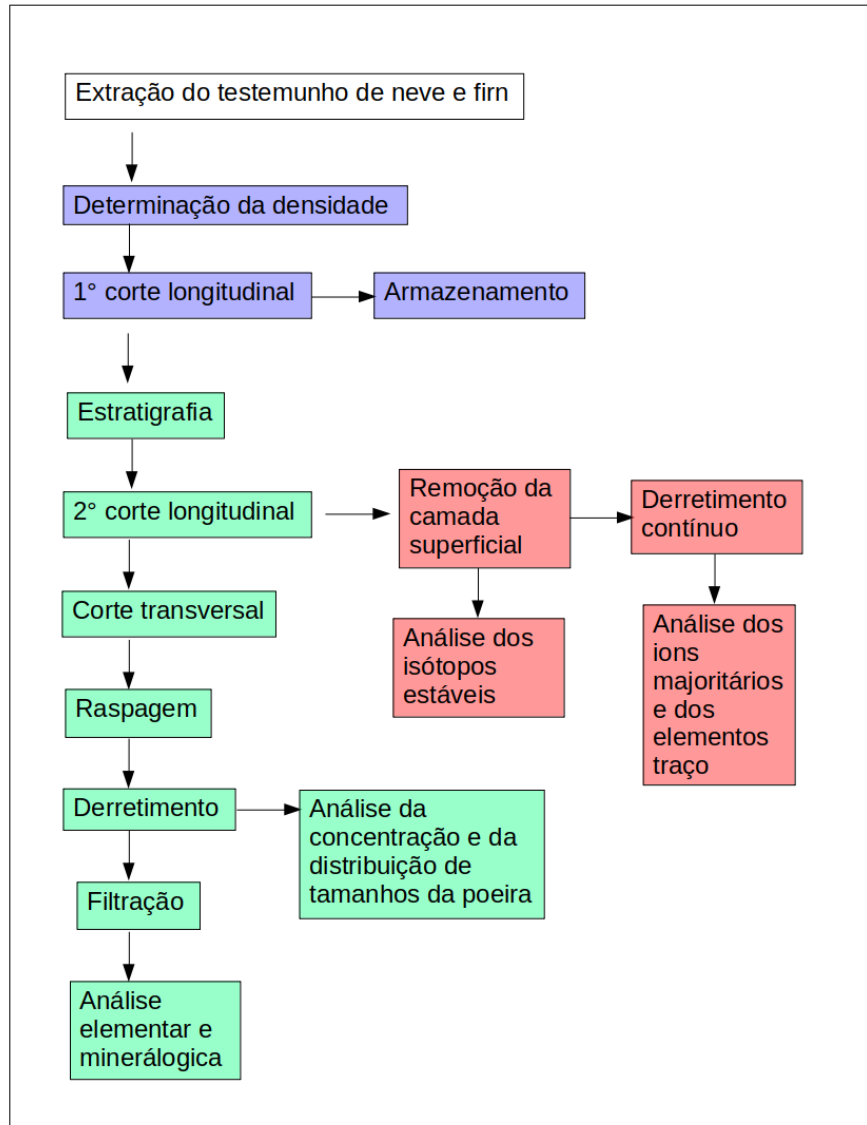


Figura 4.2: Fluxograma dos processos aplicados ao testemunho de neve e *firn* do Nevado Illimani. As cores indicam os laboratórios envolvidos: *Institut des Géosciences de l'Environnement*, Universidade Grenoble-Alpes, França (azul); EuroCold, Universidade Milano-Bicocca, Itália (verde); *Climate Change Institute*, Universidade do Maine, EUA (vermelho).

O contêiner frigorífico com os testemunhos de gelo foi transportado por navio, do porto de Arica (Chile) até a Europa, chegando em Grenoble (França) em agosto de 2017, onde permaneceu à temperatura de -20°C no interior de um frigorífico comercial.

Em dezembro de 2017, as quatro caixas com as 24 seções do testemunho foram levadas até as câmaras frias do *Institut des Géosciences de l'Environment* (IGE, Universidade Grenoble-Alpes) mantidas a -20°C, onde as seções foram pesadas para determinação do perfil de densidades. Após, o testemunho foi cortado

longitudinalmente ao meio com uma serra de fita vertical de bancada. Assim as duas metades resultantes mantinham toda a estratigrafia do testemunho original. A Figura 4.3 resume a subdivisão do testemunho. Metade do testemunho permaneceu em Grenoble e a outra metade foi transportada para Milão (Itália) em furgão refrigerado a -15°C, onde foi armazenado a -30°C na câmara fria do Eurocold (Universidade Milano-Bicocca).

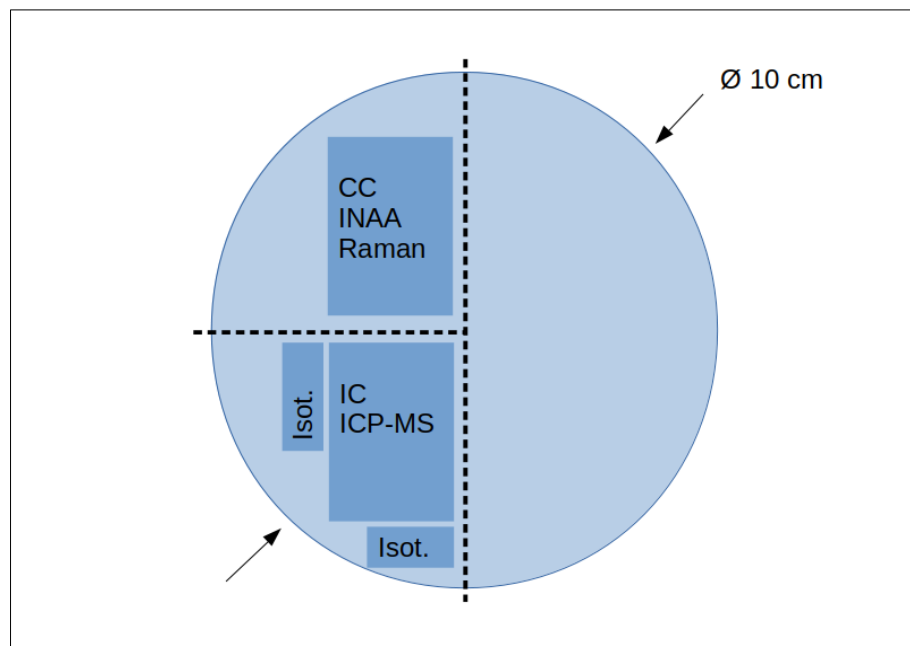


Figura 4.3: Seção transversal do testemunho de 10 cm de diâmetro indicando as frações (proporções aproximadas) destinadas às análises realizadas neste estudo. As linhas pontilhadas representam os cortes longitudinais.

A estratigrafia do testemunho foi determinada pela identificação da espessura e profundidade das camadas de gelo presentes na matriz de neve e *firn* (Fig. 4.4a). Em seguida as seções foram mais uma vez cortadas longitudinalmente ao meio com serra de fita vertical de bancada (Fig. 4.4b). Um quarto do testemunho original foi disposto em uma caixa de isopor e transportado por via aérea para o *Climate Change Institute* (CCI), Universidade do Maine, EUA, para determinação das concentrações dos íons majoritários, dos elementos-traço e das razões dos isótopos estáveis da água.



Figura 4.4: (a) estratigrafia sob luz, as linhas mais claras são lentes de gelo; (b) o segundo corte longitudinal do testemunho; (c) o corte transversal a cada 5 cm gerando às frações destinadas à análise da poeira.

4.3 Análise da Poeira

A metade remanescente no Eurocold foi cortada transversalmente na resolução de aproximadamente 5 cm (Fig. 4.4c) com serra de fita horizontal de bancada, resultando na divisão dos 23,8 m totais do testemunho em 464 amostras. Os milímetros mais superficiais das faces e arestas dessas amostras foram removidos por raspagem com faca cerâmica no interior de mesa de fluxo laminar classe ISO 5 instalada dentro de uma câmara fria limpa classe ISO 6 (Fig. 4.5a).

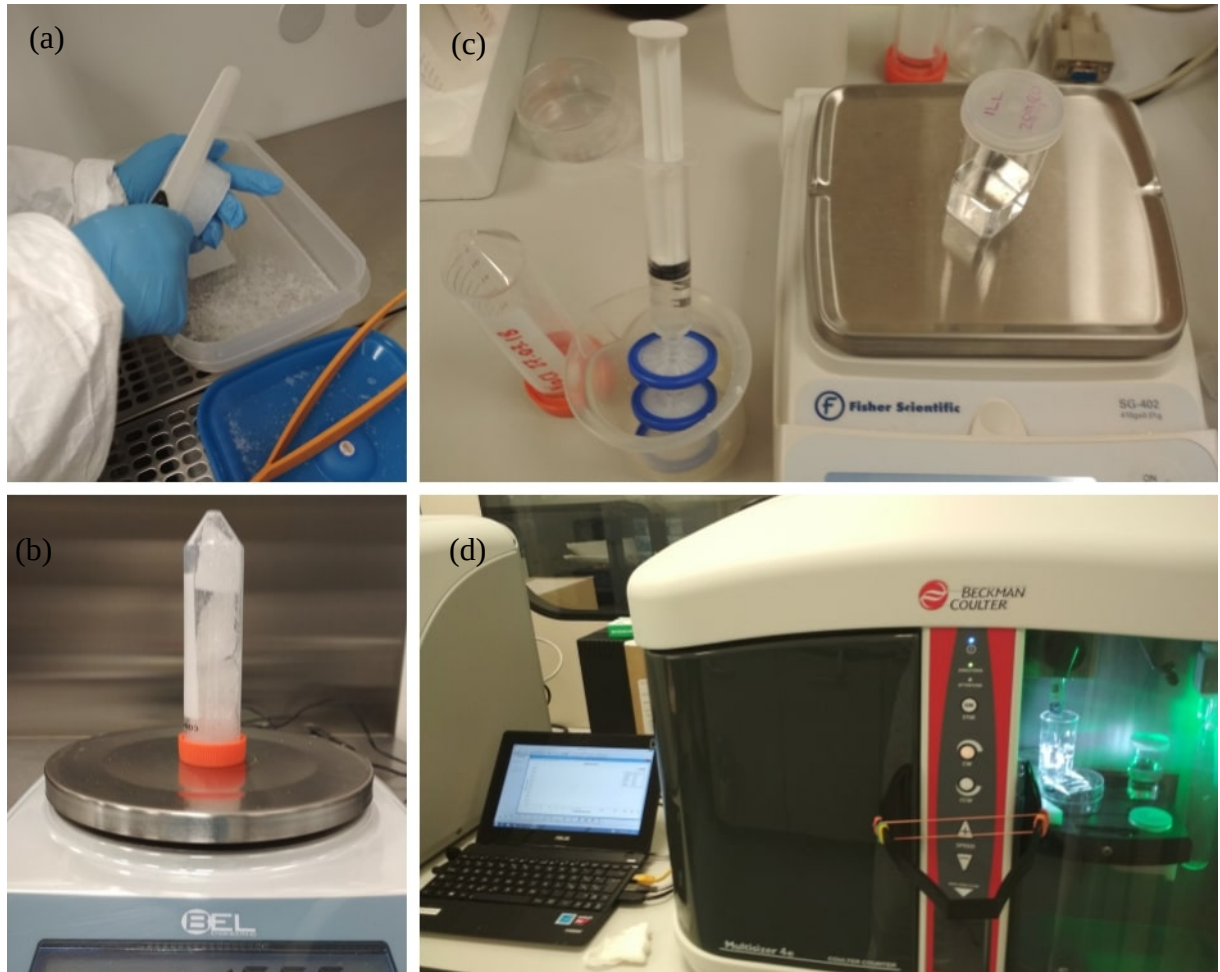


Figura 4.5: (a) raspagem para descontaminação das subamostras; (b) pesagem para controle do volume obtido após a raspagem; (c) produção da solução eletrolítica; (d) determinação da concentração e da distribuição de tamanhos das partículas na solução.

O procedimento de raspagem visava a remoção da possível contaminação da matriz porosa de *firn* gerada desde o contato com a perfuradora até o contato com as lâminas de aço da atmosfera não limpa das câmaras frias. Após a raspagem de cada amostra, o material utilizado era limpo com etanol com grau de pureza em nível analítico antes de ser utilizado novamente na descontaminação da próxima amostra.

As amostras descontaminadas eram acondicionadas em frascos limpos de 50 mL e pesadas para fins de controle do procedimento (Fig. 4.5b). A massa média das amostras após a raspagem era de 18 g. Os frascos com as amostras permaneceram armazenados a -30°C até horas antes do momento da análise.

4.3.1 Concentração e distribuição de tamanhos

As amostras foram derretidas a temperatura ambiente (aproximadamente 20°C) em laboratório limpo classe ISO 6 e separadas em duas alíquotas em mesa de fluxo laminar classe ISO 5: uma com volume médio de 10 mL colocada em frasco limpo de 25 mL modelo Accuvette Beckman Coulter, o restante permanecia no frasco de 50 mL para posterior análise elementar ou mineralógica.

As alíquotas de 10 mL separadas para análise da distribuição de tamanhos das micropartículas eram transformadas em soluções eletrolíticas pela adição de uma solução previamente filtrada de NaCl 20% resultando na concentração final de 1% (Fig. 4.5c). Até o momento das análises, as soluções de amostras permaneciam em constante agitação mecânica pela ação de um agitador orbital com o objetivo de evitar a sedimentação das partículas nos frascos. Os procedimentos adotados seguiram os protocolos para amostras de gelo da Antártica (Delmonte *et al.*, 2002).

O contador de partículas modelo Beckman Coulter Multisizer 4 (Fig. 4.5d) equipado com um orifício de 100 µm permitiu medidas de equivalentes esféricos das partículas com diâmetros entre 2 e 60 µm divididas em 400 intervalos de diâmetros. A calibração foi realizada com uma solução certificada composta por partículas esféricas de látex com 10 µm de diâmetro.

Os brancos, que eram compostos por água ultrapura Millipore Q-POD® Element e pela solução eletrolítica, eram medidos no início de cada turno de análise (composto em média pela análise de 30 amostras). Eles representavam em média uma fração menor do que 0,5% das concentrações das amostras. A razão média entre sinal e ruído foi de 97. Cada amostra foi medida duas vezes (cada medida utilizava um volume de 0,5 mL). O desvio padrão médio entre as duas medidas, em função do intervalo de tamanho das partículas, está indicado na Tabela 4.1.

Tabela 4.1: Diferença nas concentrações (em número de partículas) entre as duas medidas do contador em função do tamanho das partículas, expressa pelo desvio padrão relativo.

	2–20 (µm)	2–60 (µm)	10–20 (µm)	20–60 (µm)
Desvio padrão relativo (%)	5,4	6,6	25,0	45,0

4.3.2 Composição elementar

A composição elementar da poeira foi analisada em 10 amostras extraídas de diferentes intervalos de profundidades distribuídos ao longo do testemunho (Tabela 4.2). Nessas amostras foram usadas as frações remanescentes (em que não foram adicionadas a solução eletrolítica) das amostras medidas no contador de partículas. Das 10 amostras, cinco foram extraídas de intervalos de profundidades caracterizados por concentrações de poeira abaixo da média e as outras cinco pertencem a intervalos com concentrações acima da média. Portanto, o tamanho de cada intervalo não era constante.

Os procedimentos de preparação seguiram o protocolo para amostras de *firn* e gelo (Baccolo *et al.*, 2015). As amostras foram filtradas com membranas Millipore[®] de PTFE (tamanho de poro de 0,45 µm e 11,3 mm de diâmetro) que foram previamente deixados de molho em HNO₃ 5% (ultrapuro de dupla destilação) por 2 semanas em provetas também limpas com ácido nítrico e com renovação do banho ácido a cada 4 dias. O sistema de filtração acoplado a uma bomba de vácuo era dedicado exclusivamente à preparação de amostras de testemunhos de *firn* e gelo, a vidraria em contato com os filtros também foi limpa com HNO₃. Todo o material que passou pelo banho em HNO₃ foi lavado com água ultrapura MilliQ (Millipore[®]) em abundância momentos antes da filtração, para evitar que um ambiente ácido favorecesse a dissolução de partículas. Os filtros com amostras foram estocados e secos, em mesa de fluxo laminar ISO5, dentro de frascos de polietileno (volume de 1 mL) que passaram pelo mesmo tratamento ácido de limpeza. Além das membranas com amostras, foram preparados membranas de branco, em que foram filtrados 300 mL de água MilliQ.

Para possibilitar a quantificação dos elementos nas amostras foram usados os seguintes padrões de referência com concentrações certificadas: USGS AGV2 (composto de andesito moído), USGS BCR2 (basalto moído), NIST SRM 2709a (solo de San Joaquin) e NIST SRM 2710a (solo de Montana). Também foram preparadas soluções líquidas com concentrações conhecidas (na ordem de grandeza de ppm) para todos os elementos medidos, sendo que o procedimento utilizado para produção desses padrões de referência líquidos foram reproduzidos

na produção de um branco líquido. O branco relativo aos padrões certificados sólidos era composto do mesmo modelo de frasco em que os padrões eram colocados, porém vazio.

Tabela 4.2: Caracterização das amostras destinadas à análise elementar por ativação neutrônica.

Identificação da amostra	Profundidade do topo (m)	Profundidade da base (m)	Volume (mL)	Massa de partículas* (µg)
ILL1	1,67	2,31	86,4	241,5 ± 12,1
ILL2	2,31	3,78	181	107,8 ± 5,4
ILL3	5,57	7,02	123	164,5 ± 8,2
ILL4	8,67	8,97	25,5	230,7 ± 11,5
ILL5	10,56	11,66	116	95,6 ± 4,8
ILL6	13,60	13,69	22,0	441,3 ± 22,1
ILL7	13,69	14,78	106	257,2 ± 12,9
ILL8	19,10	19,25	19,3	194,5 ± 9,7
ILL9	20,29	20,48	32,1	172,8 ± 8,6
ILL10	21,41	22,50	100	68,6 ± 3,4

*Massa estimada a partir da concentração de partículas obtida pelo método Coulter Counter, assumindo partículas esféricas com densidade de 2,5 g cm⁻³ e incerteza de 5%.

As amostras, os brancos e os padrões de referência foram levados ao LENA (*Laboratorio Energia Nucleare Applicata*) da Universidade de Pavia (Itália), onde um reator modelo Triga Mark II de 250 kW está disponível para análises por ativação neutrônica (INAA). O reator apresenta diversos canais de diferentes especificações para introdução de amostras dentro de seu núcleo. Dois canais foram utilizados, o “Rabbit” com fluxo de nêutrons igual a $7,40 \pm 0,95 \times 10^{12} \text{ s}^{-1}\text{cm}^{-2}$ e o “Lazy Susan” cujo fluxo é de $2,40 \pm 0,24 \times 10^{12} \text{ s}^{-1}\text{cm}^{-2}$.

No canal “Rabbit” foram conduzidas irradiações de curto período para a determinação de elementos com baixo tempo de meia vida, enquanto que no canal “Lazy Susan” o período de irradiação era maior e foi utilizado para determinação de

elementos com maior tempo de meia vida (Tabela 4.3). As medidas dos espectros gama foram realizadas no LENA e no laboratório de radioatividade da Universidade Milano-Bicocca equipados com detectores de germânio de alta pureza HpGe (ORTEC, série GWL). Foram seguidos os procedimentos desenvolvidos para uma INAA com baixo ruído (Baccolo *et al.*, 2016). O cálculo para a determinação das concentrações está descrito no Anexo I.

Tabela 4.3: Características do processo de irradiação.

Material irradiado	Canal	Fluxo de Nêutrons ($s^{-1} \cdot cm^{-2}$)	Elementos Observados
Amostras, padrões de referência e brancos	Rabbit	$(7,40 \pm 0,95) \cdot 10^{12}$	Al, Mg, Mn, Si, Ti, V
Amostras, padrões de referência e brancos	Lazy Susan	$(2,40 \pm 0,24) \cdot 10^{12}$	As, Au, Ba, Ca, Ce, Co, Cs, Eu, Fe, Hf, K, La, Na, Nb, Nd, Rb, Sb, Sc, Sm, Ta, Th, W, Yb, Zn, Zr

4.3.3 Composição mineralógica

A composição mineralógica das micropartículas foi analisada em 4 amostras escolhidas por critério análogo ao utilizado na escolha das amostras para determinação da composição elementar. Portanto, as amostras eram provenientes de diferentes intervalos de profundidade, apresentando concentrações acima ou abaixo da média. As quatro amostras utilizadas estão descritas na Tabela 4.4.

Tabela 4.4: Caracterização das amostras destinadas à análise mineralógica.

Amostra	Profundidade do topo (m)	Profundidade da base (m)	Número de partículas analisadas
ILL-R1	5,79	5,82	167
ILL-R2	5,91	6,00	161
ILL-R3	9,80	9,84	138
ILL-R4	10,00	10,17	157

O método de preparação das amostras descritas na Tabela 4.4 foi similar ao aplicado em amostras de gelo da Antártica (Delmonte *et al.*, 2017; Paleari *et al.*, 2019). Após filtração em membrana de policarbonato (tamanho de poro de 0,4 µm, diâmetro de 11,3 mm, Millipore[®]), as partículas remanescentes foram resuspensas em volume de aproximadamente 1 mL de água MiliQ por ultrassom. Essa suspensão de poeira foi em seguida depositada em uma lâmina de vidro (dimensões de 2,5 por 1,5 cm) através de gotículas, utilizando uma micropipeta (regulada para 200 µL). As gotículas foram lentamente evaporadas a temperaturas entre 60° e 90°C (Figura 4.6).



Figura 4.6: Preparação das amostras destinadas à análise mineralógica. Procedimento de evaporação das gotículas de suspensão de poeira.

Análises por microespectrometria Raman foram realizadas no *Laboratory for Provenance Studies* (DISAT, Universidade Milano-Bicocca). Utilizou-se o microscópio InViaTM-Renishaw, com linha de laser Renishaw Nd:YAG a 532 nm. A faixa espectrográfica analisada foi de 400 a 1060 nm. Realizou-se, para cada grão de poeira (menores do que 5 µm), 10 aquisições de 2 segundos. Os espectros foram obtidos com potência máxima na amostra de aproximadamente 10 mW. O diâmetro do feixe de laser era de aproximadamente 2 µm. A mineralogia de mais de 630 grãos foi identificada pela comparação com espectros de referência na literatura e, quando necessário, pela comparação com minerais de referência analisados no DISAT.

4.4 Análise dos isótopos estáveis

As seções, transportadas ao CCI por transporte aéreo refrigerado, tiveram suas camadas externas removidas com uma serra de fita vertical disposta em câmara fria a -20°C. Essas camadas mais externas foram subamostradas a cada ~12 cm com serra manual de aço inoxidável, resultando em 190 amostras para isótopos estáveis. Horas antes da determinação das razões de isotópicas, as amostras foram derretidas à temperatura ambiente.

A análise das razões de isótopos estáveis de hidrogênio (D/H) e de oxigênio ($^{18}\text{O}/^{16}\text{O}$) foram realizadas com espectrômetro a laser de cavidade ressonante modelo Picarro L-2130i, ligado a um vaporizador. Obteve-se a precisão de 0,1‰. As razões isotópicas foram expressas pela notação δ :

$$\delta D \text{ ou } \delta^{18}\text{O} = \left(\frac{R_{\text{amostra}}}{R_{\text{padrão}}} - 1 \right) * 1000 \quad (\text{Eq. 4.1})$$

onde R é a razão entre o isótopo de maior massa e o isótopo leve na amostra e no padrão. O $R_{\text{padrão}}$ refere-se ao padrão Vienna-Standard Mean Ocean Water (V-SMOW).

4.5 Análise das impurezas na matriz de neve e firn

As camadas mais internas passaram por um processo de raspagem com faca cerâmica de suas partes externas. Em seguida, cada uma das 24 seções do testemunho era acondicionada em um tubo acrílico, respeitando seu posicionamento estratigráfico original. Em sala limpa classe ISO 6 do CCI, o tubo acrílico contendo uma seção do testemunho era acoplado ao sistema de derretimento contínuo (Osterberg *et al.*, 2006), comumente utilizado na análise de testemunhos de gelo da Antártica (Schwanck, 2017). Nele as seções foram destinadas de forma contínua e simultânea para a análise dos íons majoritários e dos elementos traço.

O sistema de derretimento contínuo é composto por um cone e um disco de níquel 270, dispostos sobre uma base aquecida, tudo no interior de um freezer vertical (Figura 4.7). No centro do disco há um canal interno que capta somente a porção mais interna do testemunho (com menor probabilidade de estar contaminada). A água de degelo desse canal interno é bombeada por duas bombas peristálticas, dividindo o fluxo entre dois coletores onde estão dispostos os frascos destinados às análises. Água MiliQ era bombeada pelo sistema antes do início e ao final de cada turno de derretimento, com o objetivo de limpar o sistema. No fim de cada processo de limpeza eram recolhidas amostras de branco. A resolução média obtida, ou seja, o comprimento de testemunho contido em cada amostra para íons majoritários e elementos traço, foi de aproximadamente 3 cm. Obteve-se portanto 767 amostras para cada análise.



Figura 4.7: O sistema de derretimento contínuo. A linha pontilhada representa o caminho da água de degelo, direcionada aos frascos destinados à análise de elementos traço (esquerda) e aos frascos para determinação dos íons majoritários (direita).

4.5.1 Elementos traço

As 767 amostras destinadas à análise de elementos traço foram acidificadas com HNO_3 de dupla destilação a 1%. Os frascos de polipropileno utilizados no

armazenamento das amostras foram previamente limpos com HNO_3 15% (molho de 3 dias) e água MiliQ (triplo enxágue e molho de 3 dias), seguindo o protocolo utilizado em amostras de gelo da Antártica (Schwanck, 2017). Após aproximadamente 30 dias armazenadas, visando a dissolução dos metais depositados no Nevado Illimani, os elementos-traço foram analisados por espectrometria de massas com plasma indutivamente acoplado com campo setorizado (ICP-SMFS). Utilizou-se o espectrômetro modelo Thermo Electron Element 2 instalado no CCI.

Soluções padrão, contendo todos os elementos analisados, com concentrações dentro do intervalo esperado para o Nevado Illimani foram utilizadas para calibração diária. Como padrão de referência foi utilizada a água fluvial SLRS-4 (certificada pelo Conselho Nacional de Pesquisa do Canadá, Ottawa). Os limites de detecção do método (LDM) foram definidos como iguais a três vezes o desvio padrão de cada elemento em uma série de 10 brancos. Foram determinados 29 elementos por ICP-SMFS (Li, Na, Mg, Al, Si, S, K, Ca, Sc, Ti, V, Cr, Mn, Fe, Co, Cu, Zn, As, Sr, Ag, Cd, Cs, Ba, La, Ce, Pr, Pb, Bi e U).

4.5.2 Íons majoritários

Os 767 frascos com amostras destinadas à análise dos íons majoritários foram limpos somente com água MiliQ (triplo enxágue e molho de 1 dia), seguindo o protocolo utilizado em amostras de gelo da Antártica (Thoen, 2017). Os cátions (Na^+ , K^+ , Mg^{2+} e Ca^{2+}) e ânions (Cl^- , NO_3^- , SO_4^{2-}) foram determinados por cromatografia iônica. Utilizou-se o cromatógrafo iônico Thermo Scientific™Dionex™ICS-6000 instalado no CCI. Esse sistema é dotado de detectores de condutividade com prévia supressão do sinal de fundo. A calibração foi realizada com soluções padrão externas e avaliada com padrões de referência de águas fluviais certificados. Os LDM foram definidos como iguais a três vezes o desvio padrão de cada elemento em uma série de 10 brancos (água MiliQ bombeada pelo sistema de derretimento contínuo).

4.6 O testemunho de gelo extraído em 1999

Os primeiros 45 m do testemunho profundo coletado em junho de 1999 (IL1999) e destinado ao IGE, foi cortado transversalmente a cada ~10 cm, do topo até 40 m de profundidade, e a cada ~7 cm nos 5 m mais profundos (Ramirez *et al.*, 2003). Obteve-se 666 amostras para análise de poeira em contador Beckman Coulter Multisizer II com orifício de 50 µm. Até o momento da análise, as soluções eletrolíticas preparadas a partir das amostras permaneciam sob agitação. Equivalentes esféricos das partículas entre 0,67 e 20,89 µm foram divididos em 256 intervalos de tamanho. Para cada amostra realizou-se de 2 a 3 medidas. O desvio padrão relativo médio entre as medidas foi de aproximadamente 10%, considerando o intervalo de tamanhos 2–20 µm. Essas medições foram realizadas por Alexandre L. Correia e Jefferson C. Simões em 2001 no *LGGE (Laboratoire de Glaciologie et Geophysique de l'Environnement*, atual IGE, Grenoble, França).

O testemunho IL1999 foi estudado extensivamente, portanto sua cronologia já estava definida (Knüsel *et al.*, 2003). Nele foram identificados 3 horizontes vulcânicos relativos às erupções do Pinatubo (1991), El Chicón (1982) e Agung (1963) (De Angelis *et al.*, 2003). Em adição, um pico de Trítio foi atribuído a testes nucleares em 1964 (Knüsel *et al.*, 2003). Portanto, os 45 m mais superficiais do IL1999 abrangem o período 1919–1999. A incerteza foi estimada em ± 2 anos entre 1919 e 1941 e ± 1 ano para o período 1941–1999 (De Angelis *et al.*, 2003; Correia *et al.*, 2003).

4.7 Dados atmosféricos

A obtenção de informações ambientais a partir de testemunhos de *firn* e gelo depende, além da determinação das características químicas e físicas de suas camadas, de dados que representem as condições atmosféricas no provável período de deposição de cada camada. A Tabela 4.5 indica os dados externos utilizados.

Tabela 4.5: Dados meteorológicos, atmosféricos e glaciológicos utilizados na interpretação do registro do testemunho de *firn* do Nevado Illimani.

Parâmetro (nível)	Origem (grid)	Região	Resolução	Período	Fonte	Acesso
Precipitação	Observação meteorológica	Bolívia	Mensal	1965–2017	SISMET/ SENHAMI	www.senhami.gob.bo/ sismet
Radiação de onda longa emergente	Observação de satélite (2.5° x 2.5°)	Centro em 17.5°S, 70°W	Mensal	1999–2017	PSL/NOAA	https://www.esrl.noaa.gov/ data/gridded/
Altitude do nível de congelamento	Reanálise NCEP/NCAR (2.5° x 2.5°)	Centro em 17.5°S, 67.5°W	Mensal	1948–2017	PSL/NOAA	https://www.esrl.noaa.gov/ data/gridded/
Dimensão de geleira	Fotografias aéreas	Geleira n°8, N. Illimani	~Decadal	1956–2009	SNA/ Bolívia	Ribeiro (2017)
Temperatura da superfície do mar	Reconstrução ERSST v.5 (2° x 2°)	Atlântico e Pacífico Tropicais	Mensal	1919–2017	NOAA	http://climexp.kmni.nl
Umidade específica (500 hPa)	Reanálise ERA5 (1,5° x 1,5°)	América do Sul tropical	Anual	1980–2017	ECMWF	http://climexp.kmni.nl
Vento zonal (850 hPa)	Reanálise ERA5 (1,5° x 1,5°)	América do Sul tropical	Mensal	1999–2017	ECMWF	http://climexp.kmni.nl
Vento zonal (200 hPa)	Reanálise ERA-Interim (1,5° x 1,5°)	América do Sul tropical	Mensal	1999–2017	ECMWF	https:// climatereanalyzer.org
Trajetória de massas de ar	Modelo GDAS (1° x 1°)	Nevado Illimani	Horária	2014–2015	HYSPLIT	https:// www.ready.noaa.gov/

5 Resultados

5.1 Giant dust particles at Nevado Illimani: a proxy of summertime deep convection over the Bolivian Altiplano

Artigo submetido para a revista The Cryosphere e aceito para revisão e discussão pública em seu fórum científico The Cryosphere Discussions. A versão apresentada aqui contempla as correções solicitadas pelo primeiro revisor. Email de aceite no Anexo II.

Giant dust particles at Nevado Illimani: a proxy of summertime deep convection over the Bolivian Altiplano

Filipe G. L. Lindau¹, Jefferson C. Simões^{1,2}, Barbara Delmonte³, Patrick Ginot⁴, Giovanni Baccolo³, Chiara I. Paleari³, Elena Di Stefano³, Elena Korotkikh², Douglas S. Introne², Valter Maggi³, Eduardo Garzanti³, Sergio Andò³

¹Centro Polar e Climático, Universidade Federal do Rio Grande do Sul, Porto Alegre, 91501-970, Brazil

²Climate Change Institute, University of Maine, Orono, ME 04469, USA

³Environmental and Earth Sciences Department, University Milano-Bicocca, Milan, 20126, Italy

⁴Univ. Grenoble Alpes, CNRS, IRD, Grenoble INP, IGE, 38000 Grenoble, France

Correspondence to: Filipe G. L. Lindau (filipelindau@hotmail.com)

Abstract. A deeper understanding of past atmospheric circulation variability in the Central Andes is a high-priority topic in paleoclimatology, mainly because of the necessity to validate climate models used to predict future precipitation trends and to develop mitigation and/or adaptation strategies for future climate change scenarios in this region. Within this context, we here investigate an 18-years firm core drilled at the Nevado Illimani in order to interpret its mineral dust record in relation to seasonal processes, in particular atmospheric circulation and deep convection. The core was dated by annual layer counting based on seasonal oscillations of dust, calcium and stable isotopes. Geochemical and mineralogical data show that dust is regionally-sourced in winter and summer. During austral summer (wet season) an increase in the relative proportion of giant dust particles ($\phi > 20 \mu\text{m}$) is observed, in association to oscillations of stable isotope records (δD , $\delta^{18}\text{O}$). It seems that at Nevado Illimani both the deposition of dust and the isotopic signature of precipitation are influenced by atmospheric deep convection, which is also related to the total amount of precipitation in the area. This hypothesis is corroborated by local meteorological data. The interpretation of giant particle and stable isotope records suggests that during La Niña years, summer convection activity is enhanced, in agreement with atmospheric circulation studies. Giant particles and stable isotopes, when considered together, can be therefore used as a new proxy for obtaining information about deep convective activity in the past, which is ultimately related to paleo-ENSO variability.

1 Introduction

Climate variability in the Central Andes and the Bolivian Altiplano has a strong link with atmospheric circulation and rainfall anomalies over the rest of tropical South America (e.g. Vuille, 1999). Over the Altiplano, a semi-arid plateau in the Central Andes with a mean elevation of 3800 m above the sea level (a.s.l.) (Fig. 1), climate variations have a direct effect on the availability of water resources, with severe economic and social impacts (Garreaud and

Aceituno, 2001). Recent Andean glacier retreat due to global climate change (Rabatel et al., 2013) poses issues not only for water availability (Soruco et al., 2015), but also for the preservation of glaciers as natural archives that could be soon lost. For example, in the period between years 1963 and 2009, Nevado Illimani (Fig. 1) lost approximately 35% (9.49 km²) of its total area of ice (Ribeiro et al., 2013), while on Quelccaya ice cap (13°54'S, 70°48'W, 5670 m a.s.l., Fig. 1) the seasonal variations in stable isotopes were attenuated in the latter half of the twentieth century record due to melting and percolation through the firn, although the seasonality in dust was still preserved (Thompson et al., 2017).



Figure 1: Location of the Nevado Illimani and the Quelccaya ice cap. The numbers indicate the location of the meteorological stations used for comparison with our results: 1 – El Alto; 2 – Calacoto; 3 – Patacamaya; 4 – Oruro and 5 – Potosi. The white areas in Bolivia, Chile and Argentina indicate salars from the Altiplano and Puna regions. The land basemap was derived from satellite data (Natural Earth I with Shaded Relief from <http://www.naturalearthdata.com>).

Precipitation on the Bolivian Altiplano is largely concentrated in the summer months (Garreaud et al., 2003), in response to the peak phase of the South American Summer Monsoon (SAMS). During summer (DJF), the intensification and southward displacement of the Bolivian High promotes strong easterly winds and a turbulent entrainment of easterly air masses over the Andean ridge. In addition, the upward motion over western Amazon, which is part of the meridional circulation between the tropical North Atlantic and western tropical South America, leads to increased convection and reduced tropospheric stability over the Central Andes (Segura et al., 2020). Such an atmospheric context favours the establishment of an eastward upslope air-flow and the advection of moisture from the Amazon basin toward the Andes (Zhou and Lau, 1998). Furthermore, there is the occurrence of transient

disturbances within the SAMS, such as midlatitude cold air incursions that migrate equatorward from southern South America to the Amazon basin, and are responsible to most of the precipitation in the Quelccaya ice cap (Vera et al., 2006; Hurley et al., 2015). Accordingly, summer precipitation is strongly associated with deep convective activity, enhanced by high amounts of water vapor in the boundary layer which destabilize the tropospheric column over the Altiplano (Garreaud, 1999). Precipitation during the rest of the year is scarce: during winter months (JJA) the Altiplano is generally very dry, and advection of dry air from the Pacific region is promoted, being moist air advection from the east suppressed. Strong winter westerly winds and dry conditions allow massive local transport and deposition of dust over the Central Andean glaciers, and for this reason high seasonal contrast exists between wet summer and dry winter snow layers in terms of dust and aerosol content (Knüsel et al., 2005).

Besides seasonal variability, year-to-year climate over the Altiplano is also influenced by conditions in the tropical Pacific Ocean. During warm phase of the El Niño-Southern Oscillation (ENSO), the Altiplano climate is dry. Dry summers associated with El Niño events in the tropical Pacific are characterized by enhanced westerly flow over the tropical Andes inhibiting moisture advection from the Amazon basin (Knüsel et al., 2005; Thompson et al., 2013). Conversely, wet summers associated to a cooling of the tropical Pacific (La Niña events) promote further ingressions of humid easterly air masses from the Amazon Basin.

Developing an annually-resolved ice core record from the Altiplano represents a great opportunity to enhance our knowledge about present and past climate variability in the tropical Andes region. Previous ice core studies (Correia et al., 2003; Knüsel et al., 2005; Osmont et al., 2019) from the Central Andes reveal that the aerosol content of ice is dominated by local and regional soil dust during the winter, when black carbon from biomass burning in the Amazon basin is also present. During the summer, conversely, the concentration of aerosol and particulate matter is much lower while species of anthropogenic origin (e.g. Cu, As and Cd) are observed in higher proportions (Correia et al., 2003).

With the aim to enhance our knowledge about past and present climate variability in the tropical Andes region, a new shallow firn core (23.8 m long) was drilled on the Nevado Illimani (Cordillera Real, Eastern Bolivian Altiplano), as an integration of the Ice Memory project (<https://www.ice-memory.org>). In this study we investigate mineral dust aerosol variability and provenance in this firn core, through the analysis of dust concentration, grain size, geochemistry and mineralogy. The very pronounced seasonal variations of the analyzed

proxies allowed for the development of a precise chronology, which covers the 1999–2017 period, and for the investigation of correlation between dust records and other proxies. Dust particles entrapped in firn samples seem to originate from regional sources during both winter and summer, despite minor mineralogical differences between the two seasons are observed. An interesting result concerns the presence of giant dust particles (presenting a diameter larger than 20 µm), whose variability is correlated to the stable isotope record. Our data and local meteorological observations suggest that this relationship could be explained as a consequence of atmospheric deep convection over the Bolivian Altiplano during summer. This study shows for the first time that the presence of giant dust particles in Andean firn and ice is strictly controlled by climatic processes. We found clear evidence that the convective activity over the Altiplano, reconstructed through the analysis of giant particles, is enhanced during summer periods and in particular during La Niña years, in agreement with observations concerning atmospheric circulation anomalies in the area (Vuille, 1999). From this perspective, this study demonstrates the great potential of giant particles records, which is strongly influenced by climatic and meteorological processes at high altitude continental glaciers. This is a first exploratory work, analysis of a longer ice core would be desirable in the future to investigate the relationships between giant dust particles deposition, atmospheric deep convection and periodic climatic phenomena (ENSO).

2 Material and Method

2.1 Field campaign and firn core sampling

Nevado Illimani ($16^{\circ}37'S$, $67^{\circ}46'W$, 6438 m a.s.l.) is located 50 km southeast of the Bolivian capital, La Paz, and 180 km southeast of Lake Titicaca (Fig. 1). Its approximate dimensions are 10 per 4 km, with some peaks above 6,000 m a.s.l. Nevado Illimani consists of a granodiorite pluton of Late Oligocene age, with a short belt composed by a coeval dacitic flow located near the south-western border of the pluton (McBride et al., 1983; Jiménez and López-Velásquez, 2008). In June 2017, a 23.8 m firn core (corresponding to 13.75 m water equivalent) was drilled at an altitude of 6350 m a.s.l. on the saddle between the two Nevado Illimani summits, approximately where two deep ice cores were recovered in June 1999 (Knüsel et al., 2003). The expedition was coordinated by a French, Russian, Bolivian and Brazilian team and integrated the Ice Memory project (Université Grenoble Alpes Foundation). An EM-100-1000 electromechanical ice core drill (Cryosphere Research

Solutions, Columbus, Ohio, USA) was used for the drilling and three cores were extracted, two down the bedrock (136 and 134 m) and the core for this study (23.8 m).

The cores (diameter of 10 cm), consisting of 24 sections of approximately 1 m length, were transported by mountain porters from the drilling site to the base camp during the night in order to prevent melting. Once at the base camp, they were immediately transported to a refrigerated container located in La Paz, where temperature was set at -20 °C. After the drilling campaign, the container was shipped to the Institut des Géosciences de l'Environnement (IGE, Université Grenoble Alpes, France) where the core sections were weighted and cut longitudinally using a vertical band saw in a cold room (at -15 °C). Ice layers (less than 5 cm thick) occurred frequently along the firn core (Fig. S1), generally in closely spaced groups of 2 or 3 individual layers. In addition, less than 1 cm thick ice layers (or possibly wind crusts, hardly distinguishable from the former at greater depths) commonly occurred along the core. These features indicate few events of meltwater percolation, and ensure the proxies recorded in the firn core are well-preserved.

One quarter of the original core was dedicated to dust analyses and transported for this purpose to the EUROCOLD facility of the University of Milano-Bicocca (Italy). There, firn sections were transversely cut at 5 cm using a horizontal band saw with a cobalt steel blade and 464 samples were obtained. These were manually decontaminated by mechanical scraping with a clean ceramic knife inside a laminar flow high-efficiency particle air (HEPA) ISO 5 Class bench located in an ISO 6 Class cold room. Once decontaminated, the samples were put into clean Corning centrifuge tubes and kept frozen until the measurements.

2.2 Coulter Counter Analysis

Samples were melted at room temperature, and a ~10 mL aliquot from each was transferred to an Accuvette Beckman Coulter vial, previously washed with Millipore Q-POD® Element ultra-pure water (in an ISO 5 Class laminar flow bench located inside an ISO 6 Class clean laboratory). Each sample was treated following standardized protocols (Delmonte et al., 2002). A Beckman Coulter Multisizer 4 equipped with a 100 µm orifice was used to measure dust concentration and grain size (400 size channels within the 2–60 µm interval of spherical equivalent diameter). Samples were continuously stirred until the moment of the analysis, as the larger particles tend to settle rapidly. Systematic analysis of ultra-pure water blanks allows estimating a mean signal to noise ratio around 97. Each sample was measured twice,

consuming 0.5 mL per measurement. The mean relative standard deviation (RSD) between these two measurements considering both the number and the mass of particles was 7% and 29%, respectively.

The higher deviation for the mass in comparison to the total number of particles was expected due to the presence of heavy giant particles having diameters $>20\text{ }\mu\text{m}$ (coarse silt), for which small differences in size estimation lead to higher uncertainties. Indeed, when considering only the giant particles the mean RSDs were 55% and 63% for the number and mass distributions, respectively. Thus, the proportion (%) of giant particles (GPPnb) as well as total particle concentration, were calculated from the number size distribution. Approximately 14% of the samples showed very large uncertainties (RSD $>100\%$) for GPPnb and were discarded. The mean RSD for GPPnb was 45%.

2.3 Instrumental Neutron Activation Analysis

A set of 10 samples was dedicated to Instrumental Neutron Activation Analysis (INAA). Samples were selected from different depth intervals along the core (see Table 1, “N” series, and Table S1 for precise depths), in order to be representative of both the dry and the wet seasons. The samples were filtered using PTFE Millipore[®] membranes (0.45 μm pore size, 11.3 mm diameter) previously rinsed in an ultra-pure 5% solution of bi-distilled HNO_3 —according to the procedures adopted by Baccolo et al. (2015). The filtration took place in an ISO 5 Class laminar flow bench. Two blank membranes, that underwent the same cleaning procedures, were prepared by filtering 300 mL of MilliQ (Millipore[®]) water.

For calibration and quality control, we used certified solid standards: USGS AGV2 (ground andesite), USGS BCR2 (ground basalt), NIST SRM 2709a (San Joaquin soil) and NIST SRM 2710a (Montana soil). In addition, standard acid solutions for each analyzed element were prepared with concentrations in the order of $\mu\text{g g}^{-1}$. Blanks for the empty flask and for the ultra-pure acid solution used to prepare the liquid standards were also measured. Samples, standards and blanks were irradiated at the Applied Nuclear Energy Laboratory (LENA, University of Pavia, Italy) by a Triga Mark II reactor of 250 kW. The “Lazy Susan” channel, neutron flux equal to $2.40 \pm 0.24 \times 10^{12}\text{ s}^{-1}\text{ cm}^{-2}$, was used to identify Ce, Cs, Eu, Hf, La, Sc, Sm, Th, and Yb. Samples were successively transferred at the Radioactivity Laboratory of the University of Milano-Bicocca, in order to acquire gamma spectra by means of a high-purity

Germanium detector HpGe (ORTEC, GWL series), following the standardized procedure developed for low-background INAA (Baccolo et al., 2016).

Table 1: Characterization of the Nevado Illimani samples analyzed for elemental (N1 to N10) and mineralogical (R1 to R4) composition.

Sample	Year	Season	Dust (part. mL ⁻¹)	GPPnb (%)
N1	2016	Dry	14,737	0.1
N2	2015 – 2016	Wet	7,283	0.2
N3	2013 – 2014	Wet – Dry	6,340	0.3
N4	2012	Dry	30,405	0.2
N5	2010 – 2011	Wet	2,605	1.3
N6	2008	Dry	25,816	0.7
N7	2007 – 2008	Wet – Dry	6,424	1.0
N8	2003	Dry	29,923	0.2
N9	2002	Dry	21,057	0.2
N10	2000 – 2001	Wet	4,180	1.9
R1	2010	Dry	17,409	0.1
R2	2009 – 2010	Wet	8,234	0.2
R3	2004	Dry	86,918	0.2
R4	2003 – 2004	Wet	2,303	0.9

The masses of the elements in each sample were determined by comparing spectra related to standards and samples (Baccolo et al., 2016). In order to compare different spectra, the time of acquisition, the radionuclide decay constant, the cooling time and a factor considering radioactive decay during the acquisition were kept into account. The detection limits were calculated considering three times the standard deviation of the blank signal. The uncertainties for each element were calculated based on the mass measurements, the adjustment for the spectrum, the subtraction of the blanks and the standard concentration uncertainties. Errors for the elemental concentrations in our samples ranged from 3% for La to 17% for Cs, and the detection limits ranged from 0.1 µg per gram of dust for Sm to 7 µg g⁻¹ for Ce (Table S2). Full analytical details can be found in Baccolo et al. (2016).

The Enrichment Factor (EF) normalization was calculated for each element considering as a reference the mean composition of the upper continental crust (UCC) (Rudnick and Gao, 2003). Scandium (Sc) was chosen as the crustal reference element following Eq. (1):

$$EF(X) = \frac{\left(\frac{[X]}{[Sc]}\right)_{sample}}{\left(\frac{[X]}{[Sc]}\right)_{UCC}} \quad (1)$$

Scandium was chosen as reference element because it is poorly affected by processes altering its mobility in hosting minerals, and its biogeochemical cycle is almost unaffected by anthropogenic activities (Sen and Peucker-Ehrenbrink, 2012). In addition, Sc is highly correlated with other lithogenic elements, such as Ce ($r = 0.997$), used by Eichler et al. (2015) as a crustal reference for Nevado Illimani samples, and La ($r = 0.989$). The choice of Sc has been also determined by its easy and precise determination through INAA.

2.4 Micro-Raman Spectroscopy

We used single-grain Raman spectroscopy to identify mineralogy of dust particles having a diameter smaller than 5 μm . This because this kind of analysis was carried out for provenance purposes, thus excluding the large and the giant particles of obvious local origin. A set of four samples (see Table 1, “R” series, and Table S1) was prepared, following the procedure described in previous studies (Delmonte et al., 2017; Paleari et al., 2019) specifically developed for small dust grains. Two samples are representative of mineral dust deposited in the dry season (high dust concentration) whereas two represent dust from the wet season (low dust concentration, or “background”). Measurements were performed by using an InVia Renishaw micro-Raman spectrometer (Nd YAG laser source, $\lambda = 532$ nm) available at the Laboratory for Provenance Studies (UNIMIB). We identified the mineralogy of more than 630 grains, excluding organic particles possibly related to contamination and particles with an undetermined spectrum or with no signal.

2.5 Stable Isotope and Ion Chromatography Analysis

The dust analyses described above used one quarter of the longitudinally-cut firn core. A second quarter was shipped in a frozen state to the Climate Change Institute (CCI, University of Maine, USA) for ion chromatography (IC) and water stable isotope analysis.

At the CCI, in a cold room set at -20 °C, we cut longitudinal sections of the core with a vertical band saw to separate an inner and an outer part. The latter was sampled by transverse cuts approximately every 12 cm using a stainless-steel hand saw (resulting in 190 samples) and stored in plastic bottles for stable isotope ratio determination. Decontamination of the

inner part was performed by scraping with a clean ceramic knife under a laminar flow HEPA bench inside the cold room. Then, the decontaminated inner part was sampled for IC analysis by a continuous melter system (Osterberg et al., 2006) also in an ISO 6 Class clean room. The mean sample resolution was 3 cm, resulting in 767 samples. We measured Ca^{2+} concentration using a Thermo Scientific™Dionex™ Ion Chromatograph ICS-6000 analytical system fitted with suppressed conductivity detectors with a Dionex AS-HV autosampler. The method detection limit (MDL) was defined as 3 times the standard deviation of the blank samples (MilliQ water, 10 blank samples). The detection limit for Ca^{2+} was $21.05 \mu\text{g L}^{-1}$.

The δD and the $\delta^{18}\text{O}$ were determined using a Picarro L2130-i wavelength-scanned cavity ring-down spectroscopy instrument (Picarro Inc., USA) with a precision of 0.1 ‰.

3 Results and discussion

3.1 Seasonal variability of proxies and firn core chronology

We established a chronology for the Nevado Illimani firn core based on annual layer counting (ALC), considering the pronounced seasonal oscillation of dust concentration, calcium and water stable isotopes (Fig. 2). Dust concentration variations, which are recognized for being useful for ALC in tropical and continental ice cores (Ramirez et al., 2003; Kutuzov et al., 2019), span about two-orders of magnitude between the summer and the winter. Dust concentration varies from $\sim 2,000$ particles mL^{-1} (hereafter part. mL^{-1}) during the wetter season, to $\sim 10,000$ part. mL^{-1} during the dryer season (median values). The two size distributions shown in Fig. S2, illustrate this variability. When considering extreme values, the variation range exceeds three orders of magnitude, being the lowest concentration during the wet season 150 part. mL^{-1} and the highest one during the dry season 140,000 part. mL^{-1} . Our results are in agreement with average dust concentrations from Quelccaya ice cap during the 20th century, $\sim 10,000$ part. mL^{-1} and $\sim 25,000$ part. mL^{-1} for the size ranges of 1.6–16 μm and 0.6–20 μm , respectively (Thompson et al., 1986, 2013).

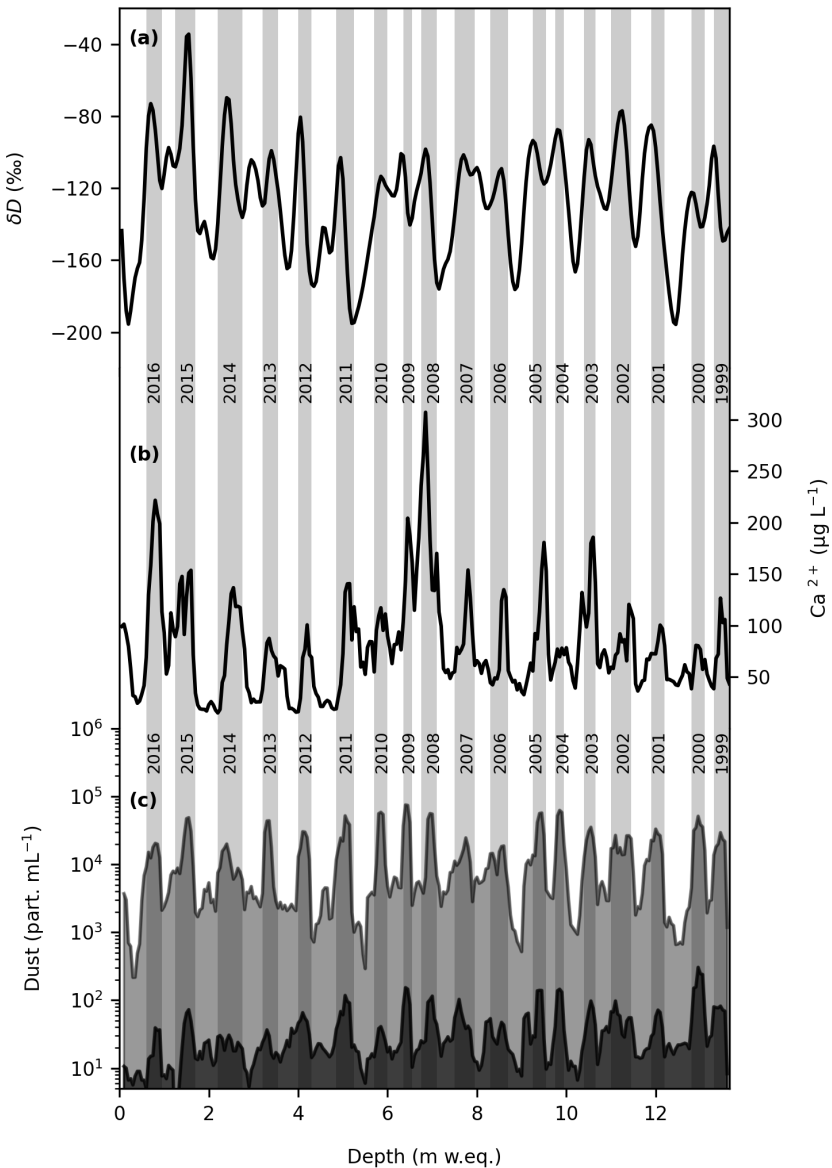


Figure 2: Dating of the Nevado Illimani firn core by annual layer counting (ALC) based on different proxies discussed in the text: (a) δD , (b) ionic Calcium, and (c) total and giant dust particles concentrations (light and dark gray, respectively, both are in logarithmic scale). Gray shaded vertical bands correspond to the dry season for each calendar year. All data are reported as 3-point running average of data re-sampled at 0.05 m w.eq.

By considering just the giant particles we also observed a seasonal pattern, with median concentrations of 15 part. mL^{-1} during the wet season and 30 part. mL^{-1} during the dry season. The well-defined oscillatory pattern of dust concentration variability reflects the extreme seasonality of precipitation over both local and regional dust sources, and the succession of dry and wet conditions. Therefore, each sample was classified as belonging to the wet or to the dry season according to dust concentration. Sublimation has a limited influence to this seasonality (Ginot et al., 2002).

Dust concentration is in accordance with the Ca^{2+} record and in agreement with literature studies (Knüsel et al., 2003). Ionic calcium can be primarily associated to calcium sulphate (CaSO_4) and/or calcium carbonate (CaCO_3) (Kutuzov et al., 2019). Because scarcity of calcium carbonates was revealed by mineralogical analyses (Fig. 4, see below), we argue that most of the ionic calcium observed in firn samples is present as a soluble species, probably CaSO_4 , and not detectable through Raman spectroscopy on single insoluble particles. However, we consider the possibility of calcium carbonate depletion due to scavenging during dust transport and/or dissolution during the melting of the samples, as discussed by Wu et al. (2016) based on ice core samples from Tibetan Plateau. In addition, we cannot exclude that Ca-bearing aerosols might have been initially a mixture of pure gypsum and calcium carbonates that successively reacted with atmospheric H_2SO_4 (Röthlisberger et al., 2000).

The regular succession of dry dusty periods and wet periods can be associated with the seasonal onset and decay of the Bolivian High, a high pressure system which is well developed and centered over Bolivia (Lenters and Cook, 1997). When the Bolivian High is particularly strong and displaced southward of its climatological position, easterly flow in the high troposphere is enhanced as well as moisture advection from the interior of the continent to the Altiplano. This moisture transport from the Amazon Basin toward the Altiplano induces a notable amount of precipitation over the Altiplano (wet season), associated with strong summer convection. The relatively low dust concentration found in the Illimani snow during the summer period is therefore related to particle dilution in the snowpack because of increased precipitation and reduced regional dust mobilization deriving from wetter soil conditions. Conversely, during winter (JJA) months, conditions over the Altiplano are typically dry, leading to higher dust availability. At that time of the year, the winter westerly flow over the entire region promotes eastward dust transport towards the Nevado Illimani, leading to significant higher dust deposition in the firn layers representing - on average - about 85% of the total annual dust particles there deposited.

Seasonal variations of the water stable isotopes in snow precipitated over the Andes are also useful for dating. However, the Andean isotopic signal led to divergent interpretations (Vimeux et al., 2009). Whereas in polar ice cores the water isotopic signature is chiefly related to temperature (Uemura et al., 2012), the isotopic composition of tropical precipitation can be affected by a larger number of factors (Hoffmann et al., 2003). It is well known that the so called “amount effect” leads to an anti-correlation between the amount of precipitation and the proportion of heavier isotopes in the precipitation. This effect is in turn related to an

ensemble of physical and microphysical processes producing a robust signal on the isotopic composition of precipitation (Dansgaard, 1964; Risi et al., 2008; Vuille et al., 2003). In this context, deep atmospheric convection also plays a role on stable isotope composition (Vimeux et al., 2005). Modelling studies (e.g. Bony et al., 2008; Risi et al., 2008) reveal that the stronger the convective activity during a particular event, the higher the total amount of precipitation and thus the more depleted the isotopic composition of precipitation. Satellite data (Samuels-Crow et al., 2014) reveal that during the summer season the isotopic composition of water vapor strongly depends on convective activity. These observations lead the authors to conclude that the isotopic composition of snow from the tropical Andes mainly reflects tropical convection.

Convective precipitation over the Bolivian Altiplano is enhanced during the wet summer season, leading to the emergence of clear seasonal oscillations in the stable isotope records of Nevado Illimani firn core which can be used for ALC and to develop a chronology.

Considering the pronounced seasonal changes in dust concentration, Ca^{2+} and stable isotopes, it is possible to assign to the base of the Illimani firn core an age corresponding to the beginning of 1999 AD. The firn record thus covers the 18-years period from early 2017 to early 1999 and the average accumulation rate can be estimated in the order of approximately 750 mm of water equivalent per year, slightly higher than the one inferred by Knüsel et al. (2003).

Interestingly, we note a close correspondence between the variability of stable isotopes and the proportion of giant particles in firn (Fig. 3a): oscillations of the stable isotope record (δD in Fig. 3a) closely follow the percentage of giant dust particles (GPPnb in Fig. 3a). During the dry season, giant particles are proportionally less abundant (average GPPnb 0.5%) whereas the isotopic composition of snow is less negative (average $-113\text{\textperthousand}$ for δD ; $-15\text{\textperthousand}$ for $\delta^{18}\text{O}$). Conversely, during the wet season when giant dust particles are at their annual maximum (average GPPnb 1%) the isotopic composition of snow is more depleted ($-141\text{\textperthousand}$ for δD , $-18\text{\textperthousand}$ for $\delta^{18}\text{O}$), reaching its minimum. The first principal component of these two series (GPPnb and δD), reported in Fig. 3b, explains approximately 82% of the variance of the records.

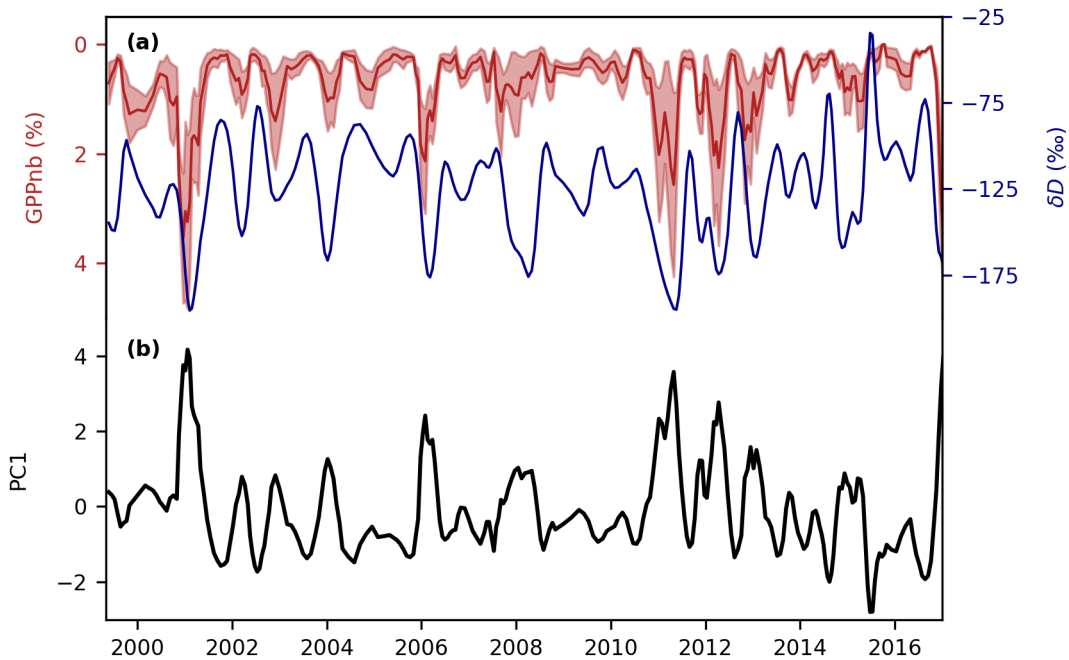


Figure 3: (a) Relationship over the 18-years record between the percentage of giant particles with respect to the total dust particles number (GPPnb, reverse scale) and the δD . Uncertainties for each GPPnb value (expressed by the red shaded area) are relative to the standard deviation between Coulter Counter measurements. (b) The first principal component of these two series (representing 82% of the total variance). All data are reported as 3-point running average of the data previously re-sampled at 0.05 m w.eq.

3.2 Dust provenance: mineralogy and geochemistry

The mineralogical composition of fine dust ($<5 \mu\text{m}$) deposited onto the Illimani firn layers reveals that the most abundant mineral phases are quartz, feldspars (alkali feldspars and plagioclase) and phyllosilicates (Fig. 4, Table S3). Phyllosilicates are mainly represented by muscovite-illite (and/or smectite, hardly distinguishable from illite by their Raman spectra) and secondarily by kaolinite (representing 7.5% in the dry season and 1.5% in the wet season). Altogether, quartz, feldspars and phyllosilicates account for 75–78% of mineral particles during both the wet and the dry season, but phyllosilicates are particularly abundant during the wet season, when they represent approximately 44% of minerals (Fig. 4a). We believe that the increased abundance of muscovite-illite during the wet season is related to different depositional regimes. During the dry winter, aerodynamic platy-like phyllosilicates can remain in the atmosphere for longer periods and are only partially deposited. On the contrary, during the wet summer strong scavenging is associated to heavy precipitations at Nevado Illimani (Bonneveira, 2004), enhancing the removal of mineral particles from the atmosphere, including phyllosilicates.

Titanium oxides and iron oxides/hydroxides are present in all samples. Hematite is twice as abundance as goethite. This is typical in regions dominated by arid conditions or where a prolonged warm and dry season is followed by a shorter and wetter period (Journet et al., 2014). Accessory minerals include carbonate and tourmaline, and very rare pyroxenes (Table S3). Such a mineralogical composition is coherent with the felsic to intermediate plutonic volcanic source rocks, suggesting that most of the dust deposited at Nevado Illimani has a local/regional provenance, both in the wet and in the dry seasons.

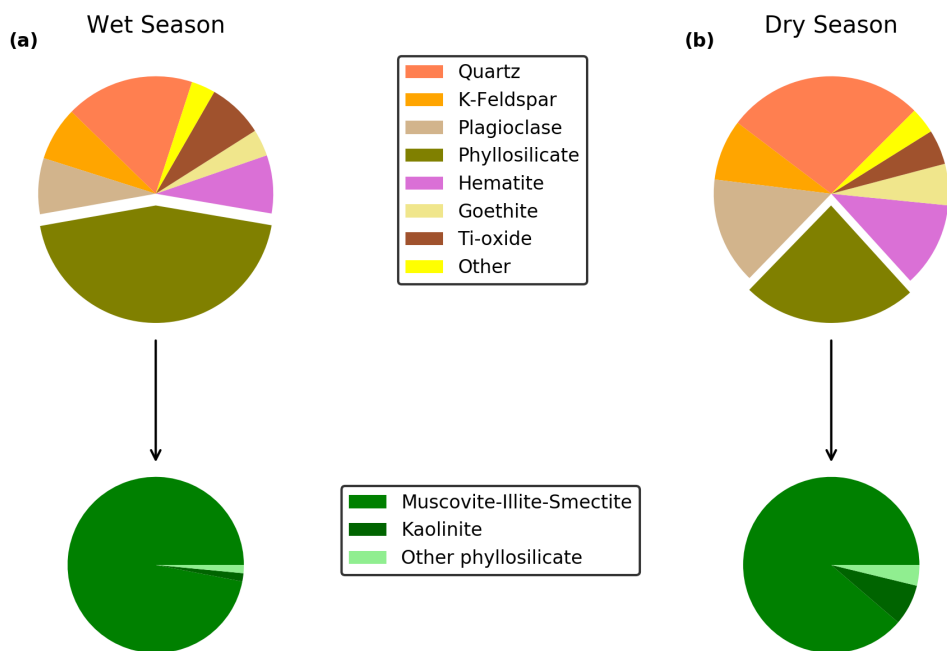


Figure 4: Changes in dust mineralogy between (a) the wet and (b) the dry seasons. The lower plots highlight the mineralogy of the phyllosilicates.

Low-background INAA analyses allowed determining the EFs for different rare earth elements (REEs), which are non-mobile and therefore widely used as provenance tracers (McLennan, 1989; Moreno et al., 2006; Gabrielli et al., 2010). In Fig. 5a the Yb/La and the Eu/Sm elemental ratios are used to compare dust samples retrieved from Nevado Illimani firn samples and literature data concerning geological samples from the Altiplano-Puna Volcanic Complex (Lindsay et al., 2001; Ort et al., 1996) and potential source areas (PSAs) in South America (Gaiero et al., 2004, 2013). The Yb/La ratio can be used to appreciate whether heavy and light REEs are enriched or depleted with respect to each other, whereas the Eu/Sm ratio is a proxy for the europium anomaly, usually calculated considering Gd, not detected by our analytical method. The comparison reveals that Nevado Illimani dust has a composition

similar to APVC crystal-rich ignimbrites, pointing to a correspondence with samples from the Northern Puna region, and not with samples from the salt lakes present in the Altiplano (Uyuni and Coipasa salars). These pieces of evidence agree with previous analyses of strontium and neodymium isotopes on Nevado Illimani ice core dust (Delmonte et al., 2010) and with the geochemical signature of local sources in the Altiplano (Gili et al., 2017), supporting the hypothesis that dust deposited at Nevado Illimani is sourced by sediments present in Southern Altiplano-Northern Puna areas.

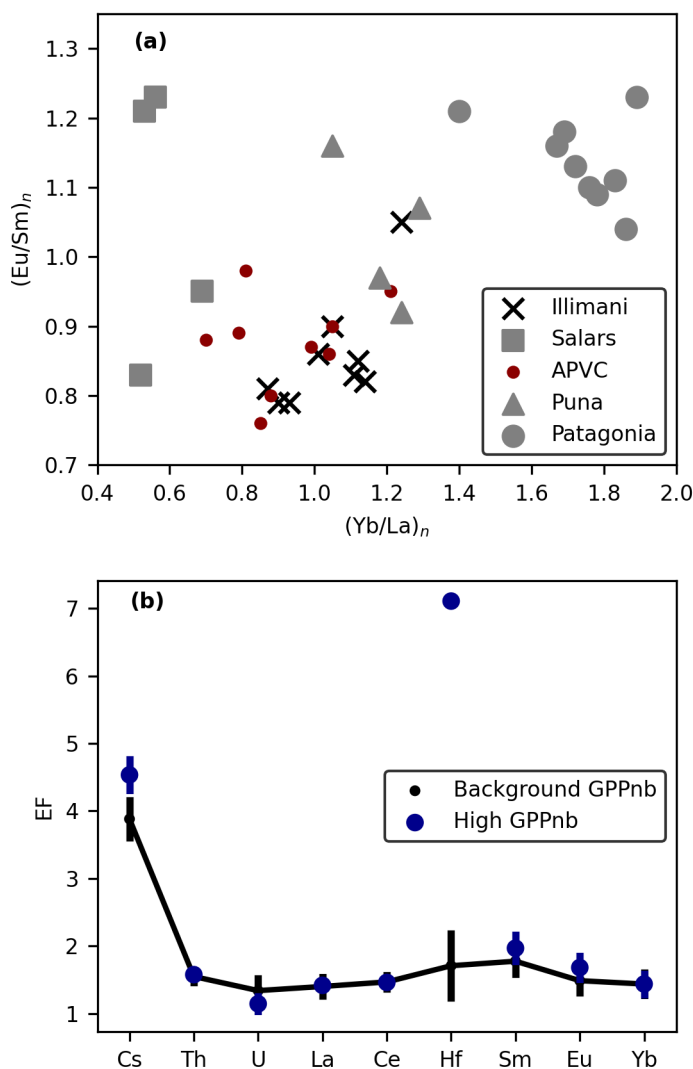


Figure 5: Geochemical signature of Nevado Illimani firn samples. (a) Relationship between the REE (normalized considering the UCC composition (Rudnick and Gao, 2003) from the Nevado Illimani firn core (this work) and sediments/soils from potential dust sources (corresponding to $< 63 \mu\text{m}$ grain size for top soils). Data from Northern Puna, and Uyuni and Coipasa salars are from Gaiero et al. (2013). Data from Patagonia are from Gaiero et al. (2004). Data for the APVC refer to geological samples from Lindsay et al. (2001) and Ort et al. (1996). (b) Enrichment Factors (EF) for different elements and standard deviations. Samples with a high GPPnb (blue circles) show anomalous enrichment for Hf and to a lesser extent for Cs (see text).

The EFs of Ce, La, Sm, Eu and Yb is similar between samples with higher percentage of giant particles ($\text{GPPnb} > 1\%$, characteristic from the wet season) and samples with background GPPnb (Fig. 5b), supporting what has been observed in relation to the mineralogical composition of samples from the wet and dry seasons. However, two important exceptions to this pattern occur in relation to Hf and Cs. High GPPnb samples show an anomalous Hf enrichment when compared to background samples, a feature that was observed also in Saharan dust samples (Castillo et al., 2008) and attributed to the presence of detrital zircon ($(\text{Zr}, \text{Hf})\text{SiO}_4$) in samples showing the coarsest grain size. As discussed by Vlastelic et al. (2015) the Hf enrichment observed in samples where the percentage of giant particles is high might be related to the presence of a few silt-sized zircon grains, which would in turn require high energy (turbulence) to lift them and keep them in suspension into the atmosphere. In this study, however, zircon grains were not detected by Raman Spectroscopy, which indicated greater abundance of phyllosilicates in dust deposited during the wet summer season. The Hf enrichment in these samples may thus be related instead to tiny zircon inclusions within phyllosilicate particles.

Another deviation from background is related to cesium. Because of the very common Cs-K exchange into interlayer sites in illite-muscovite, the Cs enrichment in samples from the wet season may also be related to the greater abundance of phyllosilicates (Cremers et al., 1988; Rosso et al., 2001).

3.3 Relationship between the giant particles and deep convection

The absolute concentration of dust in firn and ice cores depends on many factors including the snow accumulation rate, the dust *source strength* (which includes soil aridity/wetness, vegetation cover and any other factor influencing the quantity of particles available for deflation), as well as transport processes, which also affect the residence time of particles in the atmosphere (mainly in the case of long-range transport). Conversely, the dust size distribution and the relative proportion of particles within a given grain size merely depends on transport conditions (Delmonte et al., 2004, 2017).

In the case of Nevado Illimani, where dust is mostly regionally-sourced, we believe that the dust concentration is primarily modulated by the seasonally-varying source strength, mainly depending on source aridity and humidity, and by accumulation rate. Conversely, the dust size distribution, in particular the relative number (or mass) of giant particles is related to the

relative strength of local turbulence and deep convection. Indeed, we observe an interesting correlation (Fig. 3a) between the relative number of giant particle percentage (GPPnb) and δD , both related to convective activity.

Seasonal mean values (Fig. 6) show the significant correlation between these two proxies. Data located in the bottom right corner of Fig. 6 refer to dust deposited onto the Nevado Illimani glacier during the wet season, when more intense convection leads to higher percentage of giant particles and more depleted isotopic composition of precipitation. Points located in the upper left corner, conversely, are associated to winter dry periods when convection and precipitation are reduced and the relative proportion of giant particles is lower. Convective activity is known to significantly affect the isotopic composition of tropical precipitation. Intense regional convection leads to more isotopically-depleted precipitation (e.g. Risi et al., 2008). Therefore, giant particles on the Nevado Illimani glacier can be reasonably used as proxy for deep summer convective precipitation. Given their size and geochemical/mineralogical fingerprint, we confidently associate them to local/regional convective activity near the Bolivian Altiplano.

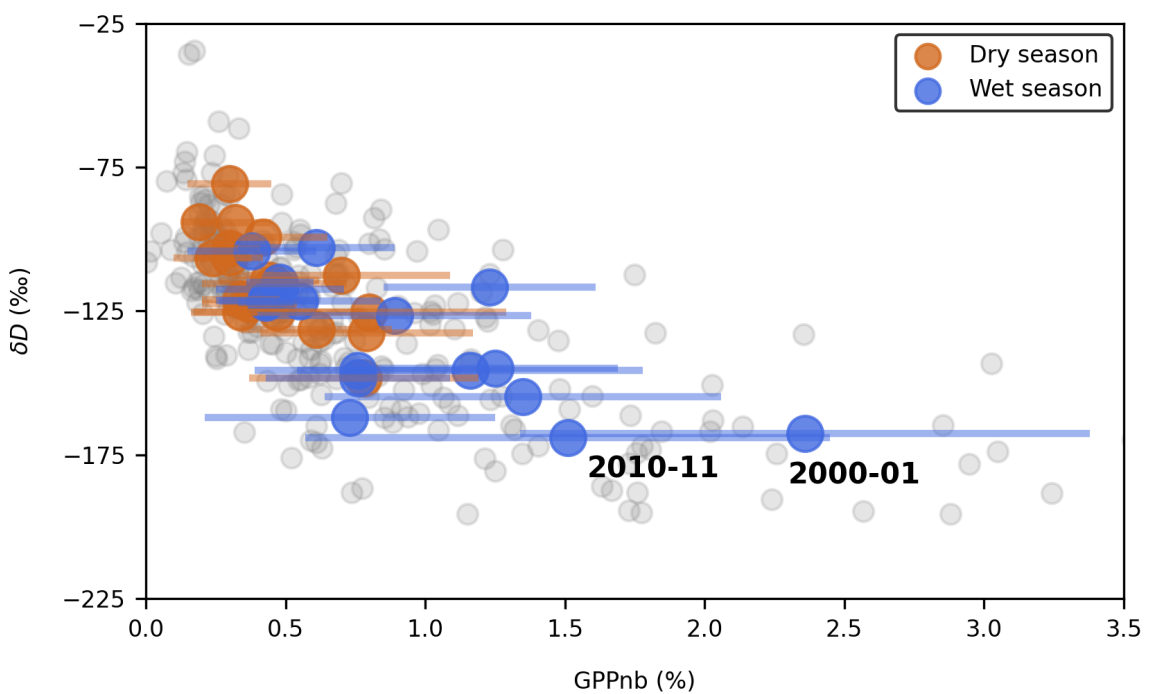


Figure 6: Seasonal mean GPPnb and δD for the dry seasons (orange circle) and the wet season (blue circle). Error bars (horizontal bands) for GPPnb are based on the mean relative standard deviation for the samples integrating each season. Light gray dots on background are raw data. The 2001-01 and 2010-11 La Niña events are reported.

In order to test the hypothesis of a relationship between giant particles and convective precipitation, we analyzed monthly precipitation and wind speed records from five meteorological stations located in the central Andes (Fig. 1). Data was provided by SENAMHI, Bolivia (www.senamhi.gob.bo/sismet), whereas monthly outgoing longwave radiation (OLR) data on a $2.5^\circ \times 2.5^\circ$ grid box (Liebmann and Smith, 1996) was obtained from NOAA/OAR/ESRL PSD, Boulder, Colorado, USA (<https://www.esrl.noaa.gov/psd/>). OLR data centered at 17.5°S , 70°W was used as an index of the convective precipitation over the Altiplano, as it presents strong negative correlations with regional rainfall observations (Garreaud and Aceituno, 2001). These datasets were re-sampled into DJF (December to February) and JJA (June to August) time series and compared with our seasonally resolved GPPnb series. For each wet and dry season, defined by dust concentration variability (Sect. 3.1), a mean GPPnb was obtained.

Results reported in Table 2 clearly show that during wet season GPPnb is positively correlated (at 95% level) to DJF precipitation at Patacamaya (17.2°S , 67.9°W , 4498 m a.s.l.). No significant correlations were found with wind speeds. Because of the convective nature of precipitation episodes, and high spatial variability in precipitation over the Bolivian Altiplano (Aceituno, 1996), it is expected that only precipitation data from stations in the closest vicinity of the Nevado Illimani show good agreement with glaciological data. Furthermore, Patacamaya was the only station in which precipitation correlated to dust related ions from Nevado Illimani during the 20th century (Knüsel et al., 2005). Thus our results also indicate that the dust record is influenced by the precipitation regime in the area south of Nevado Illimani. In agreement, by analyzing snowpits and meteorological data from 2003 to 2014 at the Quelccaya ice cap, Hurley et al. (2015) concluded that depleted δD and increased snow accumulation were related to convection along the leading edge of cold air incursions advecting from south. Both Nevado Illimani and Quellcaya ice cap show a coherent variability in their stable water isotopes record (Hoffman et al., 2003).

Table 2: Seasonal correlations between Giant Particles Percentage (GPPnb) and δD , rainfall observations and outgoing longwave radiation (OLR). The period between December and February was defined as the wet season, and the period between June and August as the dry season. Significant correlations at 95% level are shown in bold.

GPPnb	δD	El Alto	Calacoto	Patacamaya	Oruro	Potosi	OLR
Wet	-0.71	0.47	0.39	0.76	0.25	0.41	-0.69
Dry	-0.70	0.04	-0.21	-0.09	-0.08	-0.23	0.07

Also, GPPnb is negatively correlated with the DJF OLR centered over the Altiplano (Table 2), indicating that deep convection increases giant particle entrainment and suspension, humidity and precipitation over the region. We conclude that the more intense is summer convection, the higher is the relative number of giant dust particles suspended in the atmosphere and the more depleted is the δD .

During dry seasons, conversely, GPPnb is not significantly correlated with JJA OLR and precipitation (Table 2), although it is still correlated with δD , as shown by seasonal mean values reported in Fig. 6. As observed by Vimeux et al. (2005), this lack of correlation with meteorological data reflects the low and constant level of regional precipitation. However, regional JJA precipitation amounts might represent an underestimation, as considerable precipitation amounts can occur especially when cold air masses move over the Altiplano (Vuille, 1999). Thus our data potentially responds to the sparse and occasional winter convection.

Interestingly, Fig. 6 shows that over the 18-years period spanned by the Nevado Illimani firn core analyzed in this work, the summer seasons showing the most intense levels of convection were 2000-2001 and 2010-2011. Both correspond to La Niña years, as it is also clear from Fig. S3, where seasonal PC1 (proxy for convection) is compared to the Oceanic Niño Index. Some months after cooling of surface waters in the Pacific Ocean along the western coast of South America, we observe intensification of convective activity over the Altiplano. It is well known that the El Niño-Southern Oscillation phenomenon has a significant impact on climate over the Altiplano, especially during the summer season. In particular, meteorological data show that La Niña conditions intensify the meridional pressure gradient on the northern side of the Bolivian High, leading to stronger high troposphere easterly winds, increased eastward upslope flow and enhanced moisture transport (Garreaud, 1999; Vuille, 1999). Our data show that during summer seasons characterized by La Niña events, the atmospheric patterns typical of wet summer seasons are emphasized. Thus, we propose a new approach for future studies aimed at the reconstruction of paleo-ENSO at high elevation glaciological sites in the Andes based on giant particles and stable isotopes of snow, which can be used as a complement to a number of other climate proxies and modeling experiments providing insights into past ENSO variability.

Data availability

Dust (concentration, grain size, geochemistry and mineralogy), stable water isotopes and calcium data can be made available for scientific purposes upon request to the authors (contact filipelindau@hotmail.com, jefferson.simoes@ufrgs.br or barbara.delmonte@unimib.it).

Author contributions

FGLL, JCS, BD, GB wrote the original manuscript. JCS and BD designed the research. PG designed and led the drilling campaign. FGLL and PG sampled the core. FGLL, BD, GB, CIP and EDS conducted dust analyses. EK and DSI carried out the ionic and the isotopic measurements, respectively. BD, EG, SA, GB and CIP advice on data collection and interpretation. VM, CIP, PG, EG and SA provided comments to the original manuscript. VM, EG and SA provided analytical resources.

Competing interests

The authors declare that they have no conflict of interest.

Acknowledgements

We thank the drillers S. Kutuzov, L. Piard, B. Jourdain, all the operation team and the support of IRD office in Bolivia. Operations at Illimani were part of the Ice Memory project, financed by IRD, Université Grenoble Alpes, CNRS, IPEV and UMSA and by a sponsorship from the Université Grenoble Alpes Foundation. This research was partially funded by NSF project 1600018, by the Brazilian CAPES, project 88887.136384/2017-00 and a research grant from the Brazilian National Council for Scientific and Technological Development (CNPq 465680/2014-3). F.G.L. Lindau thanks CNPq for his scholarship (Processes 141013/2015-0 and 200496/2017-4).

References

- Aceituno, P.: Elementos del clima en el altiplano sudamericano, Rev. Geofis., (44), 37–55, 1996.
- Baccolo, G., Maffezzoli, N., Clemenza, M., Delmonte, B., Prata, M., Salvini, A., Maggi, V. and Previtali, E.: Low-background neutron activation analysis: a powerful tool for atmospheric mineral dust analysis in ice cores, J. Radioanal. Nucl. Chem., 306(3), 589–597, doi:10.1007/s10967-015-4206-2, 2015.
- Baccolo, G., Clemenza, M., Delmonte, B., Maffezzoli, N., Nastasi, M., Previtali, E., Prata, M., Salvini, A. and Maggi, V.: A new method based on low background instrumental neutron activation

- analysis for major, trace and ultra-trace element determination in atmospheric mineral dust from polar ice cores, *Anal. Chim. Acta*, 922, 11–18, doi:10.1016/j.aca.2016.04.008, 2016.
- Bonnaventura, H.: Etude des Phenomenes de depot et post-depot de la neige andine sur un site tropical d'altitude (Illimani - Bolivie - 6340 m) en vue de l'interpretation d'une carote de glace, Université Joseph Fourier., 2004.
- Bony, S., Risi, C. and Vimeux, F.: Influence of convective processes on the isotopic composition ($\delta^{18}\text{O}$ and δD) of precipitation and water vapor in the tropics: 1. Radiative–convective equilibrium and Tropical Ocean–Global Atmosphere-Coupled Ocean–Atmosphere Response Experiment (TOGA-COARE), *J. Geophys. Res. Atmos.*, 113(19), 1–21, doi:10.1029/2008JD009942, 2008.
- Castillo, S., Moreno, T., Querol, X., Alastuey, A., Cuevas, E., Herrmann, L., Mounkaila, M. and Gibbons, W.: Trace element variation in size-fractionated African desert dusts, *J. Arid Environ.*, 72(6), 1034–1045, doi:10.1016/j.jaridenv.2007.12.007, 2008.
- Correia, A., Freydier, R., Delmas, R. J., Simões, J. C., Taupin, J. D., Dupré, B. and Artaxo, P.: Trace elements in South America aerosol during 20th century inferred from a Nevado Illimani ice core, Eastern Bolivian Andes (6350 m asl), *Atmos. Chem. Phys.*, 3(5), 1337–1352, doi:10.5194/acp-3-1337-2003, 2003.
- Cremers, A., Elsen, A., De Preter, P. and Maes, A.: Quantitative analysis of radiocaesium retention in soils, *Nature*, 335, 247–249, 1988.
- Dansgaard, W.: Stable isotopes in precipitation, *Tellus*, 16(4), 436–468, doi:10.3402/tellusa.v16i4.8993, 1964.
- Delmonte, B., Petit, J. and Maggi, V.: Glacial to Holocene implications of the new 27000-year dust record from the EPICA Dome C (East Antarctica) ice core, *Clim. Dyn.*, 18(8), 647–660, doi:10.1007/s00382-001-0193-9, 2002.
- Delmonte, B., Petit, J. R., Andersen, K. K., Basile-Doelsch, I., Maggi, V. and Lipenkov, V. Y.: Dust size evidence for opposite regional atmospheric circulation changes over east Antarctica during the last climatic transition, *Clim. Dyn.*, 23(3–4), 427–438, doi:10.1007/s00382-004-0450-9, 2004.
- Delmonte, B., Andersson, P. S., Schöberg, H., Hansson, M., Petit, J. R., Delmas, R., Gaiero, D. M., Maggi, V. and Frezzotti, M.: Geographic provenance of aeolian dust in East Antarctica during Pleistocene glaciations: preliminary results from Talos Dome and comparison with East Antarctic and new Andean ice core data, *Quat. Sci. Rev.*, 29(1–2), 256–264, doi:10.1016/j.quascirev.2009.05.010, 2010.
- Delmonte, B., Paleari, C. I., Andò, S., Garzanti, E., Andersson, P. S., Petit, J. R., Crosta, X., Narcisi, B., Baroni, C., Salvatore, M. C., Baccolo, G. and Maggi, V.: Causes of dust size variability in central East Antarctica (Dome B): Atmospheric transport from expanded South American sources

- during Marine Isotope Stage 2, *Quat. Sci. Rev.*, 168, 55–68, doi:10.1016/j.quascirev.2017.05.009, 2017.
- Eichler, A., Gramlich, G., Kellerhals, T., Tobler, L. and Schwikowski, M.: Pb pollution from leaded gasoline in South America in the context of a 2000-year metallurgical history, *Sci. Adv.*, 1(e1400196), doi:10.1126/sciadv.1400196, 2015.
- Gabrielli, P., Wegner, A., Petit, J. R., Delmonte, B., De Deckker, P., Gaspari, V., Fischer, H., Ruth, U., Kriewa, M., Boutron, C., Cescon, P. and Barbante, C.: A major glacial-interglacial change in aeolian dust composition inferred from Rare Earth Elements in Antarctic ice, *Quat. Sci. Rev.*, 29(1–2), 265–273, doi:10.1016/j.quascirev.2009.09.002, 2010.
- Gaiero, D. M., Depetris, P. J., Probst, J. L., Bidart, S. M. and Leleyter, L.: The signature of river- and wind-borne materials exported from Patagonia to the southern latitudes: A view from REEs and implications for paleoclimatic interpretations, *Earth Planet. Sci. Lett.*, 219(3–4), 357–376, doi:10.1016/S0012-821X(03)00686-1, 2004.
- Gaiero, D. M., Simonella, L., Gassó, S., Gili, S., Stein, A. F., Sosa, P., Becchio, R., Arce, J. and Marelli, H.: Ground/satellite observations and atmospheric modeling of dust storms originating in the high Puna-Altiplano deserts (South America): Implications for the interpretation of paleoclimatic archives, *J. Geophys. Res. Atmos.*, 118(9), 3817–3831, doi:10.1002/jgrd.500362013, 2013.
- Garreaud, R., Vuille, M. and Clement, A. C.: The climate of the Altiplano: Observed current conditions and mechanisms of past changes, *Palaeogeogr. Palaeoclimatol. Palaeoecol.*, 194(1–3), 5–22, doi:10.1016/S0031-0182(03)00269-4, 2003.
- Garreaud, R. D.: Multiscale Analysis of the Summertime Precipitation over the Central Andes, *Mon. Weather Rev.*, 127(5), 901–921, doi:10.1175/1520-0493(1999)127<0901:MAOTSP>2.0.CO;2, 1999.
- Garreaud, R. D. and Aceituno, P.: Interannual rainfall variability over the South American Altiplano, *J. Clim.*, 14(1987), 2779–2789, doi:10.1175/1520-0442(2001)014<2779:IRVOTS>2.0.CO;2, 2001.
- Gili, S., Gaiero, D. M., Goldstein, S. L., Chemale, F., Jweda, J., Kaplan, M. R., Becchio, R. A. and Koester, E.: Glacial/interglacial changes of Southern Hemisphere wind circulation from the geochemistry of South American dust, *Earth Planet. Sci. Lett.*, 469, 98–109, doi:10.1016/j.epsl.2017.04.007, 2017.
- Ginot, P., Schwikowski, M., Schotterer, U., Stichler, W., Gäggeler, H. W., Francou, B., Gallaire, R. and Pouyaud, B.: Potential for climate variability reconstruction from Andean glaciochemical records, *Ann. Glaciol.*, 35(September), 443–450, doi:10.3189/172756402781816618, 2002.

- Hoffmann, G., Ramirez, E., Taupin, J. D., Francou, B., Ribstein, P., Delmas, R., Dürr, H., Gallaire, R., Simões, J., Scotterer, U., Stievenard, M. and Werner, M.: Coherent isotope history of Andean ice cores over the last century, *Geophys. Res. Lett.*, 30(4), 1179, doi:10.1029/2002GL014870, 2003.
- Hurley, J. V., Vuille, M., Hardy, D. R., Burns, S. J. and Thompson, L. G.: Cold air incursions, d₁₈O variability, and monsoon dynamics associated with snow days at Quelccaya Ice Cap, Peru, *J. Geophys. Res. Atmos.*, 120, 7467–7487, doi:10.1002/2015JD023323, 2015.
- Jiménez, N. and López-Velásquez, S.: Magmatism in the Huarina belt, Bolivia, and its geotectonic implications, *Tectonophysics*, 459(1–4), 85–106, doi:10.1016/j.tecto.2007.10.012, 2008.
- Journet, E., Balkanski, Y. and Harrison, S. P.: A new data set of soil mineralogy for dust-cycle modeling, *Atmos. Chem. Phys.*, 14(8), 3801–3816, doi:10.5194/acp-14-3801-2014, 2014.
- Knüsel, S., Ginot, P., Schotterer, U., Schwikowski, M., Gäggeler, H. W., Francou, B., Petit, J. R., Simoes, J. C. and Taupin, J. D.: Dating of two nearby ice cores from the Illimani, Bolivia, *J. Geophys. Res.*, 108(D6), 4181, doi:10.1029/2001JD002028, 2003.
- Knüsel, S., Brütsch, S., Henderson, K. A., Palmer, A. S. and Schwikowski, M.: ENSO signals of the twentieth century in an ice core from Nevado Illimani, Bolivia, *J. Geophys. Res. D Atmos.*, 110(1), 1–14, doi:10.1029/2004JD005420, 2005.
- Kutuzov, S., Legrand, M., Preunkert, S., Ginot, P., Mikhaleko, V., Shukurov, K., Poliukhov, A. and Toropov, P.: The Elbrus (Caucasus, Russia) ice core record – Part 2: history of desert dust deposition, *Atmos. Chem. Phys.*, 19(22), 14133–14148, doi:10.5194/acp-19-14133-2019, 2019.
- Lenters, J. D. and Cook, K. H.: On the Origin of the Bolivian High and Related Circulation Features of the South American Climate, *J. Atmos. Sci.*, 54(5), 656–678, doi:10.1175/1520-0469(1997)054<0656:OTOOTB>2.0.CO;2, 1997.
- Liebmann, B. and Smith, C. A.: Description of a Complete (Interpolated) Outgoing Longwave Radiation Dataset, *Bull. Am. Meteorol. Soc.*, 77(6), 1275–1277, 1996.
- Lindsay, J. M., Schmitt, A. K., Trumbull, R. B., De Silva, S. L., Siebel, W. and Emmermann, R.: Magmatic Evolution of the La Pacana Caldera System, Central Andes, Chile: Compositional Variation of Two Cogenetic, Large-Volume Felsic Ignimbrites, *J. Petrol.*, 42(3), 459–486, doi:10.1093/petrology/42.3.459, 2001.
- McBride, S. L., Robertson, R. C. R., Clark, A. H. and Farrar, E.: Magmatic and metallogenetic episodes in the northern tin belt, cordillera real, Bolivia, *Geol. Rundschau*, 72(2), 685–713, doi:10.1007/BF01822089, 1983.
- McLennan, S. M.: Rare earth elements in sedimentary rocks: influence of provenance and sedimentary processes, in *Geochemistry and Mineralogy of Rare Earth Elements*, vol. 21, pp. 169–200, De Gruyter, Berlin, Boston., 1989.

- Moreno, T., Querol, X., Castillo, S., Alastuey, A., Cuevas, E., Herrmann, L., Mounkaila, M., Elvira, J. and Gibbons, W.: Geochemical variations in aeolian mineral particles from the Sahara-Sahel Dust Corridor, *Chemosphere*, 65(2), 261–270, doi:10.1016/j.chemosphere.2006.02.052, 2006.
- Ort, M. H., Coira, B. L. and Mazzoni, M. M.: Generation of a crust-mantle magma mixture: Magma sources and contamination at Cerro Panizos, central Andes, *Contrib. to Mineral. Petrol.*, 123(3), 308–322, doi:10.1007/s004100050158, 1996.
- Osmont, D., Sigl, M., Eichler, A., Jenk, T. M. and Schwikowski, M.: A Holocene black carbon ice-core record of biomass burning in the Amazon Basin from Illimani, Bolivia, *Clim. Past*, 15(2), 579–592, doi:10.5194/cp-15-579-2019, 2019.
- Osterberg, E. C., Handley, M. J., Sneed, S. B., Mayewski, P. A. and Kreutz, K. J.: Continuous ice core melter system with discrete sampling for major ion, trace element, and stable isotope analyses, *Environ. Sci. Technol.*, 40(10), 3355–3361, doi:10.1021/es052536w, 2006.
- Paleari, C. I., Delmonte, B., Andò, S., Garzanti, E., Petit, J. R. and Maggi, V.: Aeolian Dust Provenance in Central East Antarctica During the Holocene: Environmental Constraints From Single Grain Raman Spectroscopy, *Geophys. Res. Lett.*, 1–12, doi:10.1029/2019gl083402, 2019.
- Rabatel, A., Francou, B., Soruco, A., Gomez, J., Cáceres, B., Ceballos, J. L., Basantes, R., Vuille, M., Sicart, J. E., Huggel, C., Scheel, M., Lejeune, Y., Arnaud, Y., Collet, M., Condom, T., Consoli, G., Favier, V., Jomelli, V., Galarraga, R., Ginot, P., Maisincho, L., Mendoza, J., Ménégoz, M., Ramirez, E., Ribstein, P., Suarez, W., Villacis, M. and Wagnon, P.: Current state of glaciers in the tropical Andes: A multi-century perspective on glacier evolution and climate change, *Cryosphere*, 7(1), 81–102, doi:10.5194/tc-7-81-2013, 2013.
- Ramirez, E., Hoffmann, G., Taupin, J. D., Francou, B., Ribstein, P., Caillon, N., Ferron, F. A., Landais, A., Petit, J. R., Pouyaud, B., Schotterer, U., Simoes, J. C. and Stievenard, M.: A new Andean deep ice core from Nevado Illimani (6350 m), Bolivia, *Earth Planet. Sci. Lett.*, 212(3–4), 337–350, doi:10.1016/S0012-821X(03)00240-1, 2003.
- Ribeiro, R. da R., Ramirez, E., Simões, J. C. and Machaca, A.: 46 years of environmental records from the Nevado Illimani glacier group, Bolivia, using digital photogrammetry, *Ann. Glaciol.*, 54(63), 272–278, doi:10.3189/2013AoG63A494, 2013.
- Risi, C., Bony, S. and Vimeux, F.: Influence of convective processes on the isotopic composition ($\delta^{18}\text{O}$ and δD) of precipitation and water vapor in the tropics: 2. Physical interpretation of the amount effect, *J. Geophys. Res. Atmos.*, 113(19), 1–12, doi:10.1029/2008JD009943, 2008.
- Rosso, K. M., Rustad, J. R. and Bylaska, E. J.: The Cs/K exchange in muscovite interlayers: An AB initio treatment, *Clays Clay Miner.*, 49(6), 500–513, doi:10.1346/CCMN.2001.0490603, 2001.

- Röhlisberger, R., Hutterli, M. A., Sommer, S., Wolff, E. W. and Mulvaney, R.: Factors controlling nitrate in ice cores: Evidence from the Dome C deep ice core, *J. Geophys. Res. Atmos.*, 105(D16), 20565–20572, doi:10.1029/2000JD900264, 2000.
- Rudnick, R. L. and Gao, S.: Composition of the Continental Crust, in *Treatise on Geochemistry*, vol. 1, pp. 1–64., 2003.
- Samuels-Crow, K. E., Galewsky, J., Hardy, D. R., Sharp, Z. D., Worden, J. and Braun, C.: Upwind convective influences on the isotopic composition of atmospheric water vapor over the tropical Andes, *J. Geophys. Res. Atmos.*, 119, 7051–7063, doi:10.1002/2014JD021487. Received, 2014.
- Segura, H., Espinoza, J. C., Junquas, C., Lebel, T., Vuille, M. and Garreaud, R.: Recent changes in the precipitation-driving processes over the southern tropical Andes/western Amazon, *Clim. Dyn.*, 54(5–6), 2613–2631, doi:10.1007/s00382-020-05132-6, 2020.
- Sen, I. S. and Peucker-Ehrenbrink, B.: Anthropogenic disturbance of element cycles at the Earth's surface, *Environ. Sci. Technol.*, 46(16), 8601–8609, doi:10.1021/es301261x, 2012.
- Soruco, A., Vincent, C., Rabatel, A., Francou, B., Thibert, E., Sicart, J. E. and Condom, T.: Contribution of glacier runoff to water resources of La Paz city, Bolivia (16° S), *Ann. Glaciol.*, 56(70), 147–154, doi:10.3189/2015AoG70A001, 2015.
- Thompson, L. G., Mosley-Thompson, E., Dansgaard, W. and Grootes, P. M.: The Little Ice Age as Recorded in the Stratigraphy of the Tropical Quelccaya Ice Cap, *Science* (80-.), 234, 361–364, 1986.
- Thompson, L. G., Mosley-Thompson, E., Davis, M. E., Zagorodnov, V. S., Howat, I. M., Mikhalenko, V. N. and Lin, P.-N.: Annually resolved ice core records of tropical climate variability over the past ~1800 years., *Science*, 340(6135), 945–50, doi:10.1126/science.1234210, 2013.
- Thompson, L. G., Davis, M. E., Mosley-Thompson, E., Beaudon, E., Porter, S. E., Kutuzov, S., Lin, P.-N., Mikhalenko, V. N. and Mountain, K. R.: Impacts of recent warming and the 2015/16 El Niño on tropical Peruvian ice fields, *J. Geophys. Res. Atmos.*, 688–701, doi:10.1002/2017JD026592, 2017.
- Uemura, R., Masson-Delmotte, V., Jouzel, J., Landais, A., Motoyama, H. and Stenni, B.: Ranges of moisture-source temperature estimated from Antarctic ice cores stable isotope records over glacial–interglacial cycles, *Clim. Past*, 8(3), 1109–1125, doi:10.5194/cp-8-1109-2012, 2012.
- Vera, C., Higgins, W., Amador, J., Ambrizzi, T., Garreaud, R., Gochis, D., Gutzler, D., Lettenmaier, D., Marengo, J., Mechoso, C. R., Nogues-Paegle, J., Silva Dias, P. L. and Zhang, C.: Toward a unified view of the American monsoon systems, *J. Clim.*, 19(20), 4977–5000, doi:10.1175/JCLI3896.1, 2006.

- Vimeux, F., Gallaire, R., Bony, S., Hoffmann, G. and Chiang, J. C. H.: What are the climate controls on δD in precipitation in the Zongo Valley (Bolivia)? Implications for the Illimani ice core interpretation, *Earth Planet. Sci. Lett.*, 240(2), 205–220, doi:10.1016/j.epsl.2005.09.031, 2005.
- Vimeux, F., Ginot, P., Schwikowski, M., Vuille, M., Hoffmann, G., Thompson, L. G. and Schotterer, U.: Climate variability during the last 1000 years inferred from Andean ice cores: A review of methodology and recent results, *Palaeogeogr. Palaeoclimatol. Palaeoecol.*, 281(3–4), 229–241, doi:10.1016/j.palaeo.2008.03.054, 2009.
- Vlastelic, I., Suchorski, K., Sellegri, K., Colomb, A., Nauret, F., Bouvier, L. and Piro, J. L.: The high field strength element budget of atmospheric aerosols (puy de Dôme, France), *Geochim. Cosmochim. Acta*, 167, 253–268, doi:10.1016/j.gca.2015.07.006, 2015.
- Vuille, M.: Atmospheric Circulation Over the Bolivian Altiplano During Dry and Wet Periods and Extreme Phases of the Southern Oscillation, , 1600, 1579–1600, 1999.
- Vuille, M., Bradley, R. S., Healy, R., Werner, M., Hardy, D. R., Thompson, L. G. and Keimig, F.: Modeling delta $d_{18}O$ in precipitation over the tropical Americas: 2. Simulation of the stable isotope signal in Andean ice cores, *J. Geophys. Res.*, 108(D6), 4175, doi:10.1029/2001JD002039, 2003.
- Wu, G., Zhang, X., Zhang, C. and Xu, T.: Mineralogical and morphological properties of individual dust particles in ice cores from the Tibetan Plateau, *J. Glaciol.*, 62(231), 46–53, doi:10.1017/jog.2016.8, 2016.
- Zhou, J. and Lau, K. M.: Does a monsoon climate exist over South America?, *J. Clim.*, 11(5), 1020–1040, doi:10.1175/1520-0442(1998)011<1020:DAMCEO>2.0.CO;2, 1998.

Supporting Information

Giant dust particles at Nevado Illimani: a proxy of summertime deep convection over the Bolivian Altiplano

Filipe G. L. Lindau¹, Jefferson C. Simões^{1,2}, Barbara Delmonte³, Patrick Ginot⁴, Giovanni Baccolo³, Chiara I. Paleari³, Elena Di Stefano³, Elena Korotkikh², Douglas S. Introne², Valter Maggi³, Eduardo Garzanti³, Sergio Andò³

¹Centro Polar e Climático, Universidade Federal do Rio Grande do Sul, Porto Alegre, 91501-970, Brazil

²Climate Change Institute, University of Maine, Orono, ME 04469, USA

³Environmental and Earth Sciences Department, University Milano-Bicocca, Milan, 20126, Italy

⁴CNRS, IRD, IGE, University Grenoble Alpes, Grenoble, 38041, France

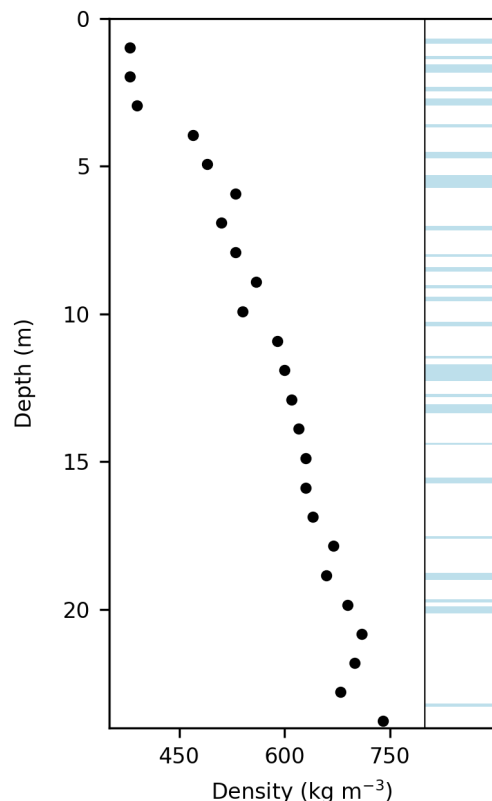


Figure S1: The Nevado Illimani firn core density profile. The right panel refer to depth intervals where groups of ice layers were observed.

Table S1: Sections of the Nevado Illimani firn core analysed for elemental (N1 to N10) and mineralogical (R1 to R4) composition.

Sample	N1	N2	N3	N4	N5	N6	N7	N8	N9	N10	R1	R2	R3	R4
Top depth (m)	1.67	2.31	5.57	8.67	10.56	13.60	13.69	19.10	20.29	21.41	5.79	5.91	9.80	10.00
Bottom depth (m)	2.31	3.78	7.02	8.97	11.66	13.69	14.78	19.25	20.48	22.50	5.82	6.00	9.84	10.17

Table S2: Average elemental concentrations measured by Instrumental Neutron Activation Analysis, and the procedural errors and the detection limits (DL). For comparison, we also present mean concentrations of dust particles from high elevation ice cores in the Alps (Thevenon et al., 2009) and in the Tibetan Plateau (Wu et al., 2009).

Element	Ce	Cs	Eu	Hf	La	Sc	Sm	Th	Yb
Concentration (ppm)	89.8	21.1	1.60	13.1	40.8	13.7	8.14	17.6	2.71
Error (%)	7.24	13.8	6.65	9.97	4.05	3.97	7.27	7.16	10.8
DL (ppm)	7	4	0.8	3	0.5	0.3	0.1	4	0.1
Colle Gnifetti ice core, Alps (ppm)	1.76	1.20	1.78	5.24	2.74	18.6	4.63	3.49	6.25
Dunde ice core, Tibetan Plateau (ppm)	65.7		1.09	4.04	32.6		5.51	14.3	2.93

Table S3: Mineral phases and relative abundance (number of grains, %) in Illimani firn from different time periods.

	R1	R2	R3	R4
Year	2010	2009-10	2004-05	2004
Season	dry	wet	wet	dry
Particles analyzed	167	161	138	167
	N (%)	N (%)	N (%)	N (%)
Quartz and polymorphs	31.7	21.7	13.8	23.4
K-feldspars	7.2	10.6	5.1	11.4
Plagioclases	10.8	9.3	7.2	18.6
Muscovite-illite-smectite	23.4	29.2	59.4	19.2
Other phyllosilicates	0.6	1.2	0.0	1.2
Clay minerals (kaolinite)	0.6	1.2	0.0	3.0
Clinopyroxenes	0.0	0.6	0.0	0.0
Orthopyroxenes	0.0	0.0	0.0	0.0
Amphiboles	0.0	0.0	0.0	0.0
Rutile	2.4	2.5	0.0	0.6
Anatase	4.2	6.8	4.3	2.4
Hematite	9.0	8.7	7.2	14.4
Goethite	8.4	5.6	1.4	3.0
Carbonates	0.0	1.2	0.0	0.0
Epidotes	0.0	0.0	0.0	0.0
Titanite	0.0	0.0	0.0	0.0
Tourmaline	1.2	0.0	0.7	0.6
Other heavy minerals	0.6	1.2	0.7	1.2
Other light minerals	0.0	0.0	0.0	1.2
Total	100	100	100	100

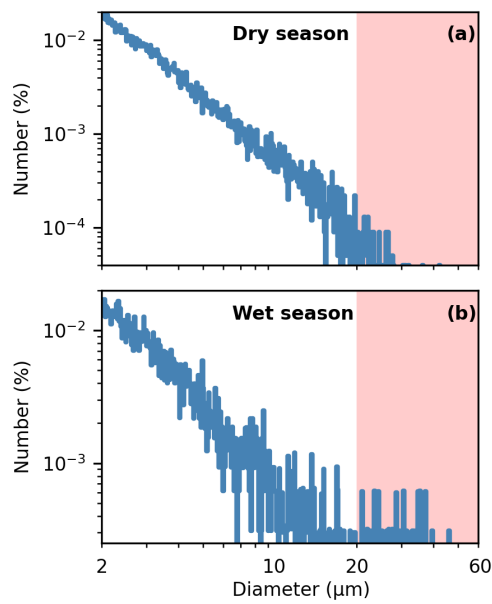


Figure S2: The number size distribution of a typical sample from the (a) dry and (b) wet season. Red areas highlight the giant particles (between 20 and 60 μm).

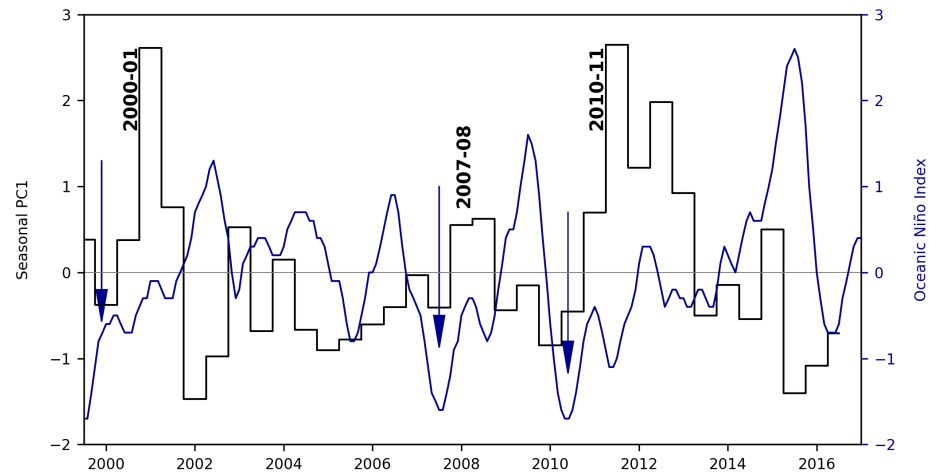


Figure S3: Comparison of the seasonal PC1 of GPPnb and δD (black line) and the Oceanic Niño Index (ONI) (blue line) typically used for identifying El Niño (warm) and La Niña (cool) events in the tropical Pacific. It is possible to note that the highest convection (high PC1) is associated to summer seasons of La Niña years.

References

- Thevenon, F., Anselmetti, F. S., Bernasconi, S. M. and Schwikowski, M.: Mineral dust and elemental black carbon records from an Alpine ice core (Colle Gnifetti glacier) over the last millennium, *J. Geophys. Res. Atmos.*, 114(17), 1–11, doi:10.1029/2008JD011490, 2009.
- Wu, G., Zhang, C., Gao, S., Yao, T., Tian, L. and Xia, D.: Element composition of dust from a shallow Dunde ice core, Northern China, *Glob. Planet. Change*, 67(3–4), 186–192, doi:10.1016/j.gloplacha.2009.02.003, 2009.

5.2 Proxies for atmospheric circulation over the Amazon basin from the aerosol composition in a Nevado Illimani firn core, Bolivia

Artigo submetido para a revista Journal of Geophysical Research – Atmospheres. Email de submissão no Anexo III.

**Proxies for atmospheric circulation over the Amazon
basin from the aerosol composition in a Nevado
Illimani firn core, Bolivia**

**Filipe G. L. Lindau¹, Jefferson C. Simões^{1,2}, Michael Handley², Elena
Korotkikh², Patrick Ginot³, Rafael R. Ribeiro¹**

¹Centro Polar e Climático, Universidade Federal do Rio Grande do Sul, Porto Alegre, 91501-970, Brazil

²Climate Change Institute, University of Maine, Orono, ME 04469, USA

³Univ. Grenoble Alpes, CNRS, IRD, Grenoble INP, IGE, 38000 Grenoble, France

Key Points

- Enhanced low level jets over the Amazon basin in 2015 increased S and Mn Efs in Illimani
- The Mn EF record can be used as a new proxy for atmospheric circulation over the Amazon basin
- 21st century Cr pollution over the Altiplano is lower than during the late 20th century

Abstract

Current changes in tropical South America due to atmospheric warming, deforestation, and glacier retreat impact moisture and water exchange between the Amazon basin and the Andes. Thus, a deeper understanding of past atmospheric variability is crucial for developing strategies for climate and environmental change scenarios in this region. Within this context, we investigated an 18-year firn core drilled at the Illimani to interpret its aerosol composition (trace elements and major ions) in relation to seasonal processes, particularly atmospheric circulation over the Amazon basin. The resulting 21st-century record showed reduced Cr contamination over the Altiplano in comparison to the late 20th century, which was probably related to reduced emissions from mining activities. Sulfur records suggest the influence of volcanic eruptions in 2006 (Rabaul) and 2014 (Nyamuragira-Nyiragongo). Overall, the aerosol composition was mainly modulated by precipitation variability over the Altiplano at both annual and seasonal timescales. However, Mn was enriched due to strengthened low-level jets in the Amazon basin during the dry season, especially in 2015. This was corroborated by the reanalysis data. Furthermore, Mn, Co, and Fe showed an unprecedented peak in the record during the wet season of 2014, which was consistent with the arrival of a dust plume from Africa over Amazonia. Therefore, the Mn enrichment record can be used as a new proxy for obtaining information about the South American Low-Level Jet, and, when considered together with more elements, might also indicate snow layers that were possibly loaded with aerosols from Africa.

1 Introduction

Atmospheric mechanisms involving Amazon-Andes connectivity in terms of evapotranspiration, moisture transport, and local convection are of particular importance to better understand hydrological disruption (related to deforestation, glacier retreat, and climate change) over that region (Espinoza et al., 2020). Beyond supplying water vapor, Amazonia exports biogenic aerosols and ashes to tropical Andes glaciers through dominant easterly trade winds. This might impact glacier mass balance by reducing the snow albedo (de Magalhães et al., 2019), but may also be recorded in their snow layers as a natural archive of the biogeochemical cycles regulating forest and climate feedbacks. Aerosols emitted from the Amazon basin have already been detected in firn and ice cores recovered at Nevado Illimani (hereafter Illimani, 16°37'S, 67°46'W, 6350 m a.s.l., Figure 1) and used as a paleothermometer of tropical South America (Kellerhals et al., 2010). In addition, higher temperatures over the Amazon basin are related to events of biomass-burning, which increases the concentration of refractive black carbon in Illimani (Osmont et al., 2019). However, aerosols deposited at Illimani mainly reflect conditions over its main source, which is the Altiplano (Figure 1), obfuscating the contribution of biogenic and/or biomass-burning material (Correia et al., 2003; Lindau et al., 2020).

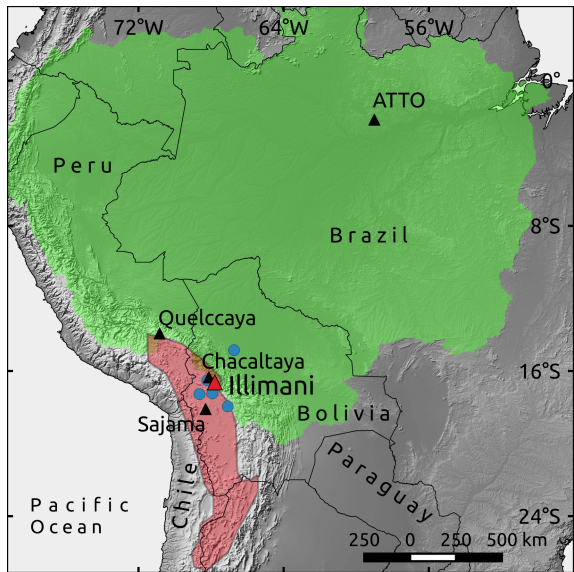


Figure 1. Location of Illimani (red triangle) whose records were compared to ice core (Quelccaya and Sajama) and atmospheric (Chacaltaya and ATTO) data (black triangles). Blue dots indicate the meteorological stations that provided precipitation data. Green and red areas delimit the Amazon basin and the Altiplano, respectively. The land basemap was obtained from Natural Earth (<http://www.naturalearthdata.com>).

Moreover, low-level northeasterly flow over the Amazon basin was found to be related to the increased deposition of Amazon-sourced aerosol (more concentrated in nitrate and ammonium) in Quelccaya ($13^{\circ}54'S$, $70^{\circ}48'W$, 5670 m a.s.l., Figure 1) (Thompson et al., 2013). This circulation, the South American Low-Level Jet (SALLJ), is a common feature of the South American climate. The SALLJ delivers vast quantities of moisture originating in the Atlantic Ocean or in the Amazon basin over regions of Bolivia, Paraguay, and southern Brazil (Marengo, 2004). It is observed throughout the year and is a dominant feature of the South American Summer Monsoon (SAMS) (Vera et al., 2006). In addition, the Bolivian high, an upper tropospheric anticyclone located over Bolivia, is established during the mature phase of the SAMS, leading to upper tropospheric easterly winds that favor the transport of moist air from the Amazon lowlands toward the Altiplano (Lenters & Cook, 1997; Garreaud, 1999). However, since the onset of the 21st century, interannual fluctuations of southern tropical Andes precipitation, which includes the Bolivian Altiplano, started to be more associated with strengthened low-level northerlies originating over the tropical North Atlantic, and less with upper-level easterly anomalies related to the Bolivian high (Segura et al., 2020). Moreover, the intensity and frequency of the SALLJ have shown an increase in the last decades in most seasons, increasing precipitation in the eastern Andes of Bolivia (Jones, 2019).

Considering that ice cores from the southern tropical Andes store high-resolution information over the last millennia (Vimeux et al., 2009), a high temporal resolution record of the aerosol composition during the current period of accentuated climate variability might be

valuable for further analyzing these changes over a longer timeframe. Therefore, we will relate atmospheric observations over both the Altiplano and the Amazon basin, with the composition of the aerosol deposited at Illimani, by analyzing the elemental and ionic composition of a firn core spanning the 1999–2016 period.

2 Methods

2.1 Field Campaign and Firn Core Sampling

In June 2017, a 23.8 m firn core (IL2017) with a diameter of 10 cm was retrieved at an altitude of 6350 m a.s.l. on the saddle between the two Illimani summits, approximately where two deep ice cores were drilled in June 1999 (IL1999) (Knüsel et al., 2003). The expedition was coordinated by a French, Russian, Bolivian, and Brazilian team and integrated the Ice Memory project (Université Grenoble Alpes Foundation). After the drilling campaign, the container was shipped to the Institut des Géosciences de l'Environnement (IGE, Université Grenoble Alpes, France), where the core sections were weighed and cut longitudinally using a vertical band saw in a cold room (at -20 °C). One quarter of the original core was used for dust analysis at EuroCold (University of Milano-Bicocca, Italy).

Another quarter of the core was shipped in a frozen state to the Climate Change Institute (CCI, University of Maine, USA) for isotopic, ionic, and elemental analyses. At the CCI, in a cold room set at -20 °C, sections of the core were cut longitudinally with a vertical band saw to separate the inner and outer parts. The inner part (used for ionic and elemental analysis) was decontaminated by scraping with a clean ceramic knife under a laminar flow HEPA bench inside the cold room. Then, the decontaminated inner part was sampled using a continuous melter system (Osterberg et al., 2006) in an ISO 6 Class clean room, yielding 767 samples (mean sample resolution of 3 cm). The samples for elemental analysis were collected into acid-cleaned (Optima HNO₃) low-density polyethylene (LDPE) vials and acidified with double-distilled HNO₃. This procedure was conducted using an ISO 5 laminar flow HEPA bench. Samples were stored for acidification at room temperature for approximately 1 month. The dilution rate reached using this acidification method may vary depending on the element. Using samples from Huascarán and Quelccaya (Figure 1), Uglietti et al. (2014) obtained a mean final recovery for Al on the order of 10% of its total concentration; conversely, Pb, As, and Mn showed final recoveries of approximately 80% (Uglietti et al., 2014).

2.2 Firn Core Analysis and Proxy Determination

The concentrations of the major ions (Na^+ , K^+ , Mg^{2+} , Ca^{2+} , Cl^- , NO_3^- and SO_4^{2-}) were measured by ion chromatography (IC). We used a Thermo Scientific™ Dionex™ Ion Chromatograph ICS-6000 analytical system at the CCI. The method detection limit (MDL, Table 1) was defined as three times the standard deviation of the blank samples (MilliQ® water, 10 blank samples). Blank concentrations were subtracted from each measurement.

Concentrations for 28 elements were measured using the CCI Thermo Scientific ELEMENT 2 inductively coupled plasma sector field mass spectrometer (ICP-SFMS) coupled to an ESI model SC-4 autosampler. The ICP-SFMS was calibrated daily with five standards, and as a reference, we used the SLRS-4 certified water (National Resource Council, Canada). Blanks were prepared with MilliQ® water, and the method blank was subtracted from each sample. The MDLs for the studied elements are listed in Table 1.

Because concentrations are partially modulated by snow accumulation at the drilling site, which can dilute the dominant dry deposition of the chemical species, we calculated the enrichment factors (EFs). They are independent of changes in accumulation, reflecting variations in emission sources and/or transport (Gabrielli et al., 2020). The EF normalization was calculated for the studied elements according to:

$$EF(X) = \frac{\left(\frac{[X]}{[CrustalElement]} \right)_{sample}}{\left(\frac{[X]}{[CrustalElement]} \right)_{UCC}} \quad (1)$$

where X is the element of interest, and the mean composition of the upper continental crust was obtained from Wedepohl (1995). We used Sr as a proxy for rock and soil dust, as its biogeochemical cycle is almost unaffected by anthropogenic activities (Sen & Peucker-Ehrenbrink, 2012). In addition, Sr is highly correlated with other lithogenic elements, such as Ba ($R^2 = 0.93$) and Ce ($R^2 = 0.88$), both of which have already been used as a crustal reference in tropical Andean ice cores (Hong et al., 2004; Eichler et al., 2015). Finally, Sr was precisely determined by ICP-SFMS (Table 1).

Furthermore, we calculated the $\text{SO}_4^{2-}exc$, which is considered to be a good proxy for atmospheric H_2SO_4 , originating exclusively from the oxidation of SO_2 in the atmosphere (Schwikowski et al., 1999; De Angelis et al., 2003). $\text{SO}_4^{2-}exc$ is the gypsum-like fraction of sulfate; thus, the calculation considers that Ca^{2+} is entirely deposited as CaSO_4 . We estimated the Cl^- present as HCl by calculating the Cl^-exc , in accordance with De Angelis et al. (2003):

$$\text{Cl}^-exc = (\text{Cl}^-_{total} - \text{Cl}^-_{soil}) - 1.7(\text{Na}^+_{total} - \text{Na}^+_{soil}) \quad (2)$$

where Cl^-_{soil} and Na^+_{soil} were calculated from Ca^{2+} concentrations using the $\text{Cl}^-/\text{Ca}^{2+}$ and $\text{Na}^+/\text{Ca}^{2+}$ mass ratio of the Ca^{2+} in the dry season of 2009, when the $\text{SO}_4^{2-}exc/\text{SO}_4^{2-}$ ratio was lower than 10%, which indicates low acid deposition.

Table 1. Method detection limit (MDL) and mean concentrations measured by ion chromatography (IC) and inductively coupled plasma sector field mass spectrometry (ICP-SFMS).

	Unit	Method blank	MDL	Mean 1999–2016
Na ⁺	ng g ⁻¹	4.4	1.9	30.9
K ⁺	ng g ⁻¹	1.0	1.1	12.7
Mg ²⁺	ng g ⁻¹	5.3	0.9	11.4
Ca ²⁺	ng g ⁻¹	16.7	21.1	88.9
Cl ⁻	ng g ⁻¹	10.9	4.9	56.7
NO ₃ ⁻	ng g ⁻¹	14.9	4.4	185.9
SO ₄ ²⁻	ng g ⁻¹	35.2	57.3	381.8
Li	pg g ⁻¹	15.8	4.4	101.5
Na	pg g ⁻¹	403	6213	39581
Mg	pg g ⁻¹	797	2269	18620
Al	pg g ⁻¹	247	2713	39855
Si	pg g ⁻¹	42523	39516	219292
S	pg g ⁻¹	823	2065	182636
K	pg g ⁻¹	872	4422	26022
Ca	pg g ⁻¹	2547	3977	58609
Sc	pg g ⁻¹	2.2	0.30	2.34
Ti	pg g ⁻¹	49.8	557	3580
V	pg g ⁻¹	0.8	10.5	68.7
Cr	pg g ⁻¹	3.7	7.7	48.8
Mn	pg g ⁻¹	32.0	114	2076
Fe	pg g ⁻¹	476	8142	52082
Co	pg g ⁻¹	0.20	2.2	33.1
Cu	pg g ⁻¹	50.8	57.7	620
Zn	pg g ⁻¹	235	417	1321
As	pg g ⁻¹	3.6	18.4	208.4
Sr	pg g ⁻¹	3.4	48.8	634
Ag	pg g ⁻¹	0.6	0.5	2.96
Cd	pg g ⁻¹	0.5	1.3	8.3
Cs	pg g ⁻¹	0.4	1.6	30.6
Ba	pg g ⁻¹	32.2	258	1512
La	pg g ⁻¹	0.1	1.1	7.34
Ce	pg g ⁻¹	0.1	2.1	14.9
Pr	pg g ⁻¹	0.01	0.3	1.73
Pb	pg g ⁻¹	2.9	5.1	234.8
Bi	pg g ⁻¹	0.2	0.5	9.44
U	pg g ⁻¹	0.1	0.1	3.9

2.2 Seasonally Resolved Chronology and Climate Records

The annual signal in ice cores from Illimani is considered to be largely preserved because precipitation and ablation seasons are relatively distinct (De Angelis et al., 2003). During the dry season, post-depositional processes such as sublimation can significantly perturb the chemical composition of the surface snow (Ginot et al., 2001). However, the sublimation rate at the Illimani site during the dry season of 2001 was -0.7 mm w.e. d⁻¹, whereas a significantly higher snow accumulation (21 cm) occurred during this same period (De Angelis et al., 2003; Wagnon et al., 2003). Thus, a detailed stratigraphy based on the

combination of three strong seasonal signals (dust particle concentration, Ca^{2+} , and water stable isotopes) allowed the identification of annual layers along the profile and provided a year-by-year dating of the IL2017 firn core (Lindau et al., 2020). The IL2017 chronology covers the period from 1999 to 2016. Then, data were classified by season following the procedures in Lindau et al. (2020) and Correia et al. (2003) by individually grouping the samples into three categories (“dry,” “wet,” and “transition”) according to dating and dust concentration levels (Figure 2). We obtained 73 (28%) cases of dry samples and 126 (49%) of wet samples.

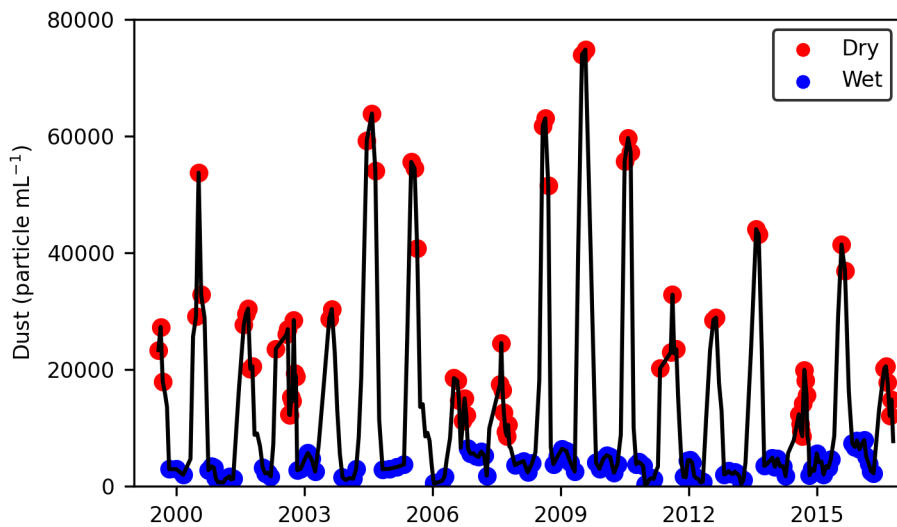


Figure 2. Seasonal classification of Illimani samples into wet (blue dots) and dry (red dots) seasons based on the dust record from (Lindau et al., 2020).

We used in situ monthly precipitation from four rain-gauge stations located in the Bolivian Altiplano (El Alto, Calacoto, Patacamaya, and Oruro) and one in the Bolivian Amazon (San Borja, Figure 1) over the 1999–2016 period obtained from the Bolivian National Service of Meteorology and Hydrology (SENAMHI) network (www.senamhi.gob.bo/sismet) with monthly resolution. For the precipitation records from the Altiplano, the seasonal variability was eliminated by subtracting the monthly mean of the respective time series in each month. Then, each time series was normalized using its mean and standard deviation values. Finally, we calculated the principal components (PC) of precipitation in the Bolivian Altiplano. The first PC (PC1r) explained 62% of the total precipitation variance. The high correlations ($r > 0.7$, $p\text{-value} < 0.01$) obtained for all stations indicate that the area we chose was influenced by a common mode of rainfall variability.

The reanalysis data set from the European Center for Medium Range Weather Forecasts (ECMWF, ERA5) and ERA-Interim were obtained at the KMNI Climate Explorer (<http://climexp.knmi.nl/getindices>) and the Climate Reanalyzer (<https://climatereanalyzer.org>), respectively, with monthly resolution. Backward and forward

air mass trajectories were calculated using HYSPLIT (<https://www.ready.noaa.gov/>). The NOAA Global Data Assimilation System data at $1^{\circ} \times 1^{\circ}$ resolution were used as meteorological input for HYSPLIT.

3 Results and Discussion

3.1 Comparison with Records from the 20th Century

To relate the elemental and ionic records in Illimani during the 1999–2016 period (IL2017) with other ice core records, we calculated a decadal (2005–2015) mean concentration for each element. Table 2 shows an equal resolution comparison between the IL2017 decadal mean and records covering the 1980–1990 period in both Illimani (IL1999) (Correia et al., 2003; De Angelis et al., 2003) and Quelccaya (Uglietti et al., 2015) ice cores. We observed a difference of one order of magnitude between the Al concentrations of the Illimani records. This is possibly related to differences in sample acidification (Section 2.2). An acid digestion method was applied by Correia et al. (2003), and we believe this was one of the major causes for the differences observed for Al, Co, and Cu. Conversely, for elements that are less sensitive to different acidification conditions (e.g., Mn, As, Pb) (Uglietti et al., 2014), we observed minor differences. In fact, the major ions showed slightly higher concentrations during the early 21st century (Table 2).

Despite the variations in elemental concentrations due to distinct leaching, EF interpretation is less affected as larger variations are allowed to classify sources in crustal or non-crustal (EF larger or smaller than 10) (Uglietti et al., 2014). Non-crustal elements for all IL2017, IL1999, and Quelccaya were As, Cu, and Cd (Table 2). Interestingly, Cr EF showed a reduction in the 21st century as it was >10 for both IL1999 and Quelccaya, but in IL2017, it was close to unity (Table 2). The presence of anthropogenic Cr in an ice core from the Alps was attributed to iron, steel, and ferro-alloy production (Van De Velde et al., 1999); ferromolybdenum is produced in northern Chile as a sub-product of Cu production. An unprecedented rise in Cu EF (over the last two millennia) was observed during the second half of the 20th century in Illimani, followed by a decrease since the 1990s due to the regulation of smelter emissions in Chile (Eichler et al., 2017). Thus, according to our record, Cr was efficiently controlled by reduced emission rates from smelters, although other mining and smelter-related elements such as Cu, Cd, Zn, As, and Ag are still enriched in Illimani. Indeed, we observed a considerable anthropogenic contribution for Zn, As, and Ag in Illimani during both the 20th and 21st centuries (Table 2).

Bi was not analyzed in IL1999, and in Quelccaya it showed a low EF during the 20th century (Table 2). Conversely, it was enriched (Bi EF = 22) in an ice core from Sajama (Figure 1) during the late 20th century (Hong et al., 2004). Bi might also be enriched by volcanic fallout; in that case, it would probably be related to a higher S EF (Ferrari et al., 2000; Kaspari et al., 2009). Although S was analyzed only in IL2017, the high mean EF observed in Table 2 was expected because S might be associated with SO₂ sourced by

smelting, fossil fuel combustion, and biomass burning, which, in turn, had an impact on records from Illimani (Eichler et al., 2015; Brugger et al., 2019; Osmont et al., 2019).

Table 2. Decadal comparison between 21st-century records from Illimani (ILL2017) and 20th century records from Illimani (ILL1999) and Quelccaya (QCY). Enrichment factors (EF) higher than 10 are shown in bold.

	2005–2015		1980–1990		Quelccaya	
	ILL2017		ILL1999		Quelccaya	
	Conc. (pg g ⁻¹)	EF	Conc. (pg g ⁻¹)	EF	Conc. (pg g ⁻¹)	EF
Li	102	2.4	216	4.1		
Na	39829	1.0	63145	1.0		
Mg	19179	0.7	29907	0.9		
Al	40409	0.3	194292	1.0	51476	1.2
S	166195	121				
K	26094	0.5	88962	1.3		
Ca	55335	1.1	82546	1.3		
Sc	2.27	0.2	39.4	2.3		
Ti	3773	0.5	13389	1.6	2302	0.6
V	70.5	0.6	298	1.6	80.9	2.2
Cr	49	0.7	2136	26	82.2	11
Mn	2026	2.0	3116	2.6		
Fe	57125	0.9	105073	1.3	43932	1.0
Co	31.9	1.6	375	15	17.4	4.0
Cu	611	27	4276	136	248	22
Zn	1297	14	3533	34		
As	216	72	668	159	147	2.7
Sr	640	1.0	1105	1.5		
Ag	3.11	33	3.52	34	1.96	8.0
Cd	8.14	48	16.1	70	4.55	70
Cs	30.7	2.9	43.2	3.0		
Ba	1626	1.0	2432	1.5		
La	8.14	0.1	111	1.4		
Ce	16.2	0.1	235	1.4		
Pr	1.92	0.1	25.0	1.6		
Pb	231	7.1	364	9.3	313	6.3
Bi	10.2	52			9.95	2.3
U	3.88	0.8	10.4	1.7	10.4	0.3
	Conc. (ng g ⁻¹)		Conc. (ng g ⁻¹)			
Na ⁺	30.6		18.4			
K ⁺	11.8		11.3			
Mg ²⁺	11.1		6.0			
Ca ²⁺	86.5		46.5			
Cl ⁻	54.8		33.5			
NO ₃ ⁻	177		138			
SO ₄ ²⁻	349		325			

3.2 Potential Volcanic Signatures

Sulfur EF showed a good correspondence with $\text{SO}_4^{2-}\text{exc}$, showing peaks when $\text{SO}_4^{2-}\text{exc}/\text{SO}_4^{2-}$ was higher than 75% (Figure 3). In ice cores, $\text{SO}_4^{2-}\text{exc}$ is often used as a proxy for volcanic eruptions. Furthermore, if $\text{SO}_4^{2-}\text{exc}$ variability is related to volcanic eruptions, the deposition of halogen gases such as HCl would also be expected (De Angelis et al., 2003). We observed a spike for both Cl^{-}exc and $\text{SO}_4^{2-}\text{exc}$ only during the transition and wet seasons of 2014/15. In September 2014, SO_2 emissions from the Nyamuragira-Nyiragongo volcanoes ($1^{\circ}24'S$; $29^{\circ}12'E$, 3058 m a.s.l, Democratic Republic of the Congo) crossed the Atlantic Ocean (Figure S1), and were detected at the Amazon Tall Tower Observatory (ATTO, Figure 1) by an anomalously high atmospheric SO_4^{2-} concentration (Saturno et al., 2018). Back trajectories indicate that the SO_2 plume that arrived in ATTO could have reached Illimani as air parcels over Illimani were mostly from the northeast (Figure 4), thus probably carrying aerosols from the Amazon basin (Chauvigné et al., 2019).

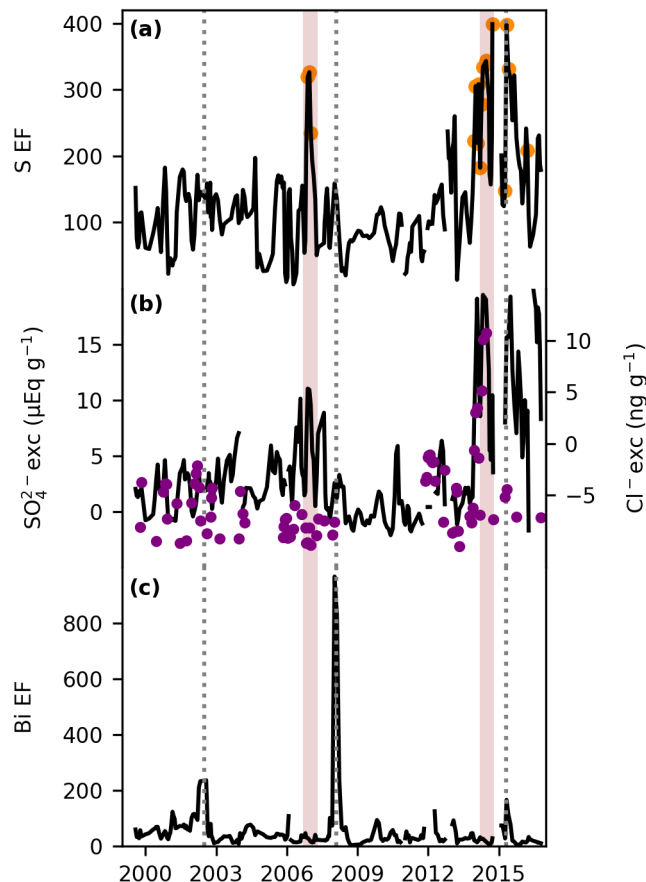


Figure 3. Volcanic proxy records, all data represent three-sample mean values. (a) The enrichment factor (EF) variability for S, the orange dots indicate periods when the excess of SO_4^{2-} represented more than 75% of the total SO_4^{2-} concentration. (b) Both the $\text{SO}_4^{2-}\text{exc}$ (black line) and the excess of Cl^{-} (purple dots). The vertical brown bands in both 2006 and 2014 indicate the probable volcanic signals of the Rabuk and Nyamuragira-Nyiragongo eruptions, respectively. (c) The EF for Bi, highlighting the period for its major spikes (vertical dotted line).

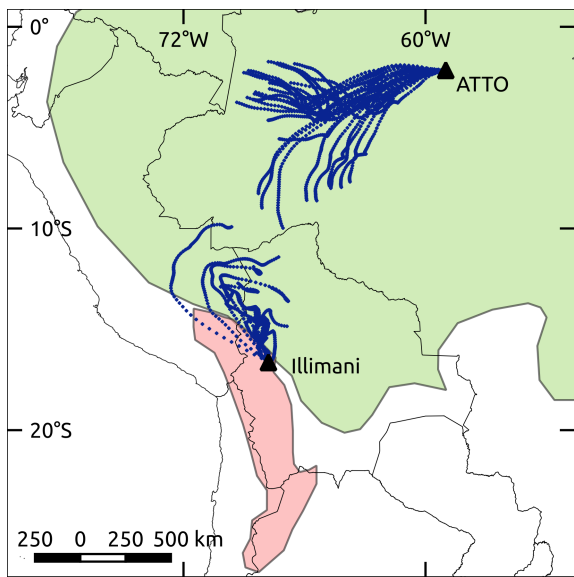


Figure 4. Six-hour air mass trajectories for the September 16–19, 2014 period (blue lines). Backward trajectories over Illimani started at 6350 m above the sea level (a.s.l.). Forward trajectories over ATTO started at 1500 m a.s.l. The green and red areas represent the Amazon basin and the Altiplano, respectively.

In addition, Figure 3a shows a spike for both S EF and $\text{SO}_4^{2-}\text{exc}$ during the wet season of 2006/07. In October 2006, the Rabaul volcano ($4^{\circ}16'S$; $152^{\circ}12'E$, Papua New Guinea) emitted 31 kt of SO_2 (VEI 4), as estimated by the Ozone Monitoring Instrument on the Aura satellite (NASA). The plume was advected eastward, probably reaching South America (Figure S2). Therefore, we consider that the 2006/07 S EF peak was most probably related to the Rabaul eruption. In 2015, another S EF peak was observed, as shown in Figure 3a; this time, we also observed a Bi EF peak. In April 2015, a VEI 4 eruption occurred in the Cabulco volcano ($41^{\circ}19'S$; $72^{\circ}37'W$, Chile); however, satellite observations indicate that the SO_2 plume advected toward the Atlantic Ocean due to predominant westerly winds over that latitude, thus not affecting the Illimani region.

Bi EF showed its most prominent peak for the 2007–08 period, which might indicate a volcanic input. However, there is no evidence for a strong tropical or South American volcanic eruption, supporting the occurrence of such a signal during that period. Similar to the observations for the Cabulco SO_2 plume, emissions from the 2008 eruption (VEI 4) of the Chaitén volcano ($42^{\circ}50'S$; $72^{\circ}38'W$, Chile) advected toward the Atlantic Ocean. Moreover, we observed a higher Bi enrichment in 2002, contemporary to another Nyiragongo eruption; however, the absence of a S signal suggests that the plume did not reach Illimani.

In fact, Bi is strongly influenced by anthropogenic sources such as fossil fuel combustion and the manufacturing of alloys (Ferrari et al., 2000). In Illimani, Bi EF was significantly correlated with EFs of mining emission-sourced elements such as As, Cd, and Cu (Table S1). It is estimated that approximately 70% of the worldwide atmospheric anthropogenic emissions of Cd and Cu are related to non-ferrous metal production (Pacyna &

Pacyna, 2001). The EF for Cu showed a higher variability until 2008, followed by a decrease that agrees with the amount of Cu processed by both smelting and fire refining in Chile (Figure 5). These processes emit large quantities of metals to the atmosphere, and since 2012, they are less used in Chile, according to the Chilean Copper Commission (COCHILCO).

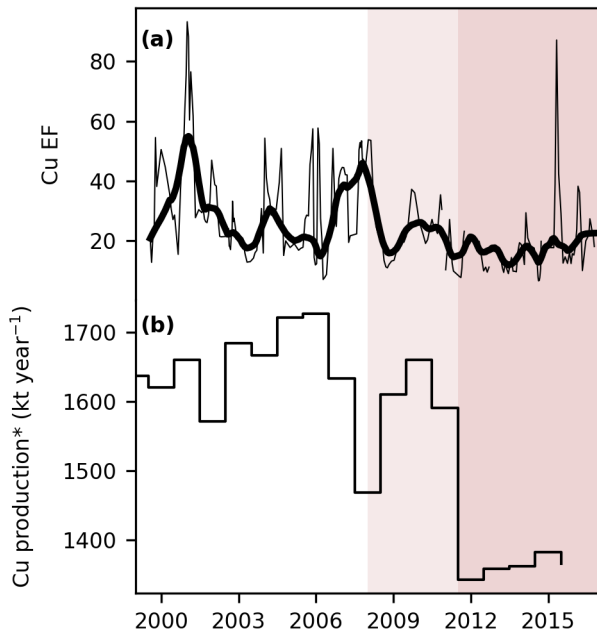


Figure 5. Comparison between the copper enrichment record and production. (a) The thinner line represents the three-sample mean Cu enrichment factor (EF) variability, and the thicker line denotes data smoothed by the LOWESS algorithm (1-year window, approximately). (b) Cu production in Chile, considering only the processes of smelting and fire refining, was obtained from COCHILCO (<http://www.cochilco.cl>). The lighter brown band represents a first decrease for both Cu EF and production, and the darker brown band denotes the greater decrease in Cu production by both smelting and fire refining.

3.3 Altiplano-Related Signal

We observed a common seasonality for the analyzed soluble species during the majority of the 1999–2016 period (Figure 6a; Figure S3). This is expected as the extreme seasonality of precipitation over the Altiplano promotes a well-defined oscillatory pattern in aerosol concentration variability in ice cores from Illimani (Correia et al., 2003; Knüsel et al., 2005; Osmont et al., 2019; Lindau et al., 2020). At this site, approximately 70% of annual precipitation occurs during the wet season (austral summer) and corresponds to the less concentrated snow layers (De Angelis et al., 2003). Furthermore, these authors observed that

large concentration peaks occurred during the dry season (austral winter) for most of the studied soluble species due to dry deposition processes and precipitation of heavily loaded snow. Such a seasonal pattern, represented by Mg^{2+} in Figure 6a, is consistent with satellite observations showing higher dust emissions from the Altiplano occurring during the austral winter (Prospero et al., 2002; Gaiero et al., 2013).

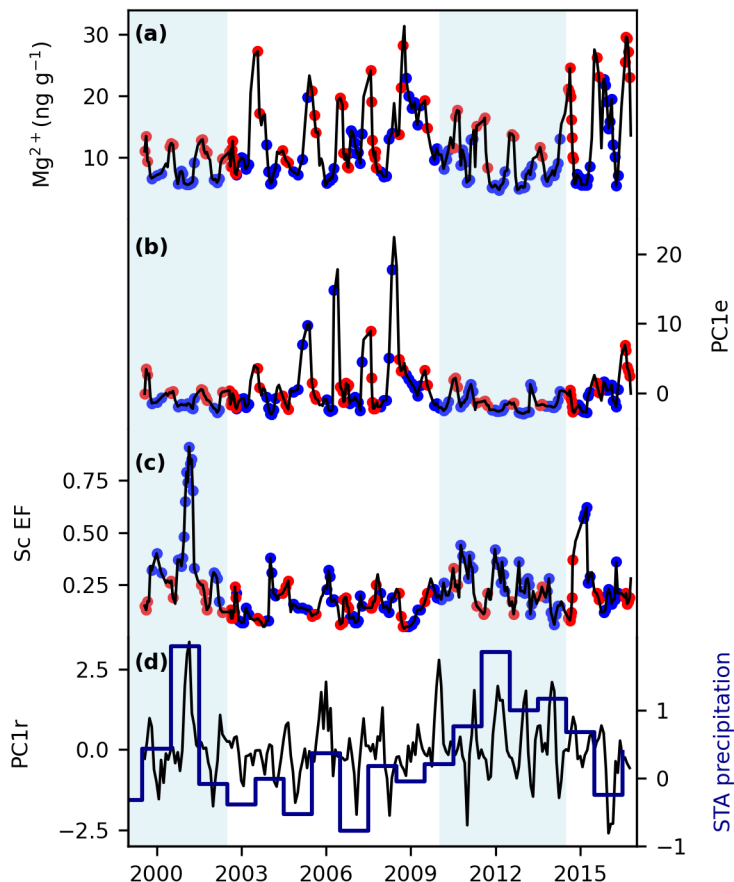


Figure 6. Responses of soluble magnesium (a), the first principal component of elemental concentrations (b), and scandium enrichment factor (c) to the first principal component of monthly precipitation variability over the Altiplano near Illimani (black line), and to annual precipitation (blue line) over the southern tropical Andes (d). Red and blue dots denote samples classified as “dry” and “wet,” respectively. Data in (a), (b), and (c) were smoothed by three-sample means. Vertical blue bands represent wetter periods discussed in the text.

Elemental concentrations exhibited a seasonal behavior similar to that observed for major ions. The first PC for elemental concentrations (PC1e, Figure 6b) explains 74% of the total variance, being strongly related ($r > 0.7$) to most of the elements, as well as correlated at the 95% level with all the major ions. However, PC1e showed spikes during the wet season,

which might be related to periods of enhanced deposition of anthropogenically sourced aerosols. Indeed, Table S2 shows that PC1e is associated ($r > 0.9$) with highly enriched elements such as As (mean EF of 69) and Cu (29). To avoid data interpolation, only the detected elements above the MDL in more than 75% of the samples (a total of 17 elements, Table S2) were considered for PC analyses.

The coherence between elemental concentrations was also observed for the EFs. For example, 70% of the EFs were correlated at the 95% level to Sc EF. This crustal-sourced element shows an increased EF during the wet season (Figure 6c). The Sc enrichment in atmospheric aerosols was related to differences in mineral proportions, probably containing little quartz and feldspars that are depleted in Sc, and more abundant clay minerals (Ferrat et al., 2011). This agrees with mineralogical data from Illimani dust, which showed a higher occurrence of aerodynamic plate-like phyllosilicates during the wet season owing to stronger scavenging caused by heavier precipitation (Lindau et al., 2020). Correia et al. (2003) proposed that during the dry season, the aerosol reaching Illimani tends to be closer to soil dust, while during the wet season, regional soil dust aerosols are more efficiently removed than fine, remotely transported aerosols from other sources. This is also observed on an interannual timescale.

As expected, precipitation over the Altiplano near Illimani (PC1r) during the 1999–2016 period shows a similar variability to the southern tropical Andes precipitation (Figure 6d) (Segura et al., 2019, 2020). The wettest year was 2001, followed by a drier period from 2003 to 2010, and then a wetter period from 2010 to 2014 (Figure 6d). Accordingly, the Sc EF is greater during these wetter periods. Conversely, higher elemental and ionic concentrations occurred within the 2003–2010 period. The 1999–2001 summer period featured a more intense and southward-positioned Bolivian High (Figure S4), favoring the transport of moist air from the Amazon lowlands toward the tropical Andes (Garreaud, 1999; Segura et al., 2019). During the summer of 2012, the upward motion over the western Amazon basin was caused by enhanced convection over this region due to the strength of low-level northerlies originating over the tropical Northern Atlantic (Segura et al., 2020).

3.4 Relationship with Atmospheric Circulation over the Amazon Basin

We observed that S enrichment was related to increased atmospheric SO₂ over Illimani, with only volcanic contribution in 2006 and 2014, although the S EF record also showed spikes in 2015 (Section 3.2). Thus, we expect that S EF is related to biomass burning in the lowlands eastward Illimani. Fires over Bolivia, Brazil, and Paraguay during August and September cause changes in aerosol optical properties in Chacaltaya (Chauvigné et al., 2019), as well as increased refractive black carbon (rBC) concentrations in Illimani (Osmont et al., 2019). However, the number of fire spots in that area was lower in 2015 than in 2004, 2007, and 2010 (Figure S5) when no dry season S EF peaks were observed. Interestingly, the dry season S EF showed a good correlation with the dry season Mn EF (Figure 7, $r = 0.64$, $p < 0.001$).

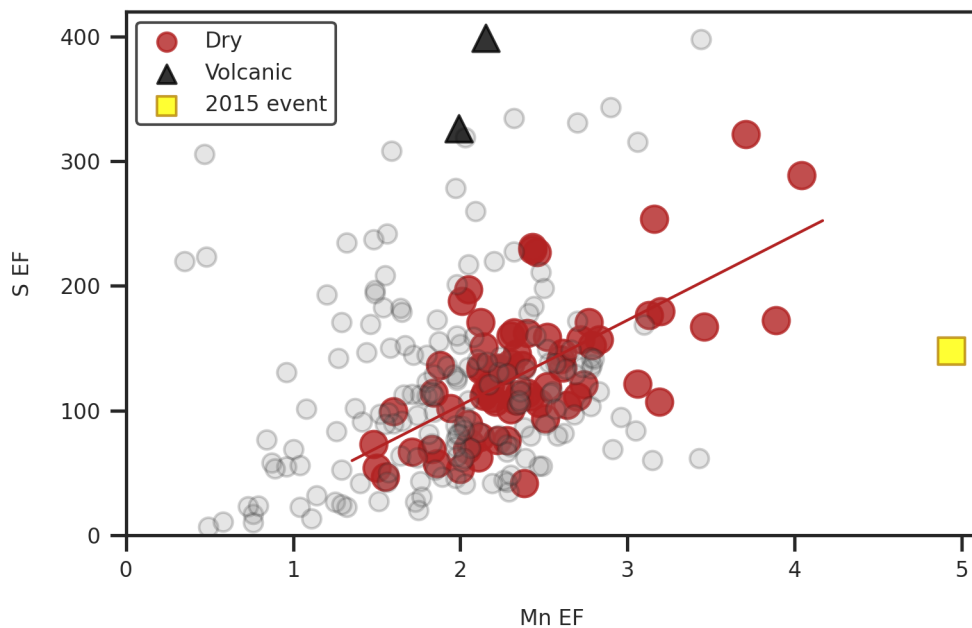


Figure 7. Linear relationship (indicated by the red line) between Mn and S enrichment factors (EFs) during the dry season (red circles). EFs related to volcanic events and to the 2015 dust event discussed in the text are represented by the black triangles and yellow square, respectively. Light gray dots in the background are the wet and transition season EFs.

The Mn EF, in turn, showed significant correlations at the 95% level with the low-level circulation over the Amazon basin during the austral winter (Figure 8), which is related to the SALLJ. In Figure 8, the more intense the SALLJ, the greater the enrichment in Mn. This is represented by its relationship with northerly wind anomalies at 850 hPa along the eastern slope of the southern tropical Andes (Figure 8), and to easterly wind anomalies at 850 hPa over the northeastern Amazon basin and westerly anomalies along the eastern slope of the southern tropical Andes (Figure S6). Enhanced SALLJ increases orographic precipitation over the Bolivian Eastern Cordillera (Jones, 2019). In accordance, Mn EF showed a positive correlation ($r = 0.53$, $p < 0.05$) with precipitation over the eastern slope of the Bolivian Eastern Cordillera during the austral winter, as indicated by meteorological observations in San Borja (Figure 1). This orographic precipitation potentially carries aerosols from the Amazon basin up to Illimani. Moreover, Thompson et al. (2013) observed that moisture bringing Amazon-sourced biogenic ammonium aerosol to Illimani arrives via winds at the 500-hPa level originating from east-southeast. We observed a positive correlation between the Mn EF and the relative humidity eastward at the 500-hPa level (Figure S7).

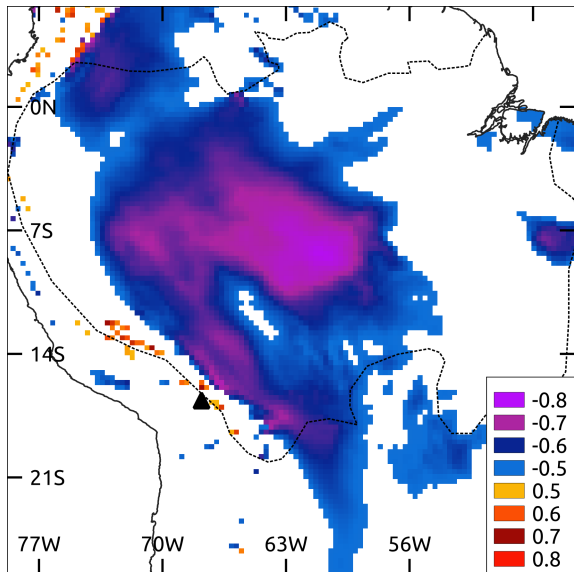


Figure 8. Spatial correlations (significant at the 95% level) during the months MJJAS (2000–2016 period) between the monthly resampled Mn enrichment factor and meridional winds at the 850-hPa level (ERA5 reanalysis). The black triangle indicates the Illimani site, and the dotted line delimits the Amazon basin.

Therefore, we believe that the dry season S EF signal is mainly controlled by atmospheric circulation over the Amazon basin. In fact, during the dry season of 2015, SALLJ intensified in comparison to the 1999–2016 period (Figure S8). This role of atmospheric circulation controlling the deposition of biomass burning proxies at Illimani has implications for interpreting rBC records in ice cores from the Andean Eastern Cordillera. Moreover, the use of Mn EF as a proxy for the austral winter intensity of the SALLJ might have implications for studying severe weather due to convective systems during the dry season in southeastern Brazil, already related to intense low-level jet flow (Rehbein et al., 2018).

We call attention to the 2014/15 wet season Mn EF peak that was unprecedented over the 1999–2016 record (Figure 7), and were followed by greater spikes of Co and Fe EF (Figure S9). On April 5 and 6 of 2015, a dust plume from the Saharan–Sahel region was detected in central Amazonia, which was supported by satellite data and air mass back trajectories, leading to peak concentrations of Fe (Rizzolo et al., 2017). According to our chronology, spikes for Co, Fe, and Mn occurred during that same period. Furthermore, air mass back trajectories for Illimani during that period indicated a predominant north-northeast direction (Figure S10), and therefore, most probably carry aerosols from the northern Amazon basin. The African dust aerosol reaching Central Amazonia is carried by northeasterly trade winds (Swap et al., 1992; Yu et al., 2015), and is enriched in crustal and biomass burning-related elements, reflecting higher concentrations of Fe, Mn, and S (Formenti et al., 2011; Moran-Zuloaga et al., 2018). The Co EF spike, by its turn, might be associated with continental biogenic sources, biomass burning, and combustion processes (Nriagu, 1989; Van De Velde et al., 1999). Interestingly, Co EF was close to unity along the IL2017 record,

indicating that it was mostly crustal sourced. Therefore, we consider that the presence of African dust in tropical Andean glaciers deserves future geochemical investigation.

4 Conclusions

The early 21st-century EF record of Illimani indicates lower anthropogenic contamination for Cr than during the late 20th century, probably due to lower emissions from mining-related activities. Indeed, a decrease in Chilean copper production via smelting and fire refining since 2008 seems to be reflected in reduced Cd and Cu EFs. Sulfur, by its turn, was highly enriched in Illimani along the 1999–2016 record (mean of 124) due to high SO₂ emissions from various anthropogenic sources. Moreover, we suggest that two S EF spikes (2006/07 and 2014) were due to volcanic eruptions.

Aerosols over the Central Amazon region can be transported to southern tropical Andes by SALLJs, which promote their uplift at the eastern Bolivian Andes. This was best reflected by Mn EF variability during the dry season (May to September), which was correlated at the 95% level to both zonal and meridional winds at the 850-hPa level and to 500 hPa relative humidity over the lowlands eastward Illimani. Furthermore, we attributed the enrichment for both Mn and S during 2015 to the enhanced SALLJ in comparison to the rest of the IL2017 record. Back trajectories and unprecedented EFs for Co, Fe, and Mn in IL2017 suggest that a dust plume from Africa might be recorded in the snow layers. We consider that this topic deserves further investigation.

Overall, concentrations for most anthropogenic and crustal-sourced elements and major ions featured a well-defined seasonal variability, modulated by the clear separation of wet and dry seasons over the southern tropical Andes. Sc was enriched during wetter periods, probably because the stronger scavenging favored by the deposition of minerals more concentrated in that element.

Acknowledgments

We thank the drillers S. Kutuzov, L. Piard, B. Jourdain, the entire operation team, and the support of the IRD office in Bolivia. Operations at Illimani were part of the Ice Memory project financed by IRD at the Université Grenoble Alpes, CNRS, IPEV, and UMSA, and by a sponsorship from the Université Grenoble Alpes Foundation. We thank B. Delmonte, G. Baccolo, and V. Maggi for their support at EuroCold, Italy. This investigation is a contribution of the Brazilian National Institute for Cryospheric Sciences (Process CNPq 465680/2014-3). It was partially funded by NSF project 1600018 and by the Brazilian CAPES, project 88887.136384/2017-00. F.G.L. Lindau thanks CNPq for his scholarship (Processes 141013/2015-0 and 200496/2017-4). The data presented in this work will be archived at the National Oceanic and Atmospheric Administration World Data Center-A for Paleoclimatology.

References

- Brugger, S. O., Gobet, E., Osmont, D., Behling, H., Fontana, S. L., Hooghiemstra, H., . . . Tinner, W. (2019). Tropical Andean glacier reveals colonial legacy in modern mountain ecosystems. *Quaternary Science Reviews*, 220, 1–13. doi: 10.1016/j.quascirev.2019.06.032
- Chauvigné, A., Diego, A., Marcos, A., Patrick, G., Radovan, K., Griša, M., . . . Laj, P. (2019). Biomass-burning and urban emission impacts in the Andes Cordillera region based on in-situ measurements from the Chacaltaya observatory, Bolivia (5240 m a.s.l.). *Atmospheric Chemistry and Physics*, 19, 4805–14824. doi: 10.5194/acp-2019-510
- Correia, A., Freydier, R., Delmas, R. J., Simões, J. C., Taupin, J. D., Dupré, B., & Artaxo, P. (2003). Trace elements in South America aerosol during 20th century inferred from a Nevado Illimani ice core, Eastern Bolivian Andes (6350 m asl). *Atmospheric Chemistry and Physics*, 3 (5), 1337–1352. doi: 10.5194/acp-3-1337-2003
- De Angelis, M., Simões, J., Bonnaveira, H., Taupin, J. D., & Delmas, R. J. (2003). Volcanic eruptions recorded in the Illimani ice core (Bolivia): 1918–1998 and Tambora periods. *Atmospheric Chemistry and Physics*, 3 (5), 1725–1741. doi: 10.5194/acp-3-1725-2003
- de Magalhães, N., Evangelista, H., Condom, T., Rabatel, A., & Ginot, P. (2019). Amazonian Biomass Burning Enhances Tropical Andean Glaciers Melting. *Scientific Reports*, 9 (1), 1–12. doi: 10.1038/s41598-019-53284-1
- Eichler, A., Gramlich, G., Kellerhals, T., Tobler, L., Rehren, T., & Schwikowski, M. (2017). Ice-core evidence of earliest extensive copper metallurgy in the Andes 2700 years ago. *Scientific Reports*, 7 , 41855. doi: 10.1038/srep41855
- Eichler, A., Gramlich, G., Kellerhals, T., Tobler, L., & Schwikowski, M. (2015). Pb pollution from leaded gasoline in South America in the context of a 2000-year metallurgical history. *Science Advances*, 1 , e1400196. doi: 10.1126/sciadv.1400196
- Espinoza, J. C., Garreaud, R., Poveda, G., Arias, P. A., Molina-Carpio, J., Masiokas, M., . . . Scaff, L. (2020). Hydroclimate of the Andes Part I: Main Climatic Features. *Frontiers in Earth Science*, 8 , 1–20. doi: 10.3389/feart.2020.00064
- Ferrari, C. P., Hong, S., Van De Velde, K., Boutron, C. F., Rudniev, S. N., Bolshov, M., . . . Rosman, K. J. (2000). Natural and anthropogenic bismuth in Central Greenland. *Atmospheric Environment*, 34 (6), 941–948. doi: 10.1016/S1352-2310(99)00257-5
- Ferrat, M., Weiss, D. J., Strekopytov, S., Dong, S., Chen, H., Najorka, J., . . . Sinha, R. (2011). Improved provenance tracing of Asian dust sources using rare earth elements and selected trace elements for palaeomonsoon studies on the eastern Tibetan Plateau. *Geochimica et Cosmochimica Acta*, 75 (21), 6374–6399. doi: 10.1016/j.gca.2011.08.025
- Formenti, P., Schütz, L., Balkanski, Y., Desboeufs, K., Ebert, M., Kandler, K., . . . Zhang, D. (2011). Recent progress in understanding physical and chemical properties of African and Asian mineral dust. *Atmospheric Chemistry and Physics*, 11 (16), 8231–8256. doi: 10.5194/acp-11-8231-2011
- Gabrielli, P., Wegner, A., Roxana Sierra-Hernández, M., Beaudon, E., Davis, M., Barker, J. D., & Thompson, L. G. (2020). Early atmospheric contamination on the top of the Himalayas since the onset of the European Industrial Revolution. *PNAS* , 117 (8), 3967–3973. doi: 10.1073/pnas.1910485117

- Gaiero, D. M., Simonella, L., Gassó, S., Gili, S., Stein, A. F., Sosa, P., . . . Marelli, H. (2013). Ground/satellite observations and atmospheric modeling of dust storms originating in the high Puna-Altiplano deserts (South America): Implications for the interpretation of paleoclimatic archives. *Journal of Geophysical Research Atmospheres*, 118 (9), 3817–3831. doi: 10.1002/jgrd.500362013
- Garreaud, R. D. (1999). Multiscale Analysis of the Summertime Precipitation over the Central Andes. *Monthly Weather Review*, 127 (5), 901–921. doi: 10.1175/1520-0493(1999)127h0901:MAOTSPi2.0.CO;2
- Ginot, P., Kull, C., Schwikowski, M., Schotterer, U., & Gäggeler, H. W. (2001). Effects of postdepositional processes on snow composition of a subtropical glacier (Cerro Tapado, Chilean Andes). *Journal of Geophysical Research*, 106 (D23), 32375. doi: 10.1029/2000JD000071
- Hong, S., Barbante, C., Boutron, C., Gabrielli, P., Gaspari, V., Cescon, P., . . . Maurice-Bourgoin, L. (2004). Atmospheric heavy metals in tropical South America during the past 22 000 years recorded in a high altitude ice core from Sajama, Bolivia. *Journal of Environmental Monitoring*, 6 (4), 322–326. doi: 10.1039/b314251e
- Jones, C. (2019). Recent changes in the South America low-level jet. *Climate and Atmospheric Science*, 2 (1), 1–8. doi: 10.1038/s41612-019-0077-5
- Kaspari, S., Mayewski, P. A., Handley, M., Osterberg, E., Kang, S., Snead, S., . . . Qin, D. (2009). Recent increases in atmospheric concentrations of Bi, U, Cs, S and Ca from a 350-year Mount Everest ice core record. *Journal of Geophysical Research Atmospheres*, 114 (4). doi: 10.1029/2008JD011088
- Kellerhals, T., Brütsch, S., Sigl, M., Knüsel, S., Gäggeler, H. W., & Schwikowski, M. (2010). Ammonium concentration in ice cores: A new proxy for regional temperature reconstruction? *Journal of Geophysical Research Atmospheres*, 115 (16), 1–8. doi: 10.1029/2009JD012603
- Knüsel, S., Brütsch, S., Henderson, K. A., Palmer, A. S., & Schwikowski, M. (2005). ENSO signals of the twentieth century in an ice core from Nevado Illimani, Bolivia. *Journal of Geophysical Research D: Atmospheres*, 110 (1), 1–14. doi: 10.1029/2004JD005420
- Knüsel, S., Ginot, P., Schotterer, U., Schwikowski, M., Gäggeler, H. W., Francou, B., . . . Taupin, J. D. (2003). Dating of two nearby ice cores from the Illimani, Bolivia. *Journal of Geophysical Research*, 108 (D6), 4181. doi: 10.1029/2001JD002028
- Lenters, J. D., & Cook, K. H. (1997). On the Origin of the Bolivian High and Related Circulation Features of the South American Climate. *Journal of the Atmospheric Sciences*, 54 (5), 656–678. doi: 10.1175/1520-0469(1997)054h0656:OTOOTBi2.0.CO;2
- Lindau, F. G. L., Simões, J. C., Delmonte, B., Ginot, P., Baccolo, G., Paleari, C. I., . . . Andò, S. (2020). Giant dust particles at Nevado Illimani: a proxy of summertime deep convection over the Bolivian Altiplano. *The Cryosphere Discussions*(April), 1–21. doi: 10.5194/tc-2020-55
- Marengo, J. A. (2004). Interdecadal variability and trends of rainfall across the Amazon basin. *Theoretical and Applied Climatology*, 78 (1-3), 79–96. doi: 10.1007/s00704-004-0045-8

- Moran-Zuloaga, D., Ditas, F., Walter, D., Saturno, J., Brito, J., Carbone, S., . . . Pöhlker, C. (2018). Long-term study on coarse mode aerosols in the Amazon rain forest with the frequent intrusion of Saharan dust plumes. *Atmospheric Chemistry and Physics*, 18 (13), 10055–10088. doi: 10.5194/acp-18-10055-2018
- Nriagu, J. (1989). A global assessment of natural sources of atmospheric trace metals. *Nature*, 338 (6210), 47–49. doi: 10.1038/338047a0
- Osmont, D., Sigl, M., Eichler, A., Jenk, T. M., & Schwikowski, M. (2019). A Holocene black carbon ice-core record of biomass burning in the Amazon Basin from Illimani, Bolivia. *Climate of the Past*, 15 (2), 579–592. doi: 10.5194/cp-15-579-2019
- Osterberg, E. C., Handley, M. J., Snead, S. B., Mayewski, P. A., & Kreutz, K. J. (2006). Continuous ice core melter system with discrete sampling for major ion, trace element, and stable isotope analyses. *Environmental Science and Technology*, 40 (10), 3355–3361. doi: 10.1021/es052536w
- Pacyna, J. M., & Pacyna, E. G. (2001). An assessment of global and regional emissions of trace metals to the atmosphere from anthropogenic sources worldwide. *Environmental Reviews*, 9 (4), 269–298. doi: 10.1139(er-9-4-269)
- Prospero, J. M., Ginoux, P., Torres, O., Nicholson, S. E., & Gill, T. E. (2002). Environmental characterization of global sources of atmospheric soil dust identified with the NIMBUS 7 Total Ozone Mapping Spectrometer (TOMS) absorbing aerosol product. *Reviews of Geophysics*, 40 (1), 1–31. doi: 10.1029/2000RG000095
- Rehbein, A., Dutra, L. M. M., Ambrizzi, T., Da Rocha, R. P., Reboita, M. S., Da Silva, G. A. M., . . . Carpenedo, C. B. (2018). Severe Weather Events over Southeastern Brazil during the 2016 Dry Season. *Advances in Meteorology*, 2018. doi: 10.1155/2018/4878503
- Rizzolo, J. A., Barbosa, C. G., Borillo, G. C., Godoi, A. F., Souza, R. A., Andreoli, R. V., . . . Godoi, R. H. (2017). Soluble iron nutrients in Saharan dust over the central Amazon rainforest. *Atmospheric Chemistry and Physics*, 17 (4), 2673–2687. doi: 10.5194/acp-17-2673-2017
- Saturno, J., Ditas, F., De Vries, M. P., Holanda, B. A., Pöhlker, M. L., Carbone, S., . . . Pöhlker, C. (2018). African volcanic emissions influencing atmospheric aerosols over the Amazon rain forest. *Atmospheric Chemistry and Physics*, 18 (14), 10391–10405. doi: 10.5194/acp-18-10391-2018
- Schwikowski, M., Döscher, A., Gäggeler, H. W., & Schotterer, U. (1999). Anthropogenic versus natural sources of atmospheric sulphate from an Alpine ice core. *Tellus B: Chemical and Physical Meteorology*, 51 (5), 938–951. doi: 10.3402/tellusb.v51i5.16506
- Segura, H., Espinoza, J. C., Junquas, C., Lebel, T., Vuille, M., & Garreaud, R. (2020). Recent changes in the precipitation-driving processes over the southern tropical Andes/western Amazon. *Climate Dynamics*, 54 (5-6), 2613–2631. doi: 10.1007/s00382-020-05132-6
- Segura, H., Junquas, C., Espinoza, J. C., Vuille, M., Jauregui, Y. R., Rabatel, A., . . . Lebel, T. (2019). New insights into the rainfall variability in the tropical Andes on seasonal and interannual time scales. *Climate Dynamics*, 53 (1-2), 405–426. doi: 10.1007/s00382-018-4590-8

- Sen, I. S., & Peucker-Ehrenbrink, B. (2012). Anthropogenic disturbance of element cycles at the Earth's surface. *Environmental Science and Technology*, 46 (16), 8601–8609. doi: 10.1021/es301261x
- Swap, R., Garstang, M., Greco, S., Talbot, R., & Kallberg, P. (1992). Saharan dust in the Amazon Basin. *Tellus, Series B*, 44 B (2), 133–149. doi: 10.3402/tellusb.v44i2.15434
- Thompson, L. G., Mosley-Thompson, E., Davis, M. E., Zagorodnov, V. S., Howat, I. M., Mikhalenko, V. N., & Lin, P.-N. (2013). Annually resolved ice core records of tropical climate variability over the past 1800 years. *Science*, 340, 945–950. doi: 10.1126/science.1234210
- Uglietti, C., Gabrielli, P., Cooke, C. A., Vallelonga, P., & Thompson, L. G. (2015). Widespread pollution of the south american atmosphere predates the industrial revolution by 240 y. *PNAS*, 112 (8), 2349–2354. doi: 10.1073/pnas.1421119112
- Uglietti, C., Gabrielli, P., Olesik, J. W., Lutton, A., & Thompson, L. G. (2014). Large variability of trace element mass fractions determined by ICP-SFMS in ice core samples from worldwide high altitude glaciers. *Applied Geochemistry*, 47, 109–121. doi: 10.1016/j.apgeochem.2014.05.019
- Van De Velde, K., Ferrari, C., Barbante, C., Moret, I., Bellomi, T., Hong, S., & Boutron, C. (1999). A 200 year record of atmospheric cobalt, chromium, molybdenum, and antimony in high altitude alpine firn and ice. *Environmental Science and Technology*, 33 (20), 3495–3501. doi: 10.1021/es990066y
- Vera, C., Higgins, W., Amador, J., Ambrizzi, T., Garreaud, R., Gochis, D., . . . Zhang, C. (2006). Toward a unified view of the American monsoon systems. *Journal of Climate*, 19 (20), 4977–5000. doi: 10.1175/JCLI3896.1
- Vimeux, F., Ginot, P., Schwikowski, M., Vuille, M., Hoffmann, G., Thompson, L. G., & Schotterer, U. (2009). Climate variability during the last 1000 years inferred from Andean ice cores: A review of methodology and recent results. *Palaeogeography, Palaeoclimatology, Palaeoecology*, 281 (3-4), 229–241. doi: 10.1016/j.palaeo.2008.03.054
- Wagnon, P., Sicart, J. E., Berthier, E., & Chazarin, J. P. (2003). Wintertime high-altitude surface energy balance of a Bolivian glacier, Illimani, 6340 m above sea level. *Journal of Geophysical Research*, 108 (D6), 4177. doi: 10.1029/2002JD002088
- Wedepohl, K. H. (1995). The composition of the continental crust. *Geochimica et Cosmochimica Acta*, 59 (7), 1217–1232. doi: 10.1016/0016-7037(95)00038-2
- Yu, H., Chin, M., Yuan, T., Bian, H., Remer, L. A., Prospero, J. M., . . . Zhao, C. (2015). The fertilizing role of African dust in the Amazon rainforest: A first multiyear assessment based on data from Cloud-Aerosol Lidar and Infrared Pathfinder Satellite Observations. *Geophysical Research Letters*, 42 (6), 1984–1991. doi: 10.1002/2015GL063040

Supporting information for “Proxies for atmospheric circulation over the Amazon basin from the aerosol composition in a Nevado Illimani firn core, Bolivia”

Filipe G. L. Lindau¹, Jefferson C. Simões^{1,2}, Michael Handley², Elena Korotkikh², Patrick Ginot³, Rafael R. Ribeiro¹

¹Centro Polar e Climático, Universidade Federal do Rio Grande do Sul, Porto Alegre, 91501-970, Brazil

²Climate Change Institute, University of Maine, Orono, ME 04469, USA

³Univ. Grenoble Alpes, CNRS, IRD, Grenoble INP, IGE, 38000 Grenoble, France

Contents of this file

1. Figures S1 to S10
2. Tables S1 to S2

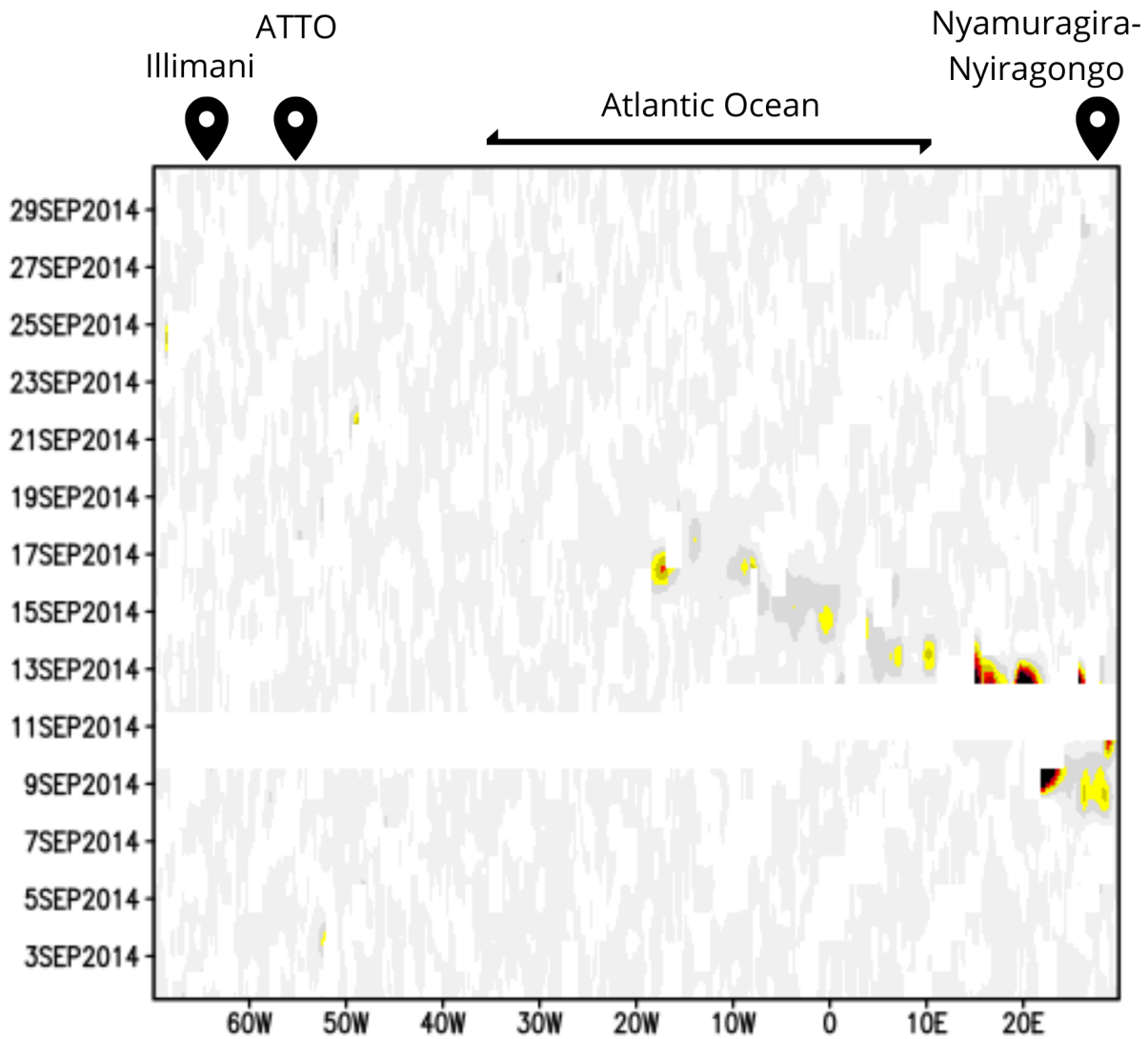


Figure S1. Planetary boundary layer OMI SO₂ Hovmöller plot corresponding to a latitude daily average (16.5°S to 0°) from September 2014. Indicated at the top of the plot are the longitude locations of: the Illimani, the ATTO station, the Nyamuragira-Nyiragongo volcanoes, and the approximate west to east extension of the south Atlantic Ocean.

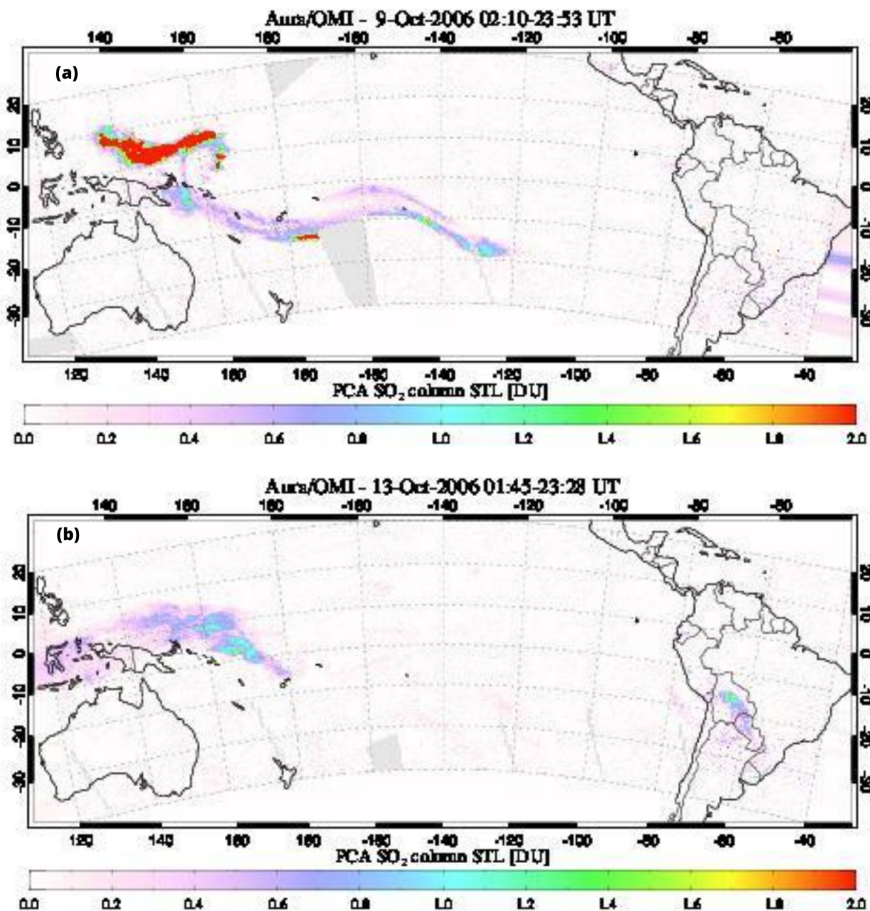


Figure S2. Rabaul volcano SO₂ plume toward South America, on October 9th (a) and 13th (b) of 2006, detected by the Ozone Monitoring Instrument (OMI) on the Aura satellite (Atmospheric Chemistry and Dynamics Laboratory, NASA, <https://so2.gsfc.nasa.gov>).

Table S1. Correlations between the enrichment factors of the elements emitted by metallurgical smelting and refining processes. All these correlations are significant at the 95% level.

	As	Bi	Cd	Cu
As	1			
Bi	0.5	1		
Cd	0.5	0.4	1	
Cu	0.6	0.4	0.4	1

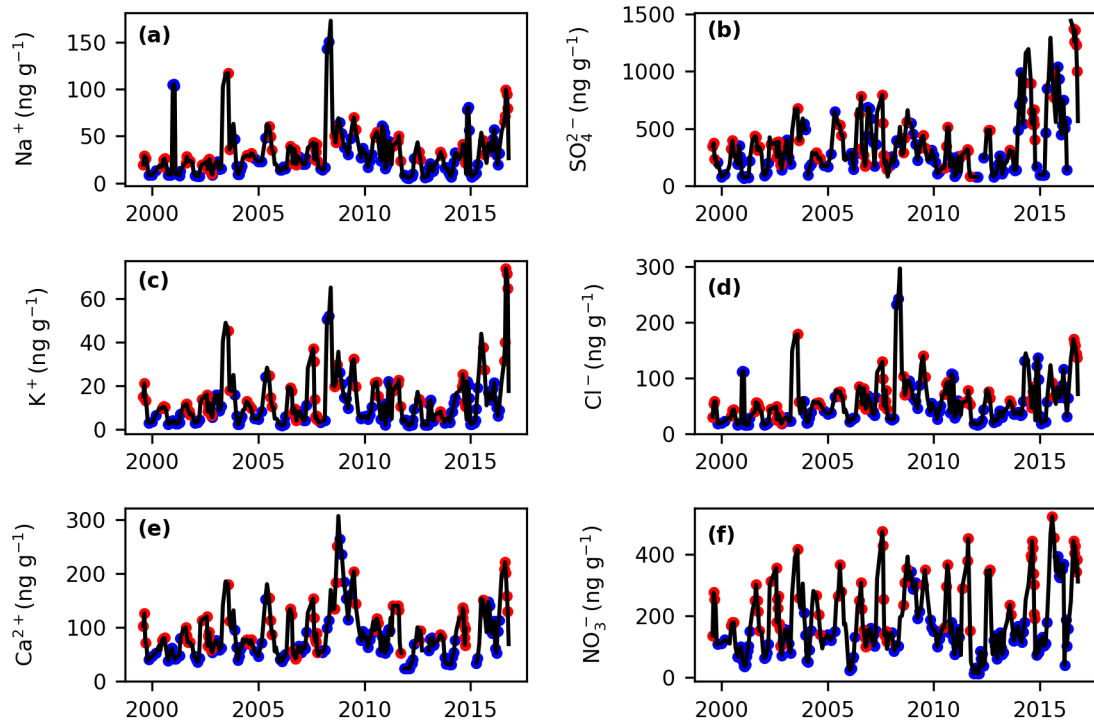


Figure S3. Major ions concentration record for the 1999–2016 period. Records are expressed by a 3-sample mean. Blue and red dots denote to samples classified as “wet” and “dry”, respectively.

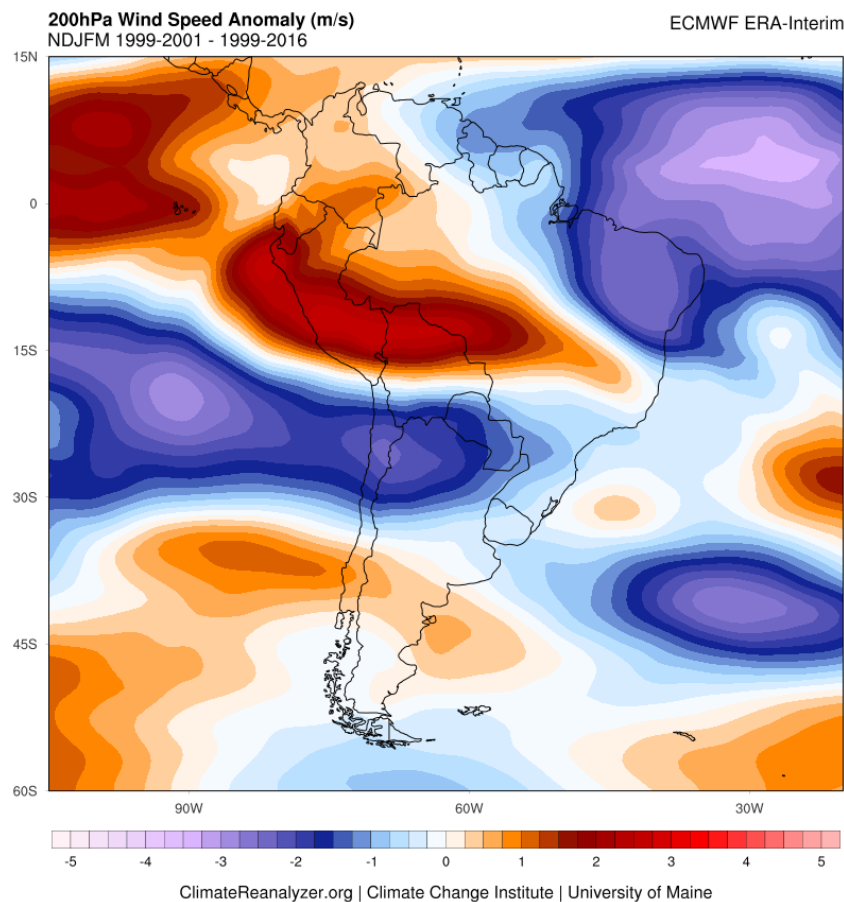


Figure S4. Austral summer (NDJFM) wind speed anomalies at the 200 hPa level, when comparing the period 1999–2001 to the 1999–2016 climatology. The higher speeds over northwestern South America suggests an intensified and southward displaced Bolivian high. Data from the ERA-Interim reanalysis, obtained at the Climate Reanalyzer (<https://climatereanalyzer.org>).

Table S2. Correlations between elemental concentrations and their first principal component. Significant correlations at the 95% and higher than 0.50 are shown in bold. The explained variance is indicated in the last line.

	PC1e
Li	0.85
Na	0.74
Mg	0.97
Al	0.94
S	0.45
K	0.83
Ca	0.76
Sc	0.91
Mn	0.88
Co	0.92
Cu	0.91
As	0.91
Sr	0.94
Cs	0.91
Pb	0.95
Bi	0.59
U	0.93
Var (%)	74

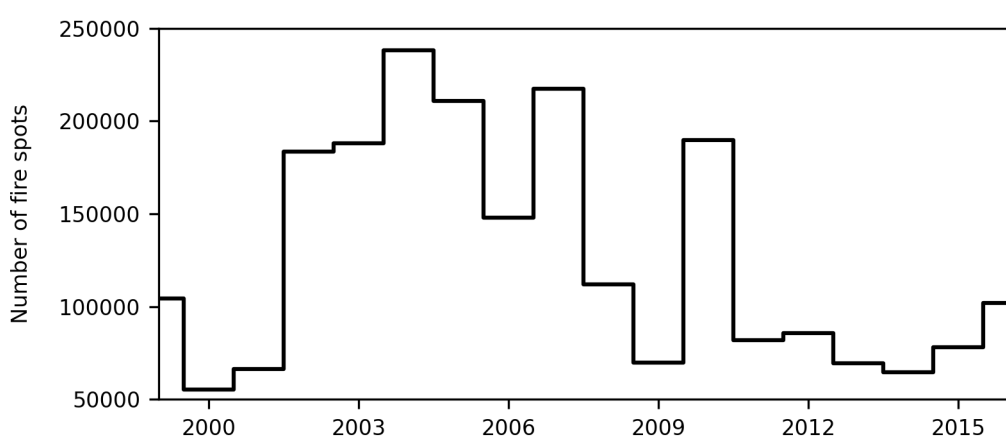


Figure S5. Total number of fire spots in Bolivia, western Brazil (states of Mato Grosso do Sul, Mato Grosso and Rondônia), and Paraguay. Data from the Brazilian Aerospace Agency (INPE) available at queimadas.dgi.inpe.br.

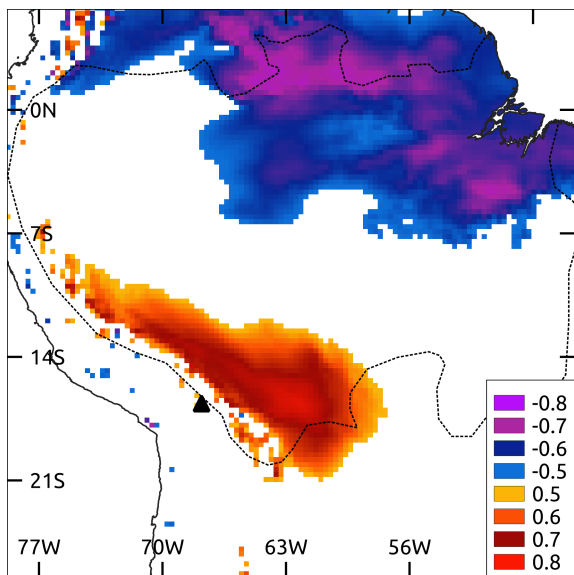


Figure S6. Spatial correlations (significant at the 95% level) during the months MJJAS (2000–2016 period) between the manganese enrichment factor and zonal winds at the 850 hPa level (ERA5 reanalysis). The black triangle indicates the Illimani site, and the dotted line delimits the Amazon basin.

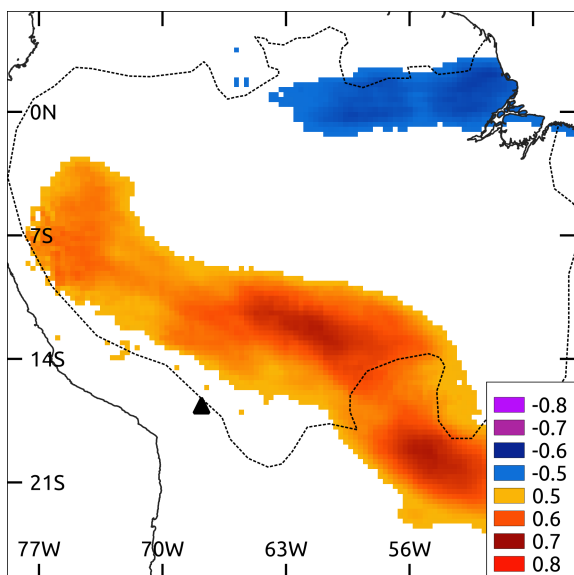


Figure S7. Spatial correlations (significant at the 95% level) during the months MJJAS (2000–2016 period) between the manganese enrichment factor and the relative humidity at the 500-hPa level (ERA5 reanalysis). The black triangle indicates the Illimani site, and the dotted line delimits the Amazon basin.

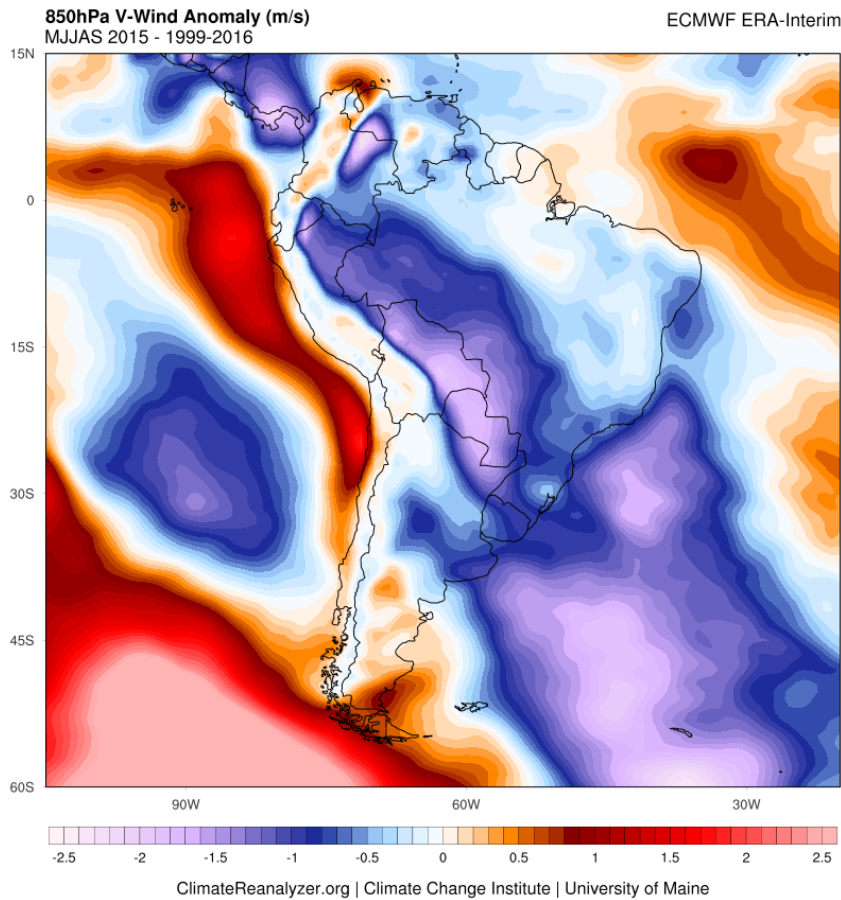


Figure S8. Austral winter (MJJAS) meridional wind anomalies at the 850 hPa level, when comparing the year of 2015 with the 1999–2016 climatology. The stronger northerly flux over western South America suggests intensified low level jets. Data from the ERA-Interim reanalysis, obtained at the Climate Reanalyzer (<https://climatereanalyzer.org>).

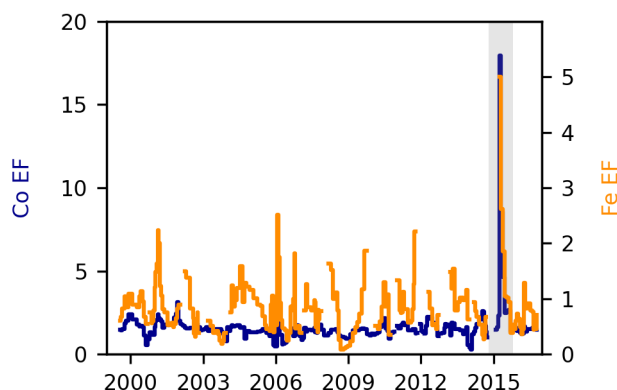


Figure S9. Anomalous enrichment for cobalt (blue) and iron (orange). The vertical gray area highlights the early 2015 period.

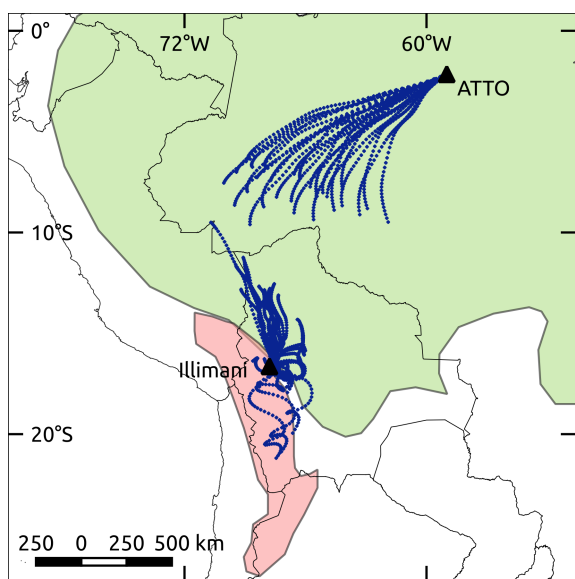


Figure S10. Two-hour air mass trajectories for the April 3–5, 2015 period (blue lines). Backward trajectories over the Illimani started at 500 m above that site. Forward trajectories over ATTO started at 1500 m a.s.l. The green and red areas represent the Amazon basin and the Altiplano, respectively.

5.3 Dust record in an ice core from tropical Andes (Nevado Illimani – Bolivia), potential for climate variability analyses in the Amazon basin

Artigo submetido para a revista Climate of the Past. Email de submissão no Anexo IV.

Dust record in an ice core from tropical Andes (Nevado Illimani – Bolivia), potential for climate variability analyses in the Amazon basin

Filipe G. L. Lindau¹, Jefferson C. Simões^{1,2}, Rafael R. Ribeiro¹, Patrick Ginot³, Barbara Delmonte⁴, Giovanni Baccolo⁴, Stanislav Kutuzov⁵, Valter Maggi⁴, and Edson Ramirez⁶

¹Centro Polar e Climático, Universidade Federal do Rio Grande do Sul, Porto Alegre, 91501-970, Brazil

²Climate Change Institute, University of Maine, Orono, ME 04469, USA

³Univ. Grenoble Alpes, CNRS, IRD, Grenoble INP, IGE, 38000 Grenoble, France

⁴Environmental and Earth Sciences Department, University Milano-Bicocca, Milan, 20126, Italy

⁵Institute of Geography, Russian Academy of Sciences, Moscow, 119017, Russia

⁶Instituto de Hidráulica e Hidrología, Universidad Mayor de San Andrés, La Paz, Bolivia

Correspondence to: Filipe G. L. Lindau (filipe.lindau@outlook.com)

Abstract. Understanding the mechanisms controlling glacial retreat in the tropical Andes can strengthen future predictions of ice cover in the region. As glaciers are a dominant freshwater source in these regions, accurate ice cover predictions are necessary for developing effective strategies to protect future water resources. In this study, we investigated a 97-year dust record from two Nevado Illimani ice cores to determine the dominant factors controlling particle concentration and size distribution. In addition, we measured the area of a Nevado Illimani glacier (glacier n°8) using aerial photographs from 1956 and 2009. We identified two dustier periods during the 20th century (1930s–1940s and 1980s–2016), which were linked to reduced moisture transport from the Amazon basin. This promoted an unprecedented increase in the percentage of coarse dust particles (CPPn, $\varnothing > 10 \mu\text{m}$) during the 1990s, as drier local conditions favored the emission and deposition of coarse particles on the glacier. Moisture advection from the Amazon basin to Nevado Illimani was influenced by tropical North Atlantic sea surface temperatures (TNA), which was supported by the correlation between TNA and CPPn ($r = 0.52$). Furthermore, glacial retreat has been accelerating since the 1980s, and a notable relationship between CPPn and the freezing level height (FLH, $r = 0.41$) was observed. This suggests that higher FLHs promote glacial retreat, which exposes fresh glacial sediments and facilitates the transport of coarse dust particles to the Nevado Illimani summit. Therefore, both the area of glacier n°8 and the ice core record of coarse dust particles were found to respond to climate variability—particularly to the warmer conditions across the southern tropical Andes and drier conditions over the Amazon basin.

1 Introduction

The tropical Andes has undergone pronounced climatic changes over the past few decades. Tropospheric warming has significantly accelerated glacial retreat, resulting in the fastest rates of retreat since the mid-Little Ice Age (mid-seventeenth to early eighteenth century) (Rabatel et al., 2013). Changes in glacier mass, length, area, and volume have been recorded since the 16th century and are strong indicators of climate change (Bojinski et al., 2014; Zemp et al., 2015). However, quantitative information on the climate-glacier relationship requires a multi-proxy approach that combines glacier geometry data with other paleoclimatic proxies, such as ice core records (Solomina et al., 2007; Jomelli et al., 2009).

The presence of large dust particles ($> 8 \mu\text{m}$ diameter) in a Renland ice core (RECAP, 71.30°N , 26.72°W , 2315 m above sea level, asl) was linked to the activity of local dust sources and inferred past changes in the ice sheet margin at the east coast of Greenland (Simonsen et al., 2019). The RECAP dust record was dominated by coarse particles during the Holocene and previous interglacial period, inferring the retreat of the East Greenland ice sheet margin and the exposure of sediment-rich areas, which increased the supply of coarse material. Similarly, the higher snowline elevation during the Holocene compared with the Last Glacial Maximum (LGM, approximately 20 ka BP) in the southern tropical Andes had caused an 8-fold increase in dust concentrations in the Sajama ice core (18.1°S , 68.88°W , 6542 m asl) (Thompson et al., 1998). Moreover, according to Nevado Illimani dust records (hereafter Illimani, 16.62°S , 67.77°W , 6438 m asl), Holocene dust concentrations were 2.5 times higher than that of glacial periods due to the drier local conditions (Ramirez et al., 2003). Higher dust concentrations during warm periods emphasizes the importance of local dust sources, as the dust cycle generally decreases during warm periods on the global scale (Maher et al., 2010). However, the Sajama and Illimani studies only assessed the total mineral concentration and did not consider the variability of mineral particle size during these climatic transitions. Due to the close link between coarse atmospheric dust and climatic and environmental processes (Baccolo et al., 2018; Simonsen et al., 2019; Lindau et al., 2020), it is necessary to investigate the relationship between coarse dust particles ($> 10 \mu\text{m}$ diameter), glacial evolution, and climate variability in the southern tropical Andes.

This study aimed to assess the relationship between ice core dust records and current glacial retreat in the tropical Andes. We analyzed the dust concentrations and particle sizes in firn and ice samples from Illimani covering 1919–2016 AD to assess past dust aerosol variability. The

samples were collected during two drilling campaigns in 1999 and 2017. To better understand the causes of dust variability, our results were compared to other climate records, meteorological observations, and aerial photographs of an Illimani glacier covering the period 1956–2009.

The Illimani is located in Cordillera Real, one of the four mountain chains forming the Eastern Cordillera of the Bolivian Andes (Fig. 1a). This mountain is 50 km southeast of the Bolivian capital La Paz and 180 km southeast of Lake Titicaca. The precipitation is distributed over 9 months of the year (Vimeux et al., 2009), with a clear dry (April to August, austral winter) and wet season (November to March, austral summer). An abrupt transition between the two seasons occurs between March and April, and intermediate conditions occur in September and October (Vimeux et al., 2005). Dust from the Illimani was almost exclusively composed of soil-derived particles during both summer and winter throughout the 20th century (Correia et al., 2003). Mineralogy, rare earth elements, and strontium/neodymium isotope ratios can also determine the local and regional (southern Altiplano) provenances of dust particles (Delmonte et al., 2010; Lindau et al., 2020).

2 Material and Method

2.1 Field campaigns and sampling

A joint expedition of scientists from the French Institut de Recherche pour le Développement (IRD) and the Paul Scherrer Institute (PSI) recovered two deep ice cores (depths of 136.7 and 138.7 m) from Illimani in June 1999 at an altitude of 6350 m asl (Fig. 1b). Both ice cores were drilled with a Fast-Electromechanical Lightweight Ice Coring System (FELICS) (Ginot et al., 2002) producing sections of up to 0.9 m in length and 7.8 cm in diameter (Knüsel et al., 2003). A 23.8 m firn core was recovered from approximately the same drilling site in June 2017 using an EM-100-1000 electromechanical drill (Cryosphere Research Solutions, Columbus, Ohio, USA), which produced a core of 10 cm in diameter. The 2017 expedition was composed of a French, Russian, Bolivian, and Brazilian team as part of the Ice Memory project (<https://www.ice-memory.org>), which extracted two additional cores down the bedrock (136 and 134 m).

The upper 45 m (35 m in water equivalent, w.e.) of one of the 1999 ice cores (IL1999) were cut into sections of approximately 10 cm (from the top to 40 m) and 7 cm (from 40 to 45 m) at the Institut des Géosciences de l'Environnement (IGE, University Grenoble Alps, France),

providing a total of 666 samples (Ramirez et al., 2003). The firn core recovered in 2017 (IL2017) was cut into sections of approximately 5 cm at the EuroCold (University of Milano-Bicocca, Italy), providing 464 additional samples.

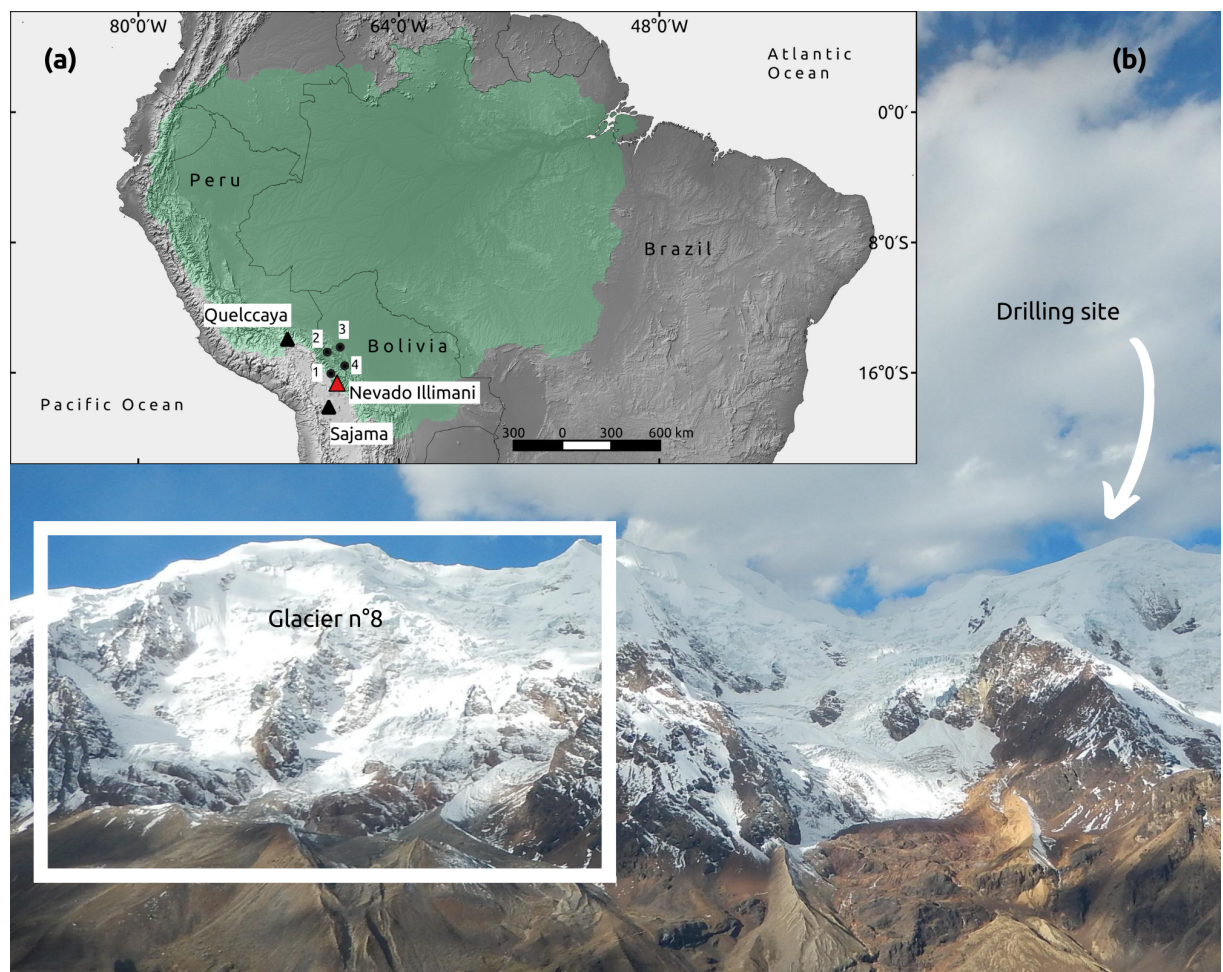


Figure 1. Map of the study region (a) indicating the locations of the ice core sites: Nevado Illimani (red triangle), Quelccaya (black triangle), and Sajama (black triangle). The green area delimits the Amazon basin (Mayorga et al. (2012); obtained from <http://daac.ornl.gov>). Also indicated are the Zongo glacier (1), and the meteorological stations in the Bolivian Amazon basin: Apolo (2), Rurrenabaque (3) and Sapeco (4). The land basemap was obtained from Natural Earth (<http://www.naturalearthdata.com>). (b) A photograph taken in June 2017 of the west/south face of Nevado Illimani, indicating the drilling site (snow and ice samples) and the selected glacier (n°8) that was analyzed by aerial photographs.

2.2 Dust concentration and size distribution

The dust content in IL1999 was analyzed in 2002 at IGE using a Beckman Coulter Multisizer IIe with a 50 μm orifice. The instrument counted the number of particles with spherical equivalent diameters of 0.67–20.89 μm , which was divided into 256 size intervals. The IL2017 dust content was measured in 2018 at the EuroCold (University Milano-Bicocca) using a Beckman Coulter Multisizer 4 equipped with a 100 μm orifice. The instrument

measured the particle distribution from 2 to 60 μm , which was divided into 400 size intervals. To increase sample conductivity for the Coulter Counter analysis, a clean prefiltered NaCl solution was added to samples to obtain a final NaCl concentration of approximately 1% (mass fraction). To reduce the sedimentation of large particles, all samples were shaken before measurement. Two or three measurements were conducted on each sample depending on the total volume, and each measurement consumed 0.5 mL of sample. The mean relative standard deviation between the measurements was approximately 10% for both IL1999 and IL2017 for the 2–20 μm particle size range. Blank background counts represented less than 0.5% of the mean particle concentration in the samples.

In order to compare the IL1999 and IL2017 analyses, we calculated the particle number concentration for the size range measured for both cores (2–20 μm). The coarse particle percentage in terms of number (CPPn) is defined as the ratio between the number of particles of $> 10 \mu\text{m}$ diameter and the total number of particles within the 2–20 μm size range. To assess the similarities between the two ice cores, we used an additional core (IL2009) spanning the period 1993–2009 (dated by multiproxy annual layer counting). The dust concentration for IL2009 was measured using an Abakus laser particle sensor (measuring particles in the range of 1–100 μm at 1 cm intervals) connected to an ice core melting continuous flow system. The overlapping period between the integrated IL1999 + IL2017 Coulter Counter dust record and the IL2009 Abakus dust concentration record suggests good reproducibility (Fig. S1).

The dust record in Illimani was then compared to the one in Quelccaya Ice Cap (13.93°S, 70.83°W, 5670 m asl) (Thompson et al., 2013). The annually resolved dust concentration record from the Quelccaya ice core, covering the 1919–2003 period, was obtained from the World Data Center for Paleoclimatology (NCDC/NOAA) available on <https://www.ncdc.noaa.gov/data-access/paleoclimatology-data/datasets/ice-core>.

2.3 Chronology and snow accumulation rates

IL2017 was dated via annual layer counting (ALC) based on its well-preserved seasonal dust content, Ca^{2+} , and δD ; the age of the core ranged from 1999 to 2016 (Lindau et al., 2020). For IL1999, the reference horizons of well-known volcanic eruptions (Pinatubo, 1991; El Chichón, 1982; Agung, 1963) were determined by the electrical conductivity method (ECM) and by the content of fluoride, chloride, and sulfate (De Angelis et al., 2003). In addition, a

tritium peak was attributed to the year 1964, signifying the nuclear weapons testing during 1964–1967 (Knüsel et al., 2003). The resulting chronology for IL1999 was 1919 to 1999 (Fig. 2), with an estimated uncertainty of ± 2 years from 1919 to 1941 and ± 1 year for 1941–1999 (De Angelis et al., 2003). As a similar approach was used to date IL2017, we estimate an uncertainty of ± 1 year for the period 1999–2016.

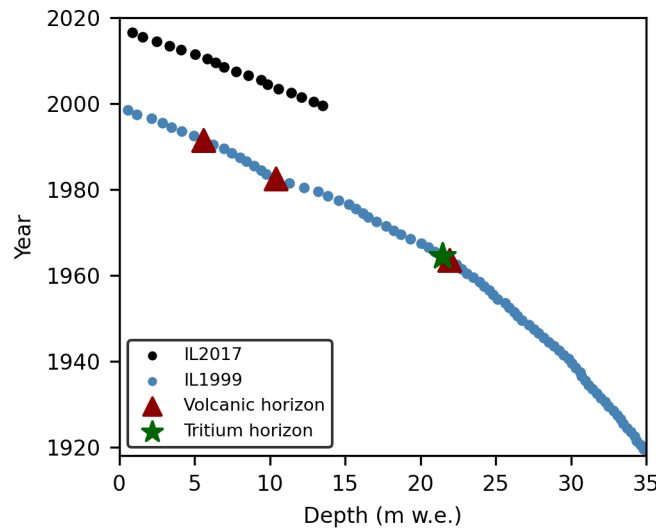


Figure 2. Depth age profiles for the IL1999 (blue points) ice core and the IL2017 (black points) firn core. The reference horizons in IL1999 are indicated by red triangles (1991, 1982, and 1963 volcanic layers) and the green star (1964 tritium peak).

The annual snow accumulation rates were reconstructed from the annual layer thicknesses, considered as the depth (in w.e.) between winter dust peaks. However, the thickness of a layer deposited on the surface decreases with depth due to compression and stretching. In order to establish the original thickness of the annual layers an exponential fit regression was applied to the layer thickness with the depth (Nye, 1963). This regression equation was used to calculate the accumulation following Eq. (1):

$$acc = \frac{(p_i - p_{i-1})a^{-b}}{a^{-b}p_i} \quad (1)$$

where acc is accumulation, p_i is depth, $(p_i - p_{i-1})$ is the layer thickness, and a and b are the constants from the best exponential fit regression. It is important to note that this method focuses on the interannual variability and can therefore mask the overall trend across the entire time range (Vimeux et al., 2009).

2.4 Glacier and climatic data

In this study, we used twelve aerial photographs of the n°8 glacier on the Illimani (Fig. 1b) during the dry seasons of 1956, 1963, 1975, 1983, and 2009 (available from the Bolivian Servicio Nacional de Aerofotogrametria [SNA]). We chose this glacier because it showed the best representation in the oldest available air photographs for this area. It is also a relatively large glacier (1.95 km^2 in 2009) in Bolivia, and most of its accumulation area is above 5000 m asl.

The photographs were digitized with a resolution of $14 \mu\text{m}$ using a photogrammetric scanner. The internal and external orientation was performed through a digital photogrammetric workstation equipped with a Planar 3D stereoscopic visualization system and the Leica Photogrammetry Suite (LPS) digital system. For the camera calibration, the radial distortion of the lenses, the focal length and the position of the fiducial marks were considered (Table S1). Eight control points were produced during fieldwork in 2010 using a pair of Astech Zmax L2 differential GPS. The ice-covered areas and drainage basins were digitized using a UTM-WGS 84 (zone 19 south) reference system. The glacier terminus was manually determined based on the aerial photographs; subsequently, we extracted a terrain digital elevation model (DEM) for each studied year. Volume glacier changes were then calculated by subtracting the DEMs of the different years (Ribeiro et al., 2013).

Freezing level heights (FLH) for the Illimani were calculated using monthly temperatures and geopotential heights from the NCEP/NCAR reanalysis (<https://psl.noaa.gov/data/gridded/data.ncep.reanalysis.html>) for the period 1948–2017. The comparison of FLH with the elevation from the glacier front helped to explain the strong ablation rates in Bolivian glaciers and their consequent retreat (Rabatel et al., 2013). The data were centered at 17.5°S , 67.5°W ($2.5^\circ \times 2.5^\circ$ resolution), and the levels around the FLH (500 and 600 hPa) were examined for a transition from positive to negative temperature. The FLHs were then linearly interpolated from the geopotential heights of the transition levels (similar to Bradley et al. 2009) and annually resampled.

Precipitation records at annual resolution for Apolo, Rurrenabaque, and Sapecho (Fig. 1a) were provided by the SENHAMÍ (Servicio Nacional de Meteorología e Hidrología, Bolivia) network (www.senhami.gob.bo/sismet). We used the Extended Reconstructed Sea Surface Temperature (ERSST, version 5, Huang et al. 2017) for the tropical Pacific (Niño 4 region, 5°N – 5°S , 160°E – 150°W) and tropical North Atlantic (TNA, 20°N – 5°N , 60°W – 30°W). We also employed the reanalysis dataset from the European Center for Medium Range Weather

Forecasts (ECMWF, ERA5). All of the data were obtained from the KMNI Climate Explorer (<http://climexp.knmi.nl/getindices>) at annual resolution.

3 Results and discussion

3.1 A 97-year tropical Andean dust record

The mean annual dust concentration in Illimani for the period 1999–2016 was 13,189 part mL^{-1} . We compared this new composite Illimani record with the Quelccaya ice core record (Thompson et al., 2013) and identified two periods of relatively high dust concentrations at both sites (Fig. 3a): 1) mid-1930s—mid-1940s, and 2) mid-1980s—2016 (the Quelccaya record finishes in 2002). In agreement, reconstructed annual precipitation from tree-ring growth in western Altiplano during 1300–2006 AD inferred a severe drought event between 1930 and 1948 (1940 was the second driest year in the entire record), which was preceded by wet conditions since the 19th century (Morales et al., 2012). In addition, the reconstructed snow accumulation in Illimani showed the lowest rate during this period ($0.35 \text{ m w.e. a}^{-1}$ in 1937), and the snow accumulation rates at Quelccaya were also relatively low (Fig. 3b). Furthermore, three of the most extreme dry years in Altiplano had occurred after the 1980s (1982, 1994, and 2006; Morales et al. 2012). We also observed a shift to lower snow accumulation rates in the mid-1980s for both Illimani and Quelccaya (Fig. 3b); this was attributed to lower moisture advection from the Amazon basin (Ribeiro et al., 2018), as Atlantic Ocean moisture via the Amazon basin is the primary moisture source for southern tropical Andes glaciers (Hoffmann et al., 2003; Thompson et al., 2013).

We detected an unprecedented rise in the ratio of coarse particles (CPPn) at Illimani during the late 20th century—particularly since the 1990s (Fig. 3c). The mean CPPn over the period 1919–2016 was 1.5%, and annual values reached $> 3\%$ by the end of the 1990s. Figure 4 shows that the late 20th century increase in CPPn correlated ($p < 0.05$) with the decrease in specific humidity at the 500 hPa (5500 m height on average) level over the Bolivian Amazon. This suggests lower regional precipitation and reduced moisture transport from the Amazon basin to the southern tropical Andes (Segura et al., 2020). Figure 4 also indicates reduced deep convection over the Bolivian Amazon (Espinoza et al., 2019). In agreement, CPPn showed a negative correlation with precipitation records from nearby meteorological stations (Fig. S2).

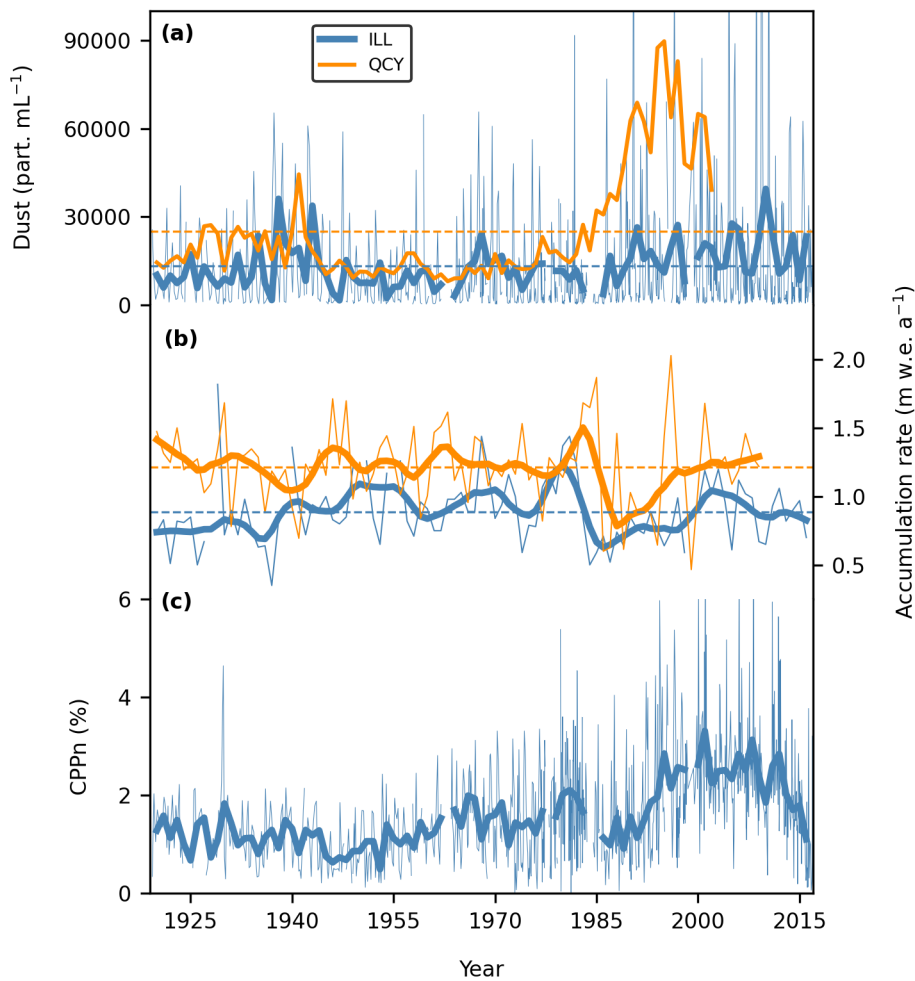


Figure 3. Comparison between dust concentration (a) and annual snow accumulation rates (b) in ice cores from Nevado Illimani (ILL, blue line, this study) and Quelccaya ice cap (QCY, orange line) (Thompson et al., 2013). Raw (thinner line) and annual (thicker line) dust concentrations from Illimani consider a particle size range of 2–20 μm . Conversely, annually resolved dust concentration from Quelccaya considers a particle size range of 0.63–20 μm . The thicker lines in (b) correspond to the 10-year LOWESS smoothed data, and the thinner lines refer to the raw data. The horizontal dashed lines refer to the mean annual dust concentration in (a) and the mean accumulation in (b) at each site. The raw (thinner line) and annual (thicker line) values in (c) refer to the coarse particle proportion in terms of number (CPPn) in the Illimani ice cores.

Moreover, CPPn variability was not directly linked to the percentage of giant dust particles ($\varnothing > 20 \mu\text{m}$) in IL2017 (Lindau et al., 2020), as giant particles respond to deep convection during wetter periods in Altiplano under enhanced atmospheric turbulence. Conversely, it is likely that coarse particles were more efficiently emitted and less efficiently scavenged under regional/local drier conditions—especially since the 1990s.

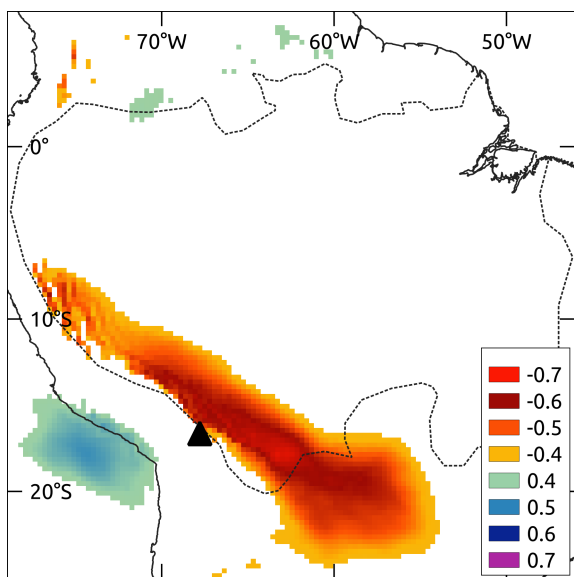


Figure 4. Spatial correlations (significant at the 95% level) between the 3-year moving average record of coarse particles (CPPn) and the specific humidity at the 500 hPa level (ERA5 reanalysis comprising the period 1980–2015). The black triangle locates the Nevado Illimani, and the dotted line delimits the Amazon basin.

3.2 Large scale controls on the percentage of coarse dust particles

The late 20th century CPPn increase is consistent with the significant decline in precipitation over the Bolivian/ southern Amazon basin during 1982–2017, which was attributed to a weakening moisture transport from the tropical North Atlantic Ocean (Espinoza et al., 2019). Warmer sea surface temperatures (SSTs) in the tropical North Atlantic (expressed by the TNA index) over the last decades (Fig. 5) altered the migration of the Intertropical Convergence Zone (ITCZ) toward warmer SSTs (Yoon and Zeng, 2010). As a result, the ITCZ was anomalously displaced northward under a warmer TNA; this weakened the northeasterly Atlantic trade winds and limited the moisture transport to the southern Amazon basin, leading to lower rainfall (Yoon and Zeng, 2010; Marengo and Espinoza, 2016). In agreement, TNA was positively correlated with the 3-year moving average of CPPn ($r = 0.52$, $p < 0.01$), and both showed increasing trends since the 1990s (Fig. 5).

We also observed a weaker positive correlation between CPPn and SSTs in the tropical Pacific by comparing the grain size data with the El Niño 4 (5° N– 5° S, 160° E– 150° W) index ($r = 0.32$, $p < 0.05$, Fig. S3). Tropical Pacific SST anomalies are associated with anomalous upper-level westerlies over the southern tropical Andes, which inhibit convection and precipitation over this region (Garreaud, 1999). Such anomalies, however, only explain approximately 13% of the total annual rainfall variability over the entire Amazon basin (Marengo, 1992; Espinoza et al., 2009).

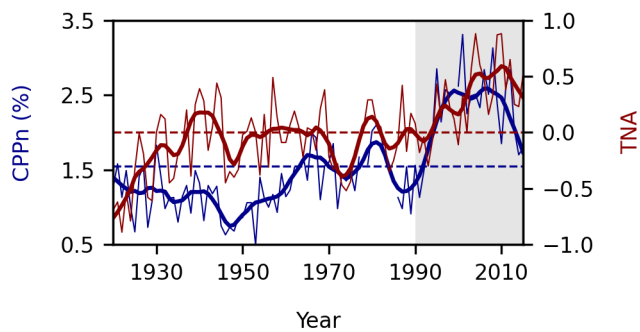


Figure 5. Relationship between the coarse particle percentage in terms of number (CPPn) and sea surface temperature anomalies in the tropical North Atlantic (TNA) referenced to the period 1981–2010. Thinner lines correspond to annually resolved data, and thicker lines correspond to the 10-year LOWESS smoothed data. Horizontal dashed lines highlight the mean for each parameter. The gray area indicates the rise of both CPPn and TNA during the 1990s.

3.3 Glacier area variability in Illimani

The glacial area of n°8 on Illimani reduced by 17% from 1956 to 2009 (Fig. 6), with an estimated area of 2.36 km^2 in 1983 and 1.95 km^2 in 2009. Fig. 6 indicates no significant variations in the glacial area of n°8 during 1956–1983, which suggests that the glacier was relatively stable. In addition, the DEMs for 1956, 1963, and 1975 showed high mean absolute errors (average of 6.3 m). From 1983 to 2009, we estimated a height reduction of -13 m and a negative mass balance of $-11.8 \pm 2.29 \text{ m w.e.}$. This is in accordance with the estimated negative mass balance of the Zongo glacier ($16.08^\circ \text{ S}, 68.28^\circ \text{ W}$, Fig. 1a) for the same period (-12 m w.e.). In addition, this glacier lost 14.4% of its area from 1956 to 2006 and has been rapidly shrinking since 1975 (Soruco et al., 2009).

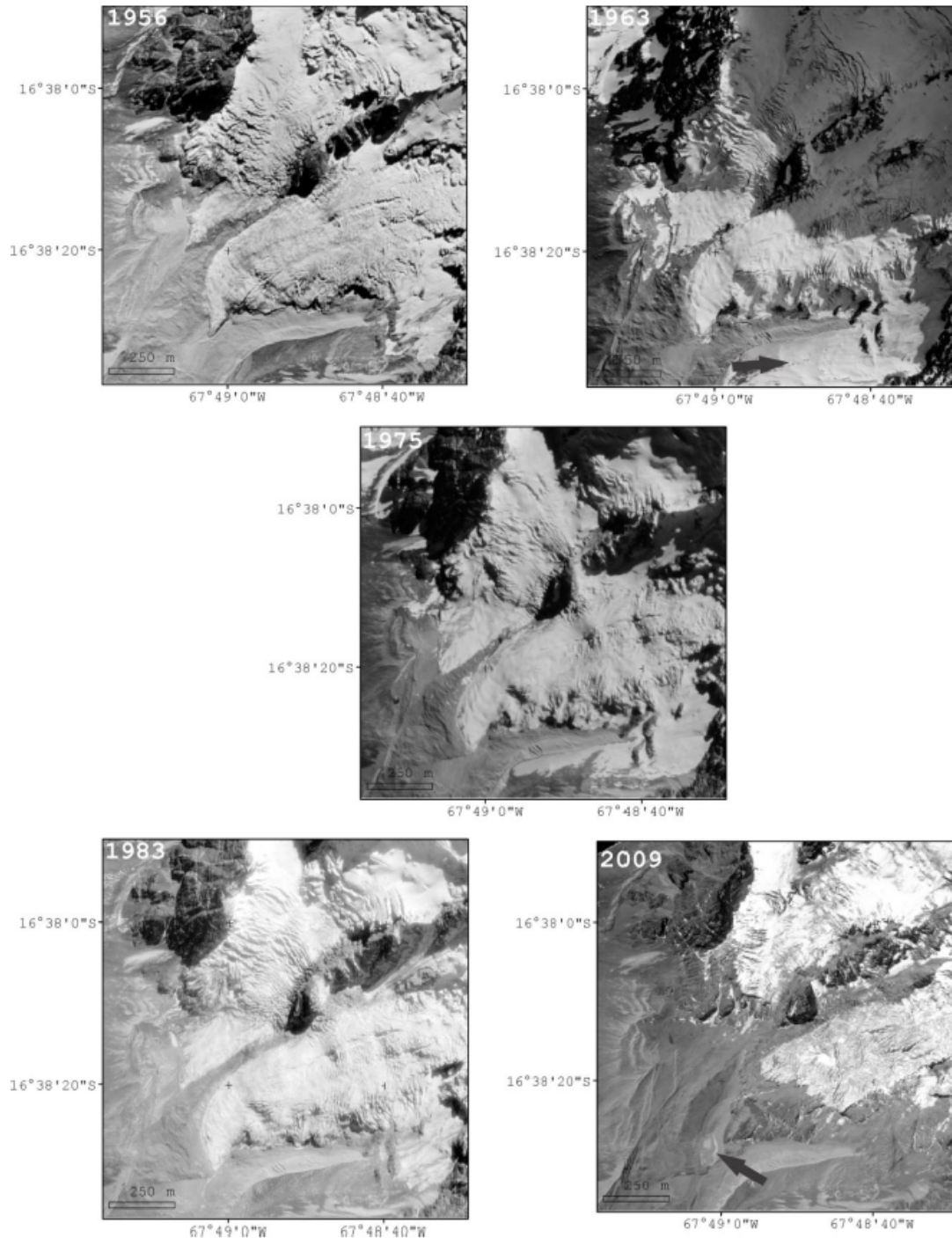


Figure 6. Aerial photograph sequences used for the analysis of glacier n ° 8 located in the southern sector of Nevado Illimani. The arrow over the left sector of the glacier in 1963 points to recent snowfall, which masks the glacier's limit. The glacier shrinkage from 1983 to 2009 formed a small proglacial lake.

Bolivian glaciers experienced rapid retreat during the early 1980s. The Chacaltaya glacier (16.33°S , 68.12°W) showed a moderate mass-balance deficit during 1940–1963, and the period 1983–1998 was marked by drastic glacial shrinkage (Ramírez et al., 2001). Moreover, Dussaillant et al. (2019) estimated a strong negative mass balance of $-0.42 \pm 0.24 \text{ m w.e. yr}^{-1}$

for glaciers of the southern tropical Andes between 2000 and 2018. The Working Group on Snow and Ice of the International Hydrological Program (GTHN-PHI-UNESCO) estimated a 50% reduction in Bolivia's glacial surface from the 1970s to 2017, and Illimani lost 9.5 km^2 of glacial coverage during the same period (Ribeiro et al., 2013). The timing of this accelerated retreat was attributed to tropospheric warming over the tropical Andes and a higher frequency of El Niño events, including changes in its spatial occurrence (Francou et al., 2003). The influence of warming in the tropical North Atlantic should also be considered, as warmer SSTs in 2005 had caused a strong negative mass balance of the Zongo glacier (Ribeiro et al., 2018).

3.4 Relationship between glacier retreat and the percentage of coarse dust particles

The timing of glacier n°8's retreat corresponds to the increase in coarse particle abundance in ice. We estimated an acceleration in the rising CPPn trend during 1987 (Fig. 7a). This period was obtained by fitting a continuous piecewise linear function to the 3-year averaged CPPn. Three line segments were obtained ($r^2 = 0.72$), and the slopes for 1920–1947, 1947–1987, and 1987–2015 were -0.01, 0.02, and 0.03 % yr^{-1} , respectively. This infers a continued increase in dust sources to Illimani in recent years, which is likely caused by the increased exposure of soil sediments in deglaciated areas and a higher deposition of locally sourced coarse particles.

The accelerated retreat of glacier n°8 and the higher deposition of coarse dust particles at Illimani coincided with rising atmospheric temperatures during the late 20th century. Gilbert et al. (2010) quantified two warming phases based on englacial temperature measurements in a borehole at the Illimani drilling site during the 1999 campaign: 1) +0.5 °C from ~1920s to 1960, and 2) +0.6 °C from 1985 to 1999. This is in agreement with the relative areal stability of n°8 during 1956–1983. However, CPPn increased during the same period, which can be attributed to a larger retreat of the smaller Illimani glaciers (area < 1 km^2) until the 1980s. The accumulation areas on the smaller glaciers are at lower elevations, and their entire surface can occasionally become an ablation zone. Moreover, the mean area loss of the small Illimani glaciers from 1963 to 1983 was 40% (a total loss of 1.6 km^2) compared to a mean reduction of 8% for glaciers larger than 1 km^2 (Ribeiro et al., 2013). Furthermore, the majority of glacier n°8 accumulation areas are above 5000 m asl.

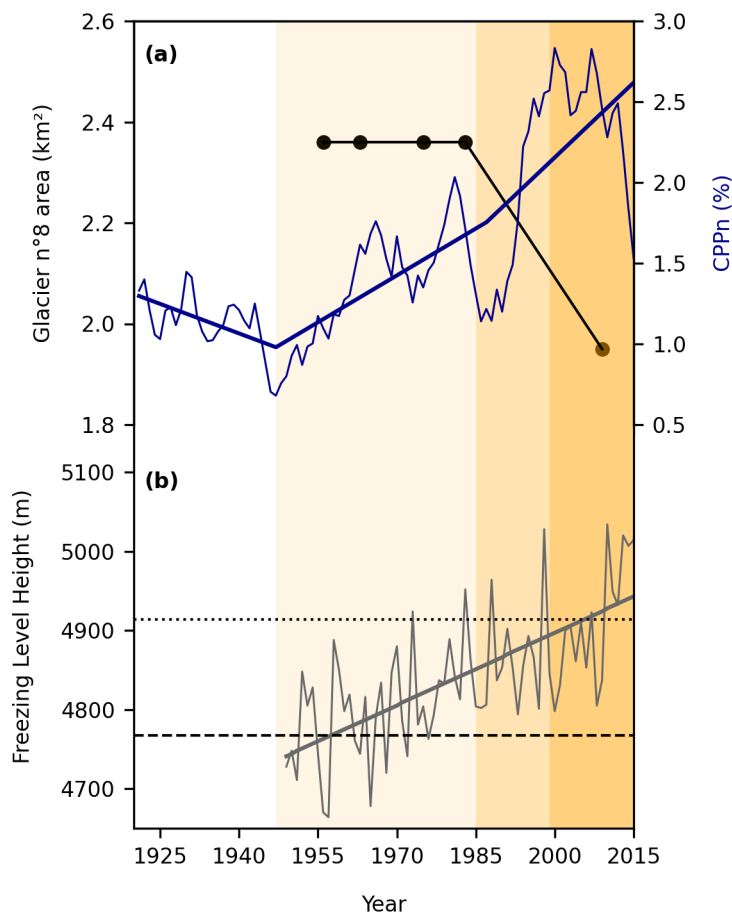


Figure 7. Relationships between glacial retreat, coarse particle percentage (CPPn), and the freezing level height over Nevado Illimani. (a) the variability in glacial area of n°8 (black line and black dots) compared with the annually resolved CPPn records (thinner blue line, 3-year moving average). The thicker blue line represents the linear piecewise fit applied to CPPn. (b) Annually resolved freezing level heights (gray line). The thicker line represents the linear increasing trend ($r^2 = 0.5$). The horizontal dashed and dotted black lines show the mean elevation of the glacial terminus for glaciers larger than 0.5 km^2 at Nevado Illimani in 1963 and 2009, respectively (Ribeiro et al., 2013). The orange bands highlight the three periods in the record (discussed in the text): 1950–1985 (light orange), 1985–1999 (orange), and 1999–2015 (dark orange).

We observed an increase in the FLH at Illimani (Fig. 7b) since 1950, which correlated with the CPPn trend ($r = 0.41$) at the 95% level. This is in accordance with the estimated 27.1 m per decade rise in freezing altitude over Cordillera Real from 1955 to 2011 (Rabatel et al., 2013). The FLH record in Fig. 7b also corresponds to the increased elevation of the glacier terminus; the mean terminus elevation of the largest Illimani glaciers was approximately 4770 m asl in 1963 and 4900 m asl in 2009 (Ribeiro et al., 2013). We therefore suggest that the ratio of coarse particles was an indirect response to the temperature rise over the southern tropical Andes. A higher FLH increases the glacier terminus elevation, which reduces the glacial area and exposes sediments; these conditions facilitate the transport of coarse material to the ice core sampling site. These observations are similar to those previously observed in

the European Alps (Oerlemans et al., 2009). However, the dust sources of the coarse particles cannot be accurately determined due to the absence of high-resolution provenance studies.

Overall, we identified three phases of CPPn increase (Fig. 7). The first phase during 1947–1985 was characterized by a moderate retreat of the Illimani glaciers driven by an increase in the FLH, which promoted the rise in CPPn. The strong El Niño events during the second phase at 1985–1999 reduced snow precipitation and increased atmospheric temperatures, which accelerated glacial retreat and increased CPPn. The final phase since 1999 was characterized by reduced glacial coverage and continued glacial shrinking in response to higher temperatures and periods of reduced snowfall driven by extreme conditions over the tropical Pacific and tropical North Atlantic. The recently deglaciated area became a new source of dust particles to the Illimani summit, which was the likely cause for the unprecedented rise in the coarse particle proportion during the 1990s.

4 Conclusions

The annually resolved mean dust concentrations (2–20 μm particle size range) in Illimani during 1919–2016 was \sim 13,000 particles per mL We identified two common periods of enhanced dust deposition when comparing the Illimani and Quelccaya ice core records (Thompson et al., 2013): 1) 1930s–1940s and 2) mid-1980s–2016. These enhanced dust periods coincided with drier conditions inferred from the observed minima in reconstructed snow accumulation rates and moisture transport from the Amazon basin.

The relative abundance of coarse dust particles in the Illimani glacier (expressed as the grain size index CPPn) correlated with SST in the tropical North Atlantic (TNA index). This suggests that a warmer tropical North Atlantic reduces the moisture advection from the Amazon basin to the Bolivian glaciers; this enhances drier conditions over the Bolivian Altiplano and promotes negative glacier mass balances, which mobilizes coarse dust particles from periglacial dust sources.

Glacier n°8 remained relatively stable from 1956 to 1983, but its area decreased by 17% in 2009. This coincided with an increase in CPPn since the late 1980s. Furthermore, the CPPn trend correlated with a rapid increase in FLHs across the region ($r = 0.41$). Thus, increasing temperatures caused glacial shrinkage, which exposed more sediments and increased the deposition of locally sourced dust to the Illimani summit. We identified distinct phases in this mechanism since the 1950s. The first phase occurred until the mid-1980s and was

characterized by moderate glacial retreat and a moderate increase in CPPn. As temperatures continued to increase from the 1980s to the 1990s, strong El Niño events and warmer conditions over the tropical North Atlantic caused an unprecedented deposition of locally sourced dust particles in the 97-year ice core Illimani record.

Data availability. Data will be available at the NOAA (US National Oceanic and Atmospheric Administration) data center for paleoclimate after the acceptance of the paper: <http://www.ncdn.noaa.gov/data-access/paleoclimatology-data/datasets/ice-core>.

Author contributions. FL, JS, RR, PG, BD and GB wrote the manuscript; JS designed the research; FL, JS, PG, BD and GB conducted dust analyses. RR and ER analyzed aerial photographs. PG, SK and VM provided analytical resources. All authors were involved in editing the manuscript.

Competing interests. The authors declare that they have no conflict of interest

Acknowledgements. The 1999 drilling campaign at Nevado Illimani was organized and covered by a joint French (IGE and IRD) and Swiss (PSI and University of Bern) project. The drilling campaign in 2017 was organized in the frame of the ICE MEMORY project (www.ice-memory.org) supported by IRD, CNRS, UGA Foundation and local Bolivian institutions (Universidad Mayor San Andres – La Paz). Drilling equipment was provided by IGE and CNRS/INSU/C2FN CLIMCOR project. We thank all participants taking part of the field campaigns. This study is part of the investigations of the Brazilian National Institute of Science and Technology of the Cryosphere (Brazilian National Council for Scientific and Technological Development - CNPq Process 465680/2014). FGL Lindau thanks CNPq (Processes 141013/2015-0 and 200496/2017-4) for scholarship to study at the EuroCold (University of Milano-Bicocca, Italy). We thank JR Petit (IGE–CNRS, Grenoble) for helping in the 1999 dust analyses on the Illimani Ice core.

References

- Baccolo, G., Delmonte, B., Albani, S., Baroni, C., Cibin, G., Frezzotti, M., Hampai, D., Marcelli, A., Revel, M., Salvatore, M. C., Stenni, B., and Maggi, V.: Regionalization of the Atmospheric Dust Cycle on the Periphery of the East Antarctic Ice Sheet Since the Last Glacial Maximum, *Geochemistry, Geophysics, Geosystems*, 19, 3540–3554, <https://doi.org/10.1029/2018GC007658>, 2018.

- Bojinski, S., Verstraete, M., Peterson, T. C., Richter, C., Simmons, A., and Zemp, M.: The concept of essential climate variables in support of climate research, applications, and policy, *Bulletin of the American Meteorological Society*, 95, 1431–1443, <https://doi.org/10.1175/BAMS-D-13-00047.1>, 2014.
- Bradley, R. S., Keimig, F. T., Diaz, H. F., and Hardy, D. R.: Recent changes in freezing level heights in the Tropics with implications for the deglaciation of high mountain regions, *Geophysical Research Letters*, 36, 2–5, <https://doi.org/10.1029/2009GL037712>, 2009.
- Correia, A., Freydier, R., Delmas, R. J., Simões, J. C., Taupin, J.-D., Dupré, B., and Artaxo, P.: Trace elements in South America aerosol during 20th century inferred from a Nevado Illimani ice core, Eastern Bolivian Andes (6350 m a.s.l.), *Atmospheric Chemistry and Physics*, 3, 1337–1352, <https://doi.org/10.5194/acpd-3-2143-2003>, 2003.
- De Angelis, M., Simões, J., Bonnaveira, H., Taupin, J. D., and Delmas, R. J.: Volcanic eruptions recorded in the Illimani ice core (Bolivia): 1918–1998 and Tambora periods, *Atmospheric Chemistry and Physics*, 3, 1725–1741, <https://doi.org/10.5194/acp-3-1725-2003>, 2003.
- Delmonte, B., Baroni, C., Andersson, P. S., Schoberg, H., Hansson, M., Aciego, S., Petit, J. R., Albani, S., Mazzola, C., Maggi, V., and Frezzotti, M.: Aeolian dust in the Talos Dome ice core (East Antarctica, Pacific/Ross Sea sector): Victoria Land versus remote sources over the last two climate cycles, *Journal of Quaternary Science*, 25, 1327–1337, <https://doi.org/10.1002/jqs.1418>, 2010.
- Dussaillant, I., Berthier, E., Brun, F., Masiokas, M., Hugonnet, R., Favier, V., Rabatel, A., Pitte, P., and Ruiz, L.: Two decades of glacier mass loss along the Andes, *Nature Geoscience*, <https://doi.org/10.1038/s41561-019-0432-5>, 2019.
- Espinoza, J. C., Ronchail, J., Guyot, J. L., Cochonneau, G., Naziano, F., Lavado, W., De Oliveira, E., Pomposa, R., and Vauchel, P.: Spatio-temporal rainfall variability in the Amazon basin countries (Brazil, Peru, Bolivia, Colombia, and Ecuador), *International Journal of Climatology*, 29, 1574–1594, <https://doi.org/10.1002/joc.1791>, 2009.
- Espinoza, J. C., Ronchail, J., Marengo, J. A., and Segura, H.: Contrasting North–South changes in Amazon wet-day and dry-day frequency and related atmospheric features (1981–2017), *Climate Dynamics*, 52, 5413–5430, <https://doi.org/10.1007/s00382-018-4462-2>, 2019.
- Francou, B., Vuille, M., Wagnon, P., Mendoza, J., and Sicart, J. E.: Tropical climate change recorded by a glacier in the central Andes during the last decades of the twentieth century: Chacaltaya, Bolivia, 16°S, *Journal of Geophysical Research*, 108, 1–12, <https://doi.org/10.1029/2002jd002959>, 2003.

- Garreaud, R. D.: Multiscale Analysis of the Summertime Precipitation over the Central Andes, *Monthly Weather Review*, 127, 901–921, [https://doi.org/10.1175/15200493\(1999\)127<0901:MAOTSP>2.0.CO;2](https://doi.org/10.1175/15200493(1999)127<0901:MAOTSP>2.0.CO;2), 1999.
- Gilbert, A., Wagnon, P., Vincent, C., Ginot, P., and Funk, M.: Atmospheric warming at a high-elevation tropical site revealed by englacial temperatures at Illimani, Bolivia (6340 m above sea level, 16°S, 67°W), *Journal of Geophysical Research Atmospheres*, 115, 1–10, <https://doi.org/10.1029/2009JD012961>, 2010.
- Ginot, P., Stampfli, F., Stampfli, D., Schwikowski, M., and Gäggeler, H. W.: FELICS, a new ice core drilling system for high-altitude glaciers, *Memoirs of National Institute of Polar Research*, pp. 38–48, 2002.
- Hoffmann, G., Ramirez, E., Taupin, J. D., Francou, B., Ribstein, P., Delmas, R., Dürr, H., Gallaire, R., Simoes, J., Schotterer, U., Stievenard, M., and Werner, M.: Coherent isotope history of Andean ice cores over the last century, *Geophysical Research Letters*, 30, 1–4, <https://doi.org/10.1029/2002GL014870>, 2003.
- Huang, B., Thorne, P. W., Banzon, V. F., Boyer, T., Chepurin, G., Lawrimore, J. H., Menne, M. J., Smith, T. M., Vose, R. S., and Zhang, H. M.: Extended reconstructed Sea surface temperature, Version 5 (ERSSTv5): Upgrades, validations, and intercomparisons, *Journal of Climate*, 30, 8179–8205, <https://doi.org/10.1175/JCLI-D-16-0836.1>, 2017.
- Jomelli, V., Favier, V., Rabatel, A., Brunstein, D., Hoffmann, G., and Francou, B.: Fluctuations of glaciers in the tropical Andes over the last millennium and palaeoclimatic implications: A review, *Palaeogeography, Palaeoclimatology, Palaeoecology*, 281, 269–282, <http://dx.doi.org/10.1016/j.palaeo.2008.10.033>, 2009.
- Knüsel, S., Ginot, P., Schotterer, U., Schwikowski, M., Gäggeler, H. W., Francou, B., Petit, J. R., Simoes, J. C., and Taupin, J. D.: Dating of two nearby ice cores from the Illimani, Bolivia, *Journal of Geophysical Research*, 108, 4181, <https://doi.org/10.1029/2001JD002028>, 2003.
- Lindau, F. G. L., Simões, J. C., Delmonte, B., Ginot, P., Baccolo, G., Paleari, C. I., Di Stefano, E., Korotkikh, E., Introne, D., Maggi, V., Garzanti, E., and Andò, S.: Giant dust particles at Nevado Illimani: a proxy of summertime deep convection over the Bolivian Altiplano, *The Cryosphere Discussions*, pp. 1–21, <https://doi.org/10.5194/tc-2020-55>, 2020.
- Maher, B. A., Prospero, J. M., Mackie, D., Gaiero, D., Hesse, P. P., and Balkanski, Y.: Global connections between aeolian dust, climate and ocean biogeochemistry at the present day and at the last glacial maximum, *Earth-Science Reviews*, 99, 61–97, <https://doi.org/10.1016/j.earscirev.2009.12.001>, 2010.

- Marengo, J. A.: Interannual variability of surface climate in the Amazon basin, *International Journal of Climatology*, 12, 853–863, <https://doi.org/10.1002/joc.3370120808>, 1992.
- Marengo, J. A. and Espinoza, J. C.: Extreme seasonal droughts and floods in Amazonia: Causes, trends and impacts, *International Journal of Climatology*, 36, 1033–1050, <https://doi.org/10.1002/joc.4420>, 2016.
- Mayorga, E., Logsdon, M. G., Ballester, M. V. R., and Richey, J. E.: LBA-ECO CD-06 Amazon River Basin Land and Stream Drainage Direction Maps, <https://doi.org/10.3334/ORNLDAA/1086>, 2012.
- Morales, M. S., Christie, D. A., Villalba, R., Argollo, J., Pacajes, J., Silva, J. S., Alvarez, C. A., Llancabure, J. C., and Gamboa, C. C.: Precipitation changes in the South American Altiplano since 1300 AD reconstructed by tree-rings, *Climate of the Past*, 8, 653–666, <https://doi.org/10.5194/cp-8-653-2012>, 2012.
- Nye, J. F.: Correction factor for accumulation measured by the thickness of the annual layers in an ice sheet, *J. Glaciol.*, 4, 785–788, 1963.
- Oerlemans, J., Giesen, R. H., and Van Den Broeke, M. R.: Retreating alpine glaciers: Increased melt rates due to accumulation of dust (Vadret da Morteratsch, Switzerland, *Journal of Glaciology*, 55, 729–736, <https://doi.org/10.3189/002214309789470969>, 2009.
- Rabaté, A., Francou, B., Soruco, A., Gomez, J., Cáceres, B., Ceballos, J. L., Basantes, R., Vuille, M., Sicart, J. E., Huggel, C., Scheel, M., Lejeune, Y., Arnaud, Y., Collet, M., Condom, T., Consoli, G., Favier, V., Jomelli, V., Galarraga, R., Ginot, P., Maisincho, L., Mendoza, J., Ménégoz, M., Ramirez, E., Ribstein, P., Suarez, W., Villacis, M., and Wagnon, P.: Current state of glaciers in the tropical Andes: A multi-century perspective on glacier evolution and climate change, *Cryosphere*, 7, 81–102, <https://doi.org/10.5194/tc-7-81-2013>, 2013.
- Ramírez, E., Francou, B., Ribstein, P., Descloitres, M., Guérin, R., Mendoza, J., Gallaire, R., Pouyaud, B., and Jordan, E.: Small glaciers disappearing in the tropical Andes: A case-study in Bolivia: Glaciar Chacaltaya (16°S), *Journal of Glaciology*, 47, 187–194, <https://doi.org/10.3189/172756501781832214>, 2001.
- Ramirez, E., Hoffmann, G., Taupin, J. D., Francou, B., Ribstein, P., Caillon, N., Ferron, F. A., Landais, A., Petit, J. R., Pouyaud, B., Schotterer, U., Simoes, J. C., and Stievenard, M.: A new Andean deep ice core from Nevado Illimani (6350 m), Bolivia, *Earth and Planetary Science Letters*, 212, 337–350, [https://doi.org/10.1016/S0012-821X\(03\)00240-1](https://doi.org/10.1016/S0012-821X(03)00240-1), 2003.
- Ribeiro, R. d. R., Ramirez, E., Simões, J. C., and Machaca, A.: 46 years of environmental records from the Nevado Illimani glacier group, Bolivia, using digital photogrammetry, *Annals of Glaciology*, 54, 272–278, <https://doi.org/10.3189/2013AoG63A494>, 2013.

- Ribeiro, R. d. R., Simões, J. C., Ramirez, E., Taupin, J. D., Assayag, E., and Dani, N.: Accumulation rate in a tropical Andean glacier as a proxy for northern Amazon precipitation, *Theoretical and Applied Climatology*, 132, 569–578, <https://doi.org/10.1007/s00704-017-2108-7>, 2018.
- Segura, H., Espinoza, J. C., Junquas, C., Lebel, T., Vuille, M., and Garreaud, R.: Recent changes in the precipitation-driving processes over the southern tropical Andes/western Amazon, *Climate Dynamics*, 54, 2613–2631, <https://doi.org/10.1007/s00382-020-05132-6>, 2020.
- Simonsen, M. F., Baccolo, G., Blunier, T., Borunda, A., Delmonte, B., Frei, R., Goldstein, S., Grinsted, A., Kjær, H. A., Sowers, T., Svensson, A., Vinther, B., Vladimirova, D., Winckler, G., Winstrup, M., and Vallelonga, P.: East Greenland ice core dust record reveals timing of Greenland ice sheet advance and retreat, *Nature Communications*, 10, <http://dx.doi.org/10.1038/s41467-019-12546-2>, 2019.
- Solomina, O., Wiles, G., Shiraiwa, T., and D'Arrigo, R.: Multiproxy records of climate variability for Kamchatka for the past 400 years, *Climate of the Past*, 3, 119–128, <https://doi.org/10.5194/cp-3-119-2007>, 2007.
- Soruco, A., Vincent, C., Francou, B., and Gonzalez, J. F.: Glacier decline between 1963 and 2006 in the Cordillera Real, Bolivia, *Geophysical Research Letters*, 36, 2–7, <https://doi.org/10.1029/2008GL036238>, 2009.
- Thompson, L. G., Davis, M. E., Thompson, E. M., Sowers, T., Henderson, K. A., Zagorodnov, V. S., Lin, P.-N., Mikhalenko, V. N., Campen, R. K., Bolzan, J. F., Cole-Dai, J., and Francou, B.: A 25,000-Year Tropical Climate History from Bolivian Ice Cores, *Science*, 282, 1858–1864, 1998.
- Thompson, L. G., Mosley-Thompson, E., Davis, M. E., Zagorodnov, V. S., Howat, I. M., Mikhalenko, V. N., and Lin, P.-N.: Annually resolved ice core records of tropical climate variability over the past 1800 years., *Science*, 340, 945–950, <http://www.ncbi.nlm.nih.gov/pubmed/23558172>, 2013.
- Vimeux, F., Gallaire, R., Bony, S., Hoffmann, G., and Chiang, J. C.: What are the climate controls on δD in precipitation in the Zongo Valley (Bolivia)? Implications for the Illimani ice core interpretation, *Earth and Planetary Science Letters*, 240, 205–220, <https://doi.org/10.1016/j.epsl.2005.09.031>, 2005.
- Vimeux, F., Ginot, P., Schwikowski, M., Vuille, M., Hoffmann, G., Thompson, L. G., and Schotterer, U.: Climate variability during the last 1000 years inferred from Andean ice cores: A review of methodology and recent results, *Palaeogeography, Palaeoclimatology, Palaeoecology*, 281, 229–241, <https://doi.org/10.1016/j.palaeo.2008.03.054>, 2009.
- Yoon, J. H. and Zeng, N.: An Atlantic influence on Amazon rainfall, *Climate Dynamics*, 34, 249–264, <https://doi.org/10.1007/s00382-009-0551-6>, 2010.

Zemp, M., Frey, H., Gärtner-Roer, I., Nussbaumer, S. U., Hoelzle, M., Paul, F., Haeberli, W., Denzinger, F., Ahlstrøm, A. P., Anderson, B., Bajracharya, S., Baroni, C., Braun, L. N., Cáceres, B. E., Casassa, G., Cobos, G., Dàvila, L. R., Delgado Granados, H., Demuth, M. N., Espizua, L., Fischer, A., Fujita, K., Gadek, B., Ghazanfar, A., Hagen, J. O., Holmlund, P., Karimi, N., Li, Z., Pelto, M., Pitte, P., Popovnin, V. V., Portocarrero, C. A., Prinz, R., Sangewar, C. V., Severskiy, I., Sigurdsson, O., Soruco, A., Usualiev, R., and Vincent, C.: Historically unprecedented global glacier decline in the early 21st century, *Journal of Glaciology*, 61, 745–762, <https://doi.org/10.3189/2015JoG15J017>, 2015.

Supplement of**Dust record in an ice core from tropical Andes (Nevado Illimani – Bolivia), potential for climate variability analyses in the Amazon basin**

Filipe G. L. Lindau¹, Jefferson C. Simões^{1,2}, Rafael R. Ribeiro¹, Patrick Ginot³, Barbara Delmonte⁴, Giovanni Baccolo⁴, Stanislav Kutuzov⁵, Valter Maggi⁴, and Edson Ramirez⁶

¹Centro Polar e Climático, Universidade Federal do Rio Grande do Sul, Porto Alegre, 91501-970, Brazil

²Climate Change Institute, University of Maine, Orono, ME 04469, USA

³Univ. Grenoble Alpes, CNRS, IRD, Grenoble INP, IGE, 38000 Grenoble, France

⁴Environmental and Earth Sciences Department, University Milano-Bicocca, Milan, 20126, Italy

⁵Institute of Geography, Russian Academy of Sciences, Moscow, 119017, Russia

⁶Instituto de Hidráulica e Hidrología, Universidad Mayor de San Andrés, La Paz, Bolivia

Correspondence to: Filipe G. L. Lindau (filipe.lindau@outlook.com)

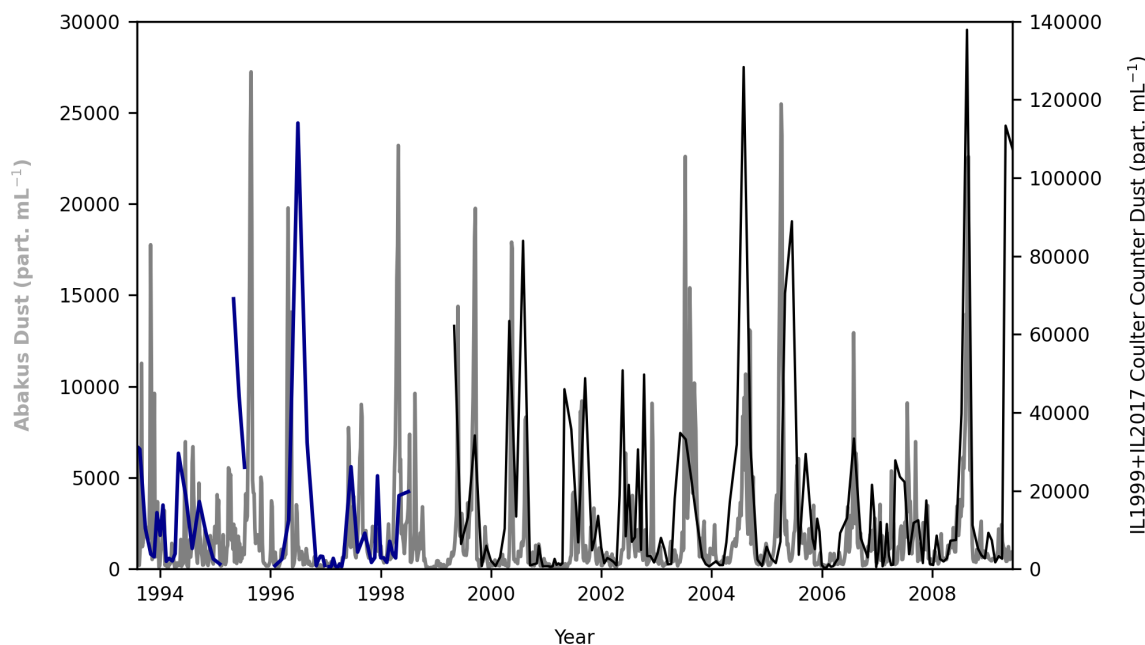


Figure S1. Overlapping between the dust measurements made with the Coulter Counter for both IL1999 (blue line) and IL2017 (black line) cores, and the ones made with Abakus for the IL2009 core (gray line). Abakus data was resampled to 5 samples per month. Concentrations were measured on different size ranges (2–20 μm for Coulter Counter) and (1–100 μm for Abakus).

Table S1. Characteristics of the aerial photographs used in the study.

Date	Scale	Number of photos	Focal length (mm)
1956	1:36000	2	153.35
1963	1:29000	2	152.44
1975	1:63000	2	152.22
1983	1:41000	2	153.26
2009	1:33000	4	152.67

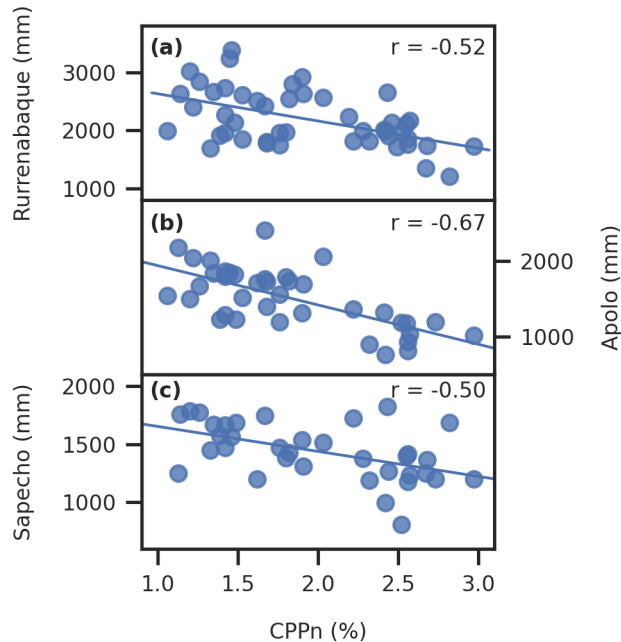


Figure S2. Relationship between the coarse particles percentage (CPPn, 3-year moving average) and annual precipitation measured by three meteorological stations in the Bolivian Amazon (Fig. 1a), (a) Rurrenabaque (1965–2015 period), (b) Apolo (1965–2006 period), and (c) Sapecho (1972–2011 period). The correlation coefficients (significant at the 95% level) are indicated in the upper right position of each plot.

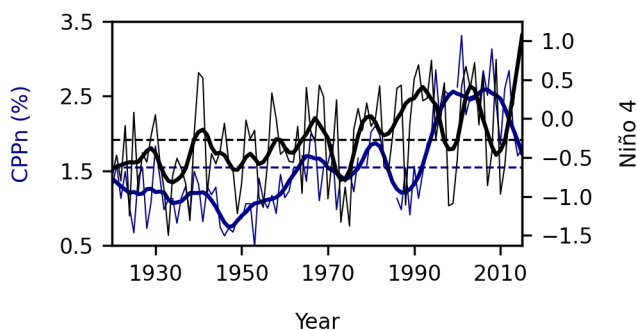


Figure S3. Relationship between the coarse particles percentage in terms of number (CPPn), and sea surface temperature anomalies in the tropical Pacific region Niño 4 referenced to the 1981–2010 period. Thinner lines correspond to annually resolved data. Thicker lines correspond to the 10-year LOWESS smoothed data. Horizontal dashed lines highlight the mean for each parameter.

6 Conclusões

Partículas de poeira contidas no testemunho de *firn* do Nevado Illimani referentes ao período 1999–2017 provêm, de acordo com suas razões de elementos terras raras, de fontes locais e regionais (mais provavelmente na porção sul do Altiplano Boliviano), tanto no inverno (estação seca), como no verão (estação úmida), embora pequenas diferenças mineralógicas serem observadas entre as duas estações. Durante o verão há uma maior deposição de minerais aerodinâmicos, como os filossilicatos, devido a maior lavagem atmosférica promovida por eventos de forte precipitação, afetando a composição dos aerossóis depositados no Illimani, principalmente observados no aumento dos fatores de enriquecimento do escândio. A forte convecção sobre o Altiplano é também responsável por aumentar a proporção de partículas gigantes (diâmetros entre 20 e 60 μm) no testemunho, ao mesmo tempo que gera um registro isotópico mais depletado. Tal relação entre as variabilidades das proporções de partículas gigantes e dos isótopos estáveis da água (δD e $\delta^{18}\text{O}$) permite, portanto, a reconstrução da atividade convectiva sobre o Altiplano que, por sua vez, é modulada pela variabilidade do fenômeno El Niño-Oscilação Sul.

As concentrações de poeira são duas ordens de grandeza maiores (valor mediano de aproximadamente 10.000 partículas por mL) durante o inverno, o que foi particularmente útil para datação do testemunho pelo método de contagem anual de camadas. De acordo, a composição dos aerossóis durante o inverno reflete a maior deposição de poeira nessa estação seca. Porém, o fator de enriquecimento crustal do manganês mostrou-se um *proxy* da circulação atmosférica sobre a bacia Amazônica, pelo seu aumento quando há a intensificação dos jatos de baixos níveis nessa região, durante o inverno. A correlação entre o manganês e o enxofre durante a estação seca indica que a circulação atmosférica sobre a bacia Amazônica pode ser determinante para o registro das queimadas em testemunhos de gelo dos Andes Centrais. O registro de enxofre, por sua vez, sugere a interferência de dois eventos vulcânicos (Rabaul em 2006 e Nyamuragira-Nyiragongo em 2014) e também de atividades relacionadas à mineração no Altiplano. O registro de elementos traço no

Illimani sugere, entretanto, uma redução recente na emissão de poluentes das fundições da região em comparação ao final do século passado. O enriquecimento do cromo durante o século XXI mostrou-se baixo o suficiente para ter sua origem classificada como crustal, enquanto que no século XX esse elemento era proveniente de fontes antrópicas.

O estudo do registro de poeira no Illimani desde o início do século XX permitiu observar uma relação entre o aumento na deposição de partículas grossas (diâmetros entre 10 e 20 µm) e uma menor advecção de umidade da bacia Amazônica para os Andes Centrais, relacionada ao aquecimento do oceano Atlântico tropical norte. Ou seja, a redução no transporte de umidade da bacia Amazônica para o Illimani, somado a uma troposfera mais quente, promove a redução da área coberta por geleiras, aumentando a exposição de sedimentos e sua consequente deflação, que é registrada no topo do Illimani por uma maior proporção de partículas grossas. A drástica redução das geleiras dos Andes Centrais, iniciada aproximadamente na década de 1980 e atualmente em curso, é portanto registrada nas camadas de neve, *firn* e gelo do Illimani.

Algumas questões abordadas nesta tese mostram a necessidade de um estudo mais detalhado da proveniência das partículas de poeira, com a inclusão de mais amostras de solo de regiões mais diversas do Altiplano e também das áreas recentemente expostas pelo degelo. Tal estudo poderia, ainda, confirmar se há deposição de poeira proveniente da África no Illimani, como ocorre na Amazônia.

A expedição Ice Memory extraiu do Illimani, além do testemunho de *firn* aqui estudado, dois testemunhos de gelo até o embasamento rochoso. Um deles será armazenado na Antártica onde está projetada a construção de um repositório de testemunhos de gelo provenientes de geleiras ameaçadas pelo aquecimento global. Porém, o outro testemunho será analisado nos próximos anos e os *proxies* obtidos nesta tese poderão ser utilizadas no maior entendimento dos mecanismos climáticos e ambientais da América do Sul tropical ao longo dos últimos milhares de anos. As relações obtidas entre o registro no Illimani e o transporte de umidade sobre a bacia Amazônica podem, por exemplo, levar a um maior entendimento dos impactos do desmatamento da floresta na dinâmica das geleiras dos Andes Centrais.

7 Referências

- Baccolo, G., Maffezzoli, N., Clemenza, M., Delmonte, B., Prata, M., Salvini, A., Maggi, V., Previtali, E. 2015. Low-background neutron activation analysis: a powerful tool for atmospheric mineral dust analysis in ice cores. **Journal of Radioanalytical Nuclear Chemistry**, v. 306, p. 589–597.
- Baccolo, G., Clemenza, M., Delmonte, B., Maffezzoli, N., Nastasi, M., Previtali, E., Prata, M., Salvini, A., Maggi, V. 2016. A new method based on low background instrumental neutron activation analysis for major, trace and ultra-trace element determination in atmospheric mineral dust from polar ice cores. **Analytica Chimica Acta**, v. 922, p. 11–18.
- Brugger, S.O., Gobet, E., Osmont, D., Behling, H., Fontana, S.L., Hooghiemstra, H., Morales-Molino, C., Sigl, M., Schwikowski, M., Tinner, W. 2019. Tropical Andean glacier reveals colonial legacy in modern mountain ecosystems. **Quaternary Science Reviews**, v. 220, p. 1–13.
- Correia, A., Freydier, R., Delmas, R.J., Simões, J.C., Taupin, J.D., Dupré, B., Artaxo, P. 2003. Trace elements in South America aerosol during 20th century inferred from a Nevado Illimani ice core, Eastern Bolivian Andes (6350 m a.s.l.). **Atmospheric Chemistry and Physics**, v. 3, p. 1337–1352.
- De Angelis, M., Simões, J., Bonnaveira, H., Taupin, J.D., Delmas, R.J. 2003. Volcanic eruptions recorded in the Illimani ice core (Bolivia): 1918-1998 and Tambora periods. **Atmospheric Chemistry and Physics**, v. 3, p. 1725–1741.
- Delmonte, B., Petit, J., Maggi, V. 2002. Glacial to Holocene implications of the new 27000-year dust record from the EPICA Dome C (East Antarctica) ice core. **Climate Dynamics**, v. 18, p. 647–660.
- Delmonte, B. 2003. **Quaternary variations and origin of continental dust in East Antarctica**. Tese de doutorado. Università degli Studi di Siena, Itália, 288 pp.
- Delmonte, B., Petit, J.R., Andersen, K.K., Basile-Doelsch, I., Maggi, V., Lipenkov, V.Y. 2004. Dust size evidence for opposite regional atmospheric circulation changes over east Antarctica during the last climatic transition. **Climate Dynamics**, v. 23, p. 427–438.

- Delmonte, B., Paleari, C.I., Andò, S., Garzanti, E., Andersson, P.S., Petit, J.R., Crosta, X., Narcisi, B., Baroni, C., Salvatore, M.C., Baccolo, G., Maggi, V. 2017. Causes of dust size variability in central East Antarctica (Dome B): Atmospheric transport from expanded South American sources during Marine Isotope Stage 2. **Quaternary Science Reviews**, v. 168, p. 55–68.
- Dussaillant, I., Berthier, E., Brun, F., Masiokas, M., Hugonnet, R., Favier, V., Rabatel, A., Pitte, P., Ruiz, L. 2019. Two decades of glacier mass loss along the Andes. **Nature Geosciences**, v. 12, p. 802–808.
- Eichler, A., Gramlich, G., Kellerhals, T., Tobler, L., Schwikowski, M. 2015. Pb pollution from leaded gasoline in South America in the context of a 2000-year metallurgical history. **Science Advances**, v. 1, e1400196.
- Eichler, A., Gramlich, G., Kellerhals, T., Tobler, L., Rehren, T., Schwikowski, M. 2017. Ice-core evidence of earliest extensive copper metallurgy in the Andes 2700 years ago. **Scientific Reports**, v. 7, 41855.
- Espinoza, J.C., Ronchail, J., Marengo, J.A., Segura, H. 2019. Contrasting North–South changes in Amazon wet-day and dry-day frequency and related atmospheric features (1981–2017). **Climate Dynamics**, v. 52, p. 5413–5430.
- Espinoza, J.C., Garreaud, R., Poveda, G., Arias, P.A., Molina-Carpio, J., Masiokas, M., Viale, M., Scaff, L. 2020. Hydroclimate of the Andes Part I: Main Climatic Features. **Frontiers in Earth Sciences**, v. 8, p. 1–20.
- Francou, B., Vuille, M., Wagnon, P., Mendoza, J., Sicart, J.E. 2003. Tropical climate change recorded by a glacier in the central Andes during the last decades of the twentieth century: Chacaltaya, Bolivia, 16°S. **Journal of Geophysical Research**, v. 108, p. 1–12.
- Garreaud, R.D. 1999. Multiscale Analysis of the Summertime Precipitation over the Central Andes. **Monthly Weather Reviews**, v. 127, p. 901–921.
- Garreaud, R.D., Aceituno, P. 2001. Interannual rainfall variability over the South American Altiplano. **Journal of Climate**, v. 14, p. 2779–2789.
- Gilbert, A., Wagnon, P., Vincent, C., Ginot, P., Funk, M. 2010. Atmospheric warming at a high-elevation tropical site revealed by englacial temperatures at Illimani, Bolivia (6340 m above sea level, 16°S, 67°W). **Journal of Geophysical Research: Atmospheres**, v. 115, p. 1–10.

- Hoffmann, G., Ramirez, E., Taupin, J.D., Francou, B., Ribstein, P., Delmas, R., Dürr, H., Gallaire, R., Simões, J., Scotterer, U., Stievenard, M., Werner, M. 2003. Coherent isotope history of Andean ice cores over the last century. **Geophysical Research Letters**, v. 30, p. 1179.
- Hong, S., Barbante, C., Boutron, C., Gabrielli, P., Gaspari, V., Cescon, P., Thompson, L., Ferrari, C., Francou, B., Maurice-Bourgoin, L. 2004. Atmospheric heavy metals in tropical South America during the past 22 000 years recorded in a high altitude ice core from Sajama, Bolivia. **Journal of Environmental Monitoring**, v. 6, p. 322–326.
- Jiménez, N., López-Velásquez, S. 2008. Magmatism in the Huarina belt, Bolivia, and its geotectonic implications. **Tectonophysics**, v. 459, p. 85–106.
- Jones, C. 2019. Recent changes in the South America low-level jet. **Climate and Atmospheric Science**, v. 2, p. 1–8.
- Kaser, G. e Osmaston, O. 2002. **Tropical Glaciers**. Cambridge University Press, Cambridge, 210p.
- Kellerhals, T., Brütsch, S., Sigl, M., Knüsel, S., Gäggeler, H.W., Schwikowski, M. 2010. Ammonium concentration in ice cores: A new proxy for regional temperature reconstruction? **Journal of Geophysical Research: Atmospheres**, v. 115, p. 1–8.
- Knüsel, S., Ginot, P., Schotterer, U., Schwikowski, M., Gäggeler, H.W., Francou, B., Petit, J.R., Simoes, J.C., Taupin, J.D. 2003. Dating of two nearby ice cores from the Illimani, Bolivia. **Journal of Geophysical Research**, v. 108, 4181.
- Knüsel, S., Brütsch, S., Henderson, K.A., Palmer, A.S., Schwikowski, M. 2005. ENSO signals of the twentieth century in an ice core from Nevado Illimani, Bolivia. **Journal of Geophysical Research: Atmospheres**, v. 110, p. 1–14.
- Kutuzov, S., Legrand, M., Preunkert, S., Ginot, P., Mikhaleko, V., Shukurov, K., Poliukhov, A., Toropov, P. 2019. The Elbrus (Caucasus, Russia) ice core record – Part 2: history of desert dust deposition. **Atmospheric Chemistry and Physics**, v. 19, p. 14133–14148.
- Lenters, J.D., Cook, K.H. 1997. On the Origin of the Bolivian High and Related Circulation Features of the South American Climate. **Journal of Atmospheric Sciences**, v. 54, p. 656–678.

- Magalhães, N. de, Evangelista, H., Condom, T., Rabatel, A., Ginot, P. 2019. Amazonian Biomass Burning Enhances Tropical Andean Glaciers Melting. **Scientific Reports**, v. 9, p. 1–12.
- Marengo, J.A., Soares, W.R., Saulo, C., Nicolini, M. 2004. Climatology of the low-level jet east of the Andes as derived from the NCEP-NCAR reanalyses: Characteristics and temporal variability. **Journal of Climate**, v. 17, p. 2261–2280.
- McBride, S.L., Robertson, R.C.R., Clark, A.H., Farrar, E. 1983. Magmatic and metallogenetic episodes in the northern tin belt, cordillera real, Bolivia. **Geologische Rundschau**, v. 72, p. 685–713.
- Osmont, D., Sigl, M., Eichler, A., Jenk, T.M., Schwikowski, M. 2019. A Holocene black carbon ice-core record of biomass burning in the Amazon Basin from Illimani, Bolivia. **Climate of the Past**, v. 15, p. 579–592.
- Osterberg, E.C., Handley, M.J., Sneed, S.B., Mayewski, P.A., Kreutz, K.J. 2006. Continuous ice core melter system with discrete sampling for major ion, trace element, and stable isotope analyses. **Environmental Science and Technology**, v. 40, p. 3355–3361.
- Paleari, C.I., Delmonte, B., Andò, S., Garzanti, E., Petit, J.R., Maggi, V. 2019. Aeolian Dust Provenance in Central East Antarctica During the Holocene: Environmental Constraints From Single Grain Raman Spectroscopy. **Geophysical Research Letters**, v. 46, p. 1–12.
- Potocki, M., Mayewski, P.A., Kurbatov, A. V., Simões, J.C., Dixon, D.A., Goodwin, I., Carleton, A.M., Handley, M.J., Jaña, R., Korotkikh, E. V. 2016. Recent increase in Antarctic Peninsula ice core uranium concentrations. **Atmospheric Environment**, v. 140, p. 381–385.
- Rabatel, A., Francou, B., Soruco, A., Gomez, J., Cáceres, B., Ceballos, J.L., Basantes, R., Vuille, M., Sicart, J.E., Huggel, C., Scheel, M., Lejeune, Y., Arnaud, Y., Collet, M., Condom, T., Consoli, G., Favier, V., Jomelli, V., Galarraga, R., Ginot, P., Maisincho, L., Mendoza, J., Ménégoz, M., Ramirez, E., Ribstein, P., Suarez, W., Villacis, M., Wagnon, P. 2013. Current state of glaciers in the tropical Andes: A multi-century perspective on glacier evolution and climate change. **The Cryosphere**, v. 7, p. 81–102.
- Ramírez, E., Francou, B., Ribstein, P., Descloitres, M., Guérin, R., Mendoza, J., Gallaire, R., Pouyaud, B., Jordan, E. 2001. Small glaciers disappearing in the tropical Andes: A case-study in Bolivia: Glaciar Chacaltaya (16°S). **Journal of Glaciology**, v. 47, p. 187–194.

- Ramirez, E., Hoffmann, G., Taupin, J.D., Francou, B., Ribstein, P., Caillon, N., Ferron, F.A., Landais, A., Petit, J.R., Pouyaud, B., Schotterer, U., Simoes, J.C., Stievenard, M. 2003. A new Andean deep ice core from Nevado Illimani (6350 m), Bolivia. **Earth and Planetary Science Letters**, v. 212, p. 337–350.
- Ribeiro, R. da R., Ramirez, E., Simões, J.C., Machaca, A. 2013. 46 years of environmental records from the Nevado Illimani glacier group, Bolivia, using digital photogrammetry. **Annals of Glaciology**, v. 54, p. 272–278.
- Ribeiro, R. da R. 2014. **Geleiras tropicais na América do Sul e as variações climáticas da Bacia Amazônica Ocidental**. Tese de doutorado, Universidade Federal do Rio Grande do Sul, 106 pp.
- Ribeiro, R. da R., Simões, J.C., Ramirez, E., Taupin, J.D., Assayag, E., Dani, N. 2018. Accumulation rate in a tropical Andean glacier as a proxy for northern Amazon precipitation. **Theoretical Applied Climatology**, v. 132, p. 569–578.
- Schwanck, F., 2016. **Variabilidade química e climática no registro do testemunho de gelo Mount Johns – Antártica**. Tese de doutorado, Universidade Federal do Rio Grande do Sul, Brasil, 144 pp.
- Schwanck, F., Simões, J.C., Handley, M., Mayewski, P.A., Bernardo, R.T., Aquino, F.E. 2016. Anomalously high arsenic concentration in a West Antarctic ice core and its relationship to copper mining in Chile. **Atmospheric Environment**, v. 125, p. 257–264.
- Segura, H., Espinoza, J.C., Junquas, C., Lebel, T., Vuille, M., Garreaud, R. 2020. Recent changes in the precipitation-driving processes over the southern tropical Andes/western Amazon. **Climate Dynamics**, v. 54, p. 2613–2631.
- Simões, J. C., 2004. Glossário da língua portuguesa da neve, do gelo e termos correlatos. **Pesquisa Antártica Brasileira**, v. 4, p. 119–154.
- Simonsen, M.F., Baccolo, G., Blunier, T., Borunda, A., Delmonte, B., Frei, R., Goldstein, S., Grinsted, A., Kjær, H.A., Sowers, T., Svensson, A., Vinther, B., Vladimirova, D., Winckler, G., Winstrup, M., Vallelonga, P. 2019. East Greenland ice core dust record reveals timing of Greenland ice sheet advance and retreat. **Nature Communications**, v. 10.
- Staal, A., Tuinenburg, O.A., Bosmans, J.H.C., Holmgren, M., Van Nes, E.H., Scheffer, M., Zemp, D.C., Dekker, S.C. 2018. Forest-rainfall cascades buffer against drought across the Amazon. **Nature Climate Change**, v. 8, p. 539–543.

- Thompson, L.G., Davis, M.E., Thompson, E.M., Sowers, T., Henderson, K.A., Zagorodnov, V.S., Lin, P.-N., Mikhalenko, V.N., Campen, R.K., Bolzan, J.F., Cole-Dai, J., Francou, B. 1998. A 25,000-Year Tropical Climate History from Bolivian Ice Cores. **Science**, v. 282, p. 1858–1864.
- Thompson, L.G., Mosley-Thompson, E., Davis, M.E., Zagorodnov, V.S., Howat, I.M., Mikhalenko, V.N., Lin, P.-N. 2013. Annually resolved ice core records of tropical climate variability over the past ~1800 years. **Science**, v. 340, p. 945–950.
- Thompson, L.G., Davis, M.E., Mosley-Thompson, E., Beaudon, E., Porter, S.E., Kutuzov, S., Lin, P.-N., Mikhalenko, V.N., Mountain, K.R. 2017. Impacts of recent warming and the 2015/16 El Niño on tropical Peruvian ice fields. **Journal of Geophysical Research: Atmospheres**, v. 122, p. 688–701.
- Thoen, I.U. 2017. **Conteúdo iônico em testemunho de firn/gelo do Monte Johns Antártica Ocidental: 1982-2008 A.D.** Dissertação de mestrado, Universidade Federal do Rio Grande do Sul, 133 pp.
- Uglietti, C., Gabrielli, P., Olesik, J.W., Lutton, A., Thompson, L.G. 2014. Large variability of trace element mass fractions determined by ICP-SFMS in ice core samples from worldwide high altitude glaciers. **Applied Geochemistry**, v. 47, p. 109–121.
- Vera, C., Higgins, W., Amador, J., Ambrizzi, T., Garreaud, R., Gochis, D., Gutzler, D., Lettenmaier, D., Marengo, J., Mechoso, C.R., Nogues-Paegle, J., Silva Dias, P.L., Zhang, C. 2006. Toward a unified view of the American monsoon systems. **Journal of Climate**, v. 19, p. 4977–5000.
- Vimeux, F. 2009. Chapter 10: Similarities and discrepancies between Andean ice cores over the last deglaciation: climate implications. In: Vimeux, F.; Sylvestre, F.; Khodri, M. (eds). **Past Climate Variability in South America and Surrounding Regions: From the Last Glacial Maximum to the Holocene**. Springer Science+Business Media, p. 239–255.
- Vimeux, F., Ginot, P., Schwikowski, M., Vuille, M., Hoffmann, G., Thompson, L.G., Schotterer, U. 2009. Climate variability during the last 1000 years inferred from Andean ice cores: A review of methodology and recent results. **Palaeogeography Palaeoclimatology Palaeoecology**, v. 281, p. 229–241.

- Vuille, M. 1999. Atmospheric Circulation Over the Bolivian Altiplano During Dry and Wet Periods and Extreme Phases of the Southern Oscillation. **International Journal of Climatology**, v. 1600, p. 1579–1600.
- Wagnon, P., Sicart, J.E., Berthier, E., Chazarin, J.P. 2003. Wintertime high-altitude surface energy balance of a Bolivian glacier, Illimani, 6340 m above sea level. **Journal of Geophysical Research**, v. 108, p. 4177.
- Yoon, J.H., Zeng, N. 2010. An Atlantic influence on Amazon rainfall. **Climate Dynamics**, v. 34, p. 249–264.
- Zemp, D.C., Schleussner, C.F., Barbosa, H.M.J., Van Der Ent, R.J., Donges, J.F., Heinke, J., Sampaio, G., Rammig, A. 2014. On the importance of cascading moisture recycling in South America. **Atmospheric Chemistry and Physics**, v. 14, p. 13337–13359.
- Zhou, J., Lau, K.M. 1998. Does a monsoon climate exist over South America? **Journal of Climate**, v. 11, p. 1020–1040.

Anexo I – Cálculo das concentrações por INAA

O método de ativação neutrônica tem como base a capacidade dos nuclídeos em capturarem nêutrons quando expostos a um forte fluxo de nêutrons. Essa captura consiste em uma reação nuclear com produtos que podem ser estáveis ou instáveis. No caso da formação de produtos instáveis, a captura do nêutron induz o decaimento radiativo do nuclídeo primitivo e a consequente emissão de partículas e de raios gama. A partir da detecção do espectro gama produzido no decaimento é possível quantificar a composição de diversos elementos.

A massa elementar foi determinada a partir do cálculo da atividade específica para cada elemento ($A_{spec.}$, *contagem. s⁻¹. g⁻¹*) obtida com base nos espectrogramas relativos aos padrões de referência, conforme a seguinte equação:

$$A_{spec.} = \frac{\frac{A}{t_{acq.}} \cdot e^{\lambda \cdot t_c} \cdot K}{(m_{el.})_{RM}} \quad (1)$$

em que A é a integral da área do pico de determinado elemento no espectrograma. Tal área foi ajustada por uma função Gaussiana, após a subtração da linha de base relativa ao ruído radioativo que foi determinado por ajuste polinomial. $t_{acq.}$ é o tempo de aquisição, λ é a constante de decaimento do radionuclídeo em questão, t_c é o tempo de resfriamento, $(m_{el.})_{RM}$ é a quantidade conhecida do elemento em questão presente no padrão de referência expressa em gramas. K é um fator corretivo que leva em consideração o decaimento radioativo que ocorre durante a aquisição, calculado pela seguinte equação:

$$K = \frac{\lambda \cdot t_{acq.}}{1 - e^{-\lambda \cdot t_{acq.}}} \quad (2)$$

o termo K torna-se mais relevante para elementos cujos tempos de meia vida são pequenos, ou seja, comparáveis ao $t_{acq.}$. A atividade das amostras ($A_{samp.}$, *contagens. s⁻¹*) foi determinada pela seguinte equação:

$$A_{\text{samp}} = \frac{A}{t_{\text{acq}}} \cdot e^{\lambda \cdot t_{\text{acq}}} \cdot K \quad (3)$$

Em seguida, a massa elementar nas amostras, $(m_{\text{el}})_{\text{samp.}}$, foi calculada de acordo com a seguinte equação:

$$(m_{\text{el.}})_{\text{samp.}} = \frac{A_{\text{sample}}}{A_{\text{spec.}}} \quad (4)$$

Nas amostras em que o tempo de irradiação foi diferente do tempo de irradiação do padrão de referência, foi aplicada uma correção adicional expressa pela equação abaixo, assim as atividades poderiam ser devidamente comparadas.

$$(A_{\text{spec.}})_{\text{corr.}} = A_{\text{spec.}} \cdot \left(\frac{1 - e^{-\lambda \cdot (t_{\text{I}})_{\text{sample}}}}{1 - e^{-\lambda \cdot (t_{\text{I}})_{\text{RM}}}} \right) \quad (5)$$

As incertezas foram quantificadas considerando as seguintes fontes: medidas de massa, tempo morto instrumental, cálculo das áreas dos picos, subtração do branco e incertezas nas concentrações dos padrões de referência. No caso dos elementos Mg e Al foi necessária uma correção em relação às reações epitermais de nêutrons, pois na produção de ^{27}Mg e ^{28}Al há a interferência de nêutrons não termais: $^{27}\text{Al}(\text{n},\text{p})^{27}\text{Mg}$, $^{28}\text{Si}(\text{n},\text{p})^{28}\text{Al}$. As contribuições dessas interferências foram avaliadas pela irradiação de Al e Si de alta pureza.

Os limites de detecção foram determinados de acordo com a seguinte equação:

$$A_{\text{DL}} = 2,71 + 4,65 \cdot \sqrt{(A_{\text{ins.}})_B} \quad (6)$$

em que A_{DL} é o limite de detecção expresso em contagens instrumentais, $(A_{\text{ins.}})_B$ é a integral observada da área bruta no branco, em correspondência à faixa de energia gama selecionada. Para obtenção do limite de detecção expresso em unidade de massa, foram combinadas as equações (3) e (4). O DL final foi calculado pelo valor médio dos brancos considerados.

Anexo II – Email de aceite do artigo “Giant dust particles at Nevado Illimani: a proxy of summertime deep convection over the Bolivian Altiplano” no fórum científico The Cryosphere Discussions

Firefox

<https://outlook.live.com/mail/0/search/id/AQM...>

tc-2020-55 (author) - manuscript available for public review and discussion

editorial@copernicus.org <editorial@copernicus.org>

Qua, 08/04/2020 01:44

Para: filipelindau@hotmail.com <filipelindau@hotmail.com>

Dear Filipe Gaudie Ley Lindau,

We are pleased to inform you that your following manuscript has been posted as a discussion paper in TCD, the scientific discussion forum of TC:

Giant dust particles at Nevado Illimani: a proxy of summertime deep convection over the Bolivian Altiplano

Author(s): Filipe Gaudie Ley Lindau et al.

MS No.: tc-2020-55

MS Type: Research article

The paper is now accessible and open for interactive public discussion until 03 Jun 2020 at: <https://www.the-cryosphere-discuss.net/tc-2020-55/>

Referees, authors and other members of the scientific community can post interactive comments alongside the discussion paper. These comments are fully citable and archived together with the discussion paper.

As the contact author, you will be informed by email about every comment posted in the interactive public discussion of your paper, and you have the opportunity to respond with author comments on behalf of all co-authors. Please inform your co-authors accordingly and make sure that all of them agree before submitting an author comment.

In addition to the author comments, you and your co-authors can individually post short comments under your names. Short comments can also be posted by all other members of the scientific community. To foster scientific discussion, please forward this information to your co-authors and any other interested colleagues.

Please respond to the referee comments and relevant short comments posted in the discussion forum of your paper as soon as possible in order to stimulate further discussion by interested scientists.

Please note that, in general, interactive comments (author comments, referee comments, short comments) should be of a substantial nature and of direct relevance to the issues raised in the discussion paper. On no account should comments contain personal insults. In case of abusive commenting, please notify the responsible Editor, who has the option of censoring abusive comments in agreement with the Co-Editors-in-Chief. More information is available via the TC website: https://www.the-cryosphere.net/peer_review/interactive_review_process.html

Firefox

<https://outlook.live.com/mail/0/search/id/AQM...>

As soon as the open discussion phase is over, no more referee comments or short comments will be accepted. During the following final response phase, however, you will have the opportunity to post final author comments. Before submitting a revised version of your manuscript for publication in TC, you are obliged to have answered all referee comments and relevant short comments in one or more author comments in the discussion forum of your paper.

You are invited to monitor the processing of your manuscript via your MS Overview: https://editor.copernicus.org/TC/my_manuscript_overview

To log in, please use your Copernicus Office user ID 535519.

In case any questions arise, please contact me.

Kind regards,

Natascha Töpfer
Copernicus Publications
Editorial Support
editorial@copernicus.org

on behalf of the TC Editorial Board

Anexo III – Email de submissão do artigo “Proxies for atmospheric circulation over the Amazon basin from the aerosol composition in a Nevado Illimani firn core, Bolivia” na revista Journal of Geophysical Research – Atmospheres

Firefox

<https://outlook.live.com/mail/0/inbox/id/AQMk...>

AGU journal submission 2020JD033900

jgr-atmospheres@agu.org <jgr-atmospheres@agu.org>

Seg, 14/09/2020 15:53

Para: filipe.lindau@outlook.com <filipe.lindau@outlook.com>

Cc: flindau9@gmail.com <flindau9@gmail.com>

Dear Dr. Lindau:

We would like to inform you that you have been listed as an author on manuscript 2020JD033900, Proxies for atmospheric circulation over the Amazon basin from the aerosol composition in a Nevado Illimani firn core, Bolivia, which has been submitted for possible publication in Journal of Geophysical Research - Atmospheres.

The corresponding author, Dr. Lindau, has indicated that the submission has been made with the consent of all authors. Please note, manuscript communications are sent to the corresponding author. All authors may check the status of the manuscript at any time using this link: <https://jgr-atmospheres-submit.agu.org/cgi-bin/main.plex?el=A6Fd4GRDR2A7HqEL6F5A9ftdUc0DQVwXaKFWLiloO48cUwZ>

ORCIDs are required for all corresponding authors and strongly encouraged for coauthors.

AGU has officially joined with many other publishers in a [commitment](#) to include the [ORCID](#) (Open Researcher and Contributor ID) for authors of all papers published starting in 2016. Funding agencies are also asking for ORCIDs.

Including the ORCID as part of published author information in papers will better enable linking of content and accurate discovery across individuals, similar to the way DOIs have enabled reference linking across journals. Given a specific scientist's permission, AGU can also add published papers to his or her ORCID record. See our statement <https://eos.org/agu-news/agu-opens-its-journals-to-author-identifiers>. We can also provide credit to you through ORCID when you serve as a reviewer.

If you have not already created an ORCID or linked it to your GEMS profile, please do so as soon as possible. You can both create and link an ORCID from your user profile. From your homepage, under General Tasks, click Modify Profile/Password. Under the ORCID field, select "Click here" to register and/or link your ORCID.

We appreciate your contribution to Journal of Geophysical Research - Atmospheres, and we will make every effort to efficiently and fairly handle your submission.

Sincerely,

Firefox

<https://outlook.live.com/mail/0/inbox/id/AQMk...>

Journal of Geophysical Research - Atmospheres Editorial Office

2 of 2

9/14/20, 4:29 PM

Anexo IV – Email de submissão do artigo “Dust record in an ice core from tropical Andes (Nevado Illimani – Bolivia), potential for climate variability analyses in the Amazon basin” na revista Climate of the Past (CP)

Firefox

<https://outlook.live.com/mail/0/inbox/id/AQMk...>

cp-2020-129 (author) - manuscript files under validation

editorial@copernicus.org <editorial@copernicus.org>

Sex, 25/09/2020 10:36

Para: filipelindau@hotmail.com <filipelindau@hotmail.com>

Dear Filipe Gaudie Ley Lindau,

Thank you very much for uploading the required files for your manuscript submitted for peer review and possible final journal publication in CP:

Title: Dust record in an ice core from tropical Andes (Nevado Illimani – Bolivia), potential for climate variability analyses in the Amazon basin

Author(s): Filipe Gaudie Ley Lindau et al.

MS No.: cp-2020-129

MS Type: Research article

Iteration: Initial Submission

Currently, your files are undergoing a technical check and you will be informed about the further steps in due time.

Please log in with your Copernicus Office user ID 535519 to monitor the processing of your manuscript via your MS overview at:

https://editor.copernicus.org/CP/my_manuscript_overview

In case any questions arise, please do not hesitate to contact me. Thank you very much for your cooperation.

Kind regards,

The editorial support team
Copernicus Publications
editorial@copernicus.org

ANEXO I

Título da Dissertação/Tese:

"CONEXÕES CLIMÁTICAS ENTRE OS ANDES TROPICAIS E A AMAZÔNIA NO REGISTRO DE AEROSSÓIS EM TESTEMUNHO DE GELO DO NEVADO ILLIMANI"

Área de Concentração: Geoquímica

Autor: **Filipe Gaudie Ley Lindau**Orientador: **Prof. Dr. Jefferson Cardia Simões**Examinador: **Prof. Dr. Alexandre Lima Correia**

Data: 05/Nov/2020

Conceito: A- Excelente

PARECER:

Avalia-se a seguir a tese de doutorado do Sr. Filipe Gaudie Ley Lindau, intitulada "Conexões climáticas entre os Andes tropicais e a Amazônia no registro de aerossóis em testemunho de gelo do Nevado Illimani". A tese descreve o trabalho de pesquisa elaborado pelo Sr. Lindau em análises químicas e físicas de amostras de aerossóis armazenadas em testemunho de firn coletado na Bolívia. O trabalho apresenta três artigos submetidos a revistas científicas tendo o Sr. Lindau como primeiro autor.

A tese apresenta uma introdução com o contexto geral do trabalho, indicando os objetivos do estudo, discutindo resultados anteriores obtidos na mesma região e sua relevância geral no contexto de estudos climáticos. A metodologia discute os aspectos técnicos da análise em laboratório em profundidade, mas carece de detalhes sobre a análise de componentes principais, uma das ferramentas estatísticas usadas no trabalho, assim como sobre a análise de trajetórias. A seção de resultados é composta por três manuscritos submetidos a revistas científicas com seletiva política de revisão por pares, nos quais são apresentadas várias análises do registro de aerossóis, sua sazonalidade, o registro glacioquímico de íons majoritários e elementos traço, assim como sobre a análise isotópica e correlações desses resultados experimentais com parâmetros meteorológicos e climáticos.

Um ponto que necessita de maior desenvolvimento no trabalho são os mecanismos físicos de conexão entre a química atmosférica na Bacia Amazônica e o registro glaciológico nos Andes. O transporte de vapor de água de leste até o sítio de amostragem em Illimani pode ser depreendido de dados de reanálises meteorológicas. Sugere-se um estudo subsequente para avaliar a correlação entre o transporte horizontal de vapor de água em altos níveis (~500 hPa), durante os meses de verão austral, e a acumulação efetiva observada no testemunho em períodos equivalentes (i.e. largura das faixas brancas na Fig 2 da pág. 54). No entanto, a contribuição de aerossóis de origem amazônica sobre os Andes é um conceito mais sutil. Por exemplo, a Fig S6 mostrada na página 102 apresenta uma

correlação positiva entre o vento zonal em baixos níveis (850 hPa) na Amazônia, a leste de Illimani, e fatores de enriquecimento do manganês no testemunho. Para o transporte entre Amazônia e Illimani seria necessário (ainda que não suficiente) uma correlação negativa (ventos de leste), ao contrário do mostrado. Há uma fraca correlação ($R=0,52$) entre a temperatura do Atlântico Norte e a percentagem de partículas de aerossol grandes no testemunho (pág. 116), que não poderia corroborar o transporte até o sítio amostral. Por outro lado a mineralogia do particulado apresentada na Fig 5 da pág. 59 é consistente com uma origem local sobre o Altiplano para o aerossol aprisionado no testemunho analisado.

Por fim, ressalto o enorme empenho físico e intelectual necessários para a realização deste trabalho. Considerando-se as condições experimentais pouco favoráveis é certamente admirável o esforço demonstrado pelo Sr. Lindau para a obtenção de medidas de qualidade no estudo do registro glacioquímico nos Andes, para melhorar o conhecimento da dinâmica de funcionamento da Bacia Amazônica, com três manuscritos submetidos para revistas científicas internacionais. Meu parecer é favorável, com conceito A – Excelente, para a tese de doutorado do Sr. Filipe Lindau.

Assinatura:



Data: 05/Nov/2020

Ciente do Orientador:

Ciente do Aluno:

ANEXO I

Título da Dissertação/Tese:

“CONEXÕES CLIMÁTICAS ENTRE OS ANDES TROPICAIS E A AMAZÔNIA NO REGISTRO DE AEROSSÓIS EM TESTEMUNHO DE GELO DO NEVADO ILLIMANI”

Área de Concentração: Geoquímica

Autor: **Filipe Gaudie Ley Lindau**Orientador: **Prof. Dr. Jefferson Cardia Simões**Examinadora: **Profa. Dra. Franciéle Schwanck Carlos**

Data: 05/11/2020

Conceito: A (excelente)

PARECER:

O tema é atual e de relevância. O trabalho apresenta novas contribuições e ferramentas para o entendimento da variabilidade de geleiras tropicais nos Andes. A revisão bibliográfica foi bem desenvolvida, se apresenta clara e objetiva porém falta uma discussão mais profunda dos processos e conceitos. A tese aborda o panorama geral sobre as mudanças ambientais pelas quais essas geleiras estão passando, além de detalhar em escala regional as mudanças que estão acontecendo na área do nevado Illimani, o que é uma importante contribuição para uma região onde poucos trabalhos de detalhe foram desenvolvidos. A metodologia escolhida consegue atingir os objetivos propostos e fornece resultados de qualidade para o desenvolvimento do estudo. Os resultados estão bem descritos e interpretados. As figuras geradas são fundamentais no entendimento dos resultados obtidos. De maneira geral, são resultados novos e de qualidade que poderão contribuir na compreensão dos mecanismos que afetam a precipitação, circulação e a mobilização de aerossóis nessa área, bem como no gerenciamento dos processos ambientais que estão em curso, ocasionando retração dessas geleiras, mudança na disponibilidade dos recursos hídricos e escassez de água no futuro.

Assinatura: *Franciéle Schwanck Carlos*

Data: 06/11/2020

Ciente do Orientador:

Ciente do Aluno: